

# DEVELOPMENT OF SUPERALLOYS BY POWDER METALLURGY FOR USE AT 1000 - 1400 °F

by

C.D. Calhoun  
(R.E. Allen, Program Manager)

GENERAL ELECTRIC COMPANY

N72-13468

Unclas  
10661

(NASA-CR-72968) DEVELOPMENT OF SUPERALLOYS  
BY POWDER METALLURGY FOR USE AT 1000 - 1400  
F C.D. Calhoun (General Electric Co.)  
Nov. 1971 92 p

CSCL 11F

G3/17

Prepared for

NATIONAL AERONAUTICS AND SPACE ADMINISTRATION

NASA-Lewis Research Center  
Contract NAS3-13202  
Fredric H. Harf, Project Manager

REPRODUCED BY  
NATIONAL TECHNICAL  
INFORMATION SERVICE  
U.S. DEPARTMENT OF COMMERCE  
SPRINGFIELD, VA. 22161

## NOTICE

This report was prepared as an account of Government sponsored work. Neither the United States, nor the National Aeronautics and Space Administration (NASA), nor any person acting on behalf of NASA:

- A.) Makes any warranty or representation, expressed or implied, with respect to the accuracy, completeness, or usefulness of the information contained in this report, or that the use of any information, apparatus, method, or process disclosed in this report may not infringe privately owned rights; or
- B.) Assumes any liabilities with respect to the use of, or for damages resulting from the use of any information, apparatus, method or process disclosed in this report.

As used above, "person acting on behalf of NASA" includes any employee or contractor of NASA, or employee of such contractor, to the extent that such employee or contractor of NASA, or employee of such contractor prepares, disseminates, or provides access to, any information pursuant to his employment or contract with NASA, or his employment with such contractor.

Requests for copies of this report should be referred to:

National Aeronautics and Space Administration  
Office of Scientific and Technical Information  
Attention: AFSS-A  
Washington, D. C. 20546

1. Report No. NASA CR-72968		2. Government Accession No.		3. Recipient's Catalog No.	
4. Title and Subtitle  Development of Superalloys by Powder Metallurgy for use at 1000 - 1400F				5. Report Date November, 1971	
				6. Performing Organization Code	
7. Author(s) C.D. Calhoun				8. Performing Organization Report No. R71AEG248	
				10. Work Unit No.	
9. Performing Organization Name and Address  General Electric Company Aircraft Engine Group Evendale, Ohio - 45215				11. Contract or Grant No. NAS3-13202	
				13. Type of Report and Period Covered Contract Report	
12. Sponsoring Agency Name and Address  National Aeronautics and Space Administration Washington, D.C. - 20546				14. Sponsoring Agency Code	
15. Supplementary Notes  Project Manager, Frederic H. Harf, Materials and Structures Div., NASA/Lewis Research Center, Cleveland, Ohio					
<p>16. Abstract Consolidated powder of four nickel-base superalloys were studied for potential application as compressor and turbine discs in jet engines. All of the alloys were based on the René 95 chemistry; three of these had variations in carbon and <math>Al_2O_3</math> contents, and the fourth alloy was chemically modified to a higher <math>\gamma'</math> volume fraction. The <math>Al_2O_3</math> was added by preoxidation of the powders prior to extrusion. The nucleus of the study was a statistical process development study where various levels of four experimental factors [(1) alloy composition, (2) grain size, (3) thermomechanical processing, and (4) room temperature deformation plus final age] were evaluated by tensile and stress rupture testing at 1200° F (650° C). Various levels of the four factors were assumed in order to construct the statistically designed experiment, but the actual levels investigated were established in preliminary studies that preceded the statistical process development study. The incorporation of <math>Al_2O_3</math> particles in the matrix of two alloys by the SAP technique did not improve tensile and stress rupture properties and was not carried beyond this point.</p> <p>Utilizing knowledge gained in the statistical process development study, four combinations of alloy and processing were selected, processed, and then evaluated by tensile testing before and after 100 hours of exposure at 1400° F (760° C). The two most promising combinations of alloy and processing were then selected for a detailed evaluation of physical and mechanical properties.</p> <p>Ultrahigh tensile strengths with good ductilities were observed in the temperature range of 72° F (22° C) to 1300° F (705° C). Excellent resistance to creep was observed at 1000° F (540° C), but creep properties deteriorated at higher temperatures. The slow-bend Charpy fracture energy was reduced with increasing yield stress in the processing schedules investigated; however, in material with elongated grain structures, attractive Charpy fracture energies were observed considering the high level of yield stress attained. Variations in yield stress and grain shape had no significant effect on <math>K_{IC}</math> - the threshold stress intensity range for Mode I crack propagation. Thermal exposure at 1200° F (650° C) for 1500 hours had no significant effect on tensile properties or notch sensitivity; however, this exposure decreased Charpy slow-bend fracture energies. Exposure at 1400° F (760° C) for 1500 hours resulted in a reduction in tensile strength but did not influence notch sensitivity.</p>					
17. Key Words (Suggested by Author(s))  Powder Metallurgy, Superalloys, René 95, Thermomechanical Processing, Mechanical Properties, Stability, Phase Analysis, Nickel Alloys, Oxide Dispersions			18. Distribution Statement  Unclassified - unlimited		
19. Security Classif. (of this report) Unclassified		20. Security Classif (of this page) Unclassified		21. No. of Pages 92	
				22. Price*	

## TABLE OF CONTENTS

<u>Section</u>	<u>Page</u>
1.0 SUMMARY	1
2.0 INTRODUCTION	3
3.0 TECHNICAL PLAN	5
4.0 EXPERIMENTAL WORK AND RESULTS	7
4.1 Powder Production and Consolidation	7
4.1.1 Melting	7
4.1.2 Atomization	8
4.1.3 Oxidation	8
4.1.4 Extrusion	9
4.2 Preliminary Studies	10
4.2.1 Rollability	11
4.2.2 Processing to Desired Grain Size	11
4.2.3 Thermomechanical Processing	13
4.2.4 Room Temperature Deformation Plus Age	14
4.3 Statistical Process Development Study	15
4.3.1 Data Analyses	17
4.3.2 Selection of Four Best Alloy/Process Combinations	19
4.3.3 Processing of Additional Material	20
4.4 Evaluation of Two Best Alloy/Process Combinations	21
4.4.1 Tensile Test Results	21
4.4.2 Creep Test Results	22
4.4.3 Fracture Resistance	22
4.4.4 Light Microscopy	23
4.4.5 Replication Electron Microscopy Evaluations	23
4.4.6 Transmission Electron Microscopy Evaluations	26
4.4.7 Phase Analysis Results	27
5.0 DISCUSSION	29
6.0 SUMMARY OF RESULTS	33
ACKNOWLEDGEMENTS	34
APPENDIX	35
REFERENCES	40

## LIST OF TABLES

<u>Table</u>		<u>Page</u>
I	Desired Composition and Limits of Consolidated Powders.	41
II	Chemical Analysis of Ingots.	42
III	Partial Chemical Analyses of As-Received -100-Mesh Powders.	43
IV	Summation of Extrusion Parameters.	44
V	Density and Average Grain Size of Extruded Bars.	45
VI	Chemical Analyses of Extruded Bars.	46
VII	Summation of Data from Flat Rollability Studies.	47
VIII	Statistical Design of Process Development Study.	48
IX	Tensile and Stress Rupture Data from Statistical Process Development Study.	49
X	Results from Statistical Analysis of Process Development Study.	50
XI	Four Best Alloy/Process Combinations.	51
XII	Tensile Screening Test Results for Four Best Alloy/Process Combinations.	52
XIII	Creep-Monitored Stress Rupture Data for Four Best Alloy/Process Combinations.	53
XIV	Comparison of 1200°F (650°C) Tensile Data for 0.35- to 0.5-Inch (0.9- to 1.3-cm) Diameter Rods.	54
XV	Tensile Data from Evaluation of Two Best Alloy/Process Combinations.	55
XVI	Tensile Data for Two Best Alloy/Process Combinations After Thermal Exposure.	56
XVII	Notched Tensile Data for Two Best Alloy/Process Combinations.	57
XVIII	Creep Data for Two Best Alloy/Process Combinations.	58
XIX	Slow-Bend Fracture Energies of Two Best Alloy/Process Combinations.	59
XX	X-Ray Analyses of Phases in Two Best Alloy/Process Combinations as Influenced by Thermal Exposure.	60

## LIST OF ILLUSTRATIONS

<u>Figure</u>		<u>Page</u>
1	Strength Advantage of Rene' 95 Over Inconel 718 and Astroloy.	61
2	Program Flow Chart.	62
3	Representative Micrographs of Gas-Atomized Powder Used in this Investigation.	63
4	Representative Particle Size Distribution of Powder Used in this Investigation.	64
5	Oxidation Data from Air Exposures of -100-Mesh Powders of Alloys A-1 and A-2.	65
6	Schematic Drawing of Extrusion Cans Used for the First Extrusion Series.	66
7	Schematic Drawing of Extrusion Can Used for Second Extrusion Series.	67
8	Photograph of Sections from Extruded Bars. Top Two Bars are from the First Extrusion Series and Bottom Two are from the Second Extrusion Series.	68
9	Photomicrographs of As-Extruded Microstructures; Extrusion Direction is Vertical.	69
10	Examples of Duplex Grain Structures that Formed when Attempting to Achieve Equiaxed Grain Growth (100X).	70
11	Preliminary Study 2 - Processing to Desired Grain Size - Effect of Variations in Rolling Reduction at 2050°F (1120°C) on Properties.	71
12	Preliminary Study 3 - TMP - Performed to Relate Dislocation Substructures from TMP to Properties.	72
13	Preliminary Study 4 - Aging Response - Performed to Relate Aging Treatments to Properties.	73
14	Preliminary Study 4 - Aging Response - Performed to Relate Aging Treatments Plus Room-Temperature Deformation to Properties.	74
15	Processing Flow Diagram.	75
16	Schematic Diagrams of Processing Schedules Selected from Statistical Process Development Study.	76
17	Tensile Data for Two Best Alloy/Process Combinations Compared to Cast-and-Forged Rene' 95.	77

# LIST OF ILLUSTRATIONS (Concluded)

<u>Figure</u>		<u>Page</u>
18	Tensile Data [1200°F (650°C)] for Two Best Alloy/Process Combinations As-Processed and After Thermal Exposure.	78
19	Comparison of the Creep Properties of Two Best Alloy/Process Combinations to Cast-and-Forged Rene' 95.	79
20	Test Results from $\hat{K}^*$ Testing at 1000°F (540°C) of Two Best Alloy/Process Combinations. $\hat{K}^*$ is the Threshold Stress Intensity Factor Range for Mode I Crack Propagation.	80
21	Photomicrographs of Four Best Alloy/Process Combinations.	81
22	Electron Micrographs of Four Best Alloy/Process Combinations (5000X).	82
23	Electron Micrographs Illustrating the Influence of Thermal Exposure on the Microstructure of Material Condition S-1 (5000X).	83
24	Electron Micrographs Illustrating the Influence of Thermal Exposure on the Microstructure of Material Condition S-3 (5000X).	84
25	Transmission Electron Micrograph of Alloy A in the Recrystallized Condition.	85
26	Transmission Electron Micrographs of Dislocation Substructures in Four Best Alloy/Process Combinations.	86
27	Drawing of Smooth Bar Specimens Used in Tensile, Stress Rupture, and Creep Testing. The Gage Length of the Creep Specimen was Increased from 0.65 to 1.0 Inch.	87
28	Drawing of Specimens for Notched Tensile Tests.	88
29	Design of Charpy V-Notched Bar that was Fatigue Cracked and Tested in Slow Bend.	89
30	Typical Charpy Bend Test Record Illustrating Calculation of Energy Absorbed at Point of Crack Instability.	90

## 1.0 SUMMARY

Consolidated powders of four nickel-base superalloys were studied for potential application as compressor and turbine discs in jet engines. All of the alloys were based on the Rene' 95 chemistry; three of these had variations in carbon and  $\text{Al}_2\text{O}_3$  contents, and the fourth alloy was chemically modified to a higher  $\gamma'$  volume fraction. The  $\text{Al}_2\text{O}_3$  was added by preoxidation of the powders prior to extrusion. The nucleus of the study was a statistical process development study where various levels of four experimental factors [(1) alloy composition, (2) grain size, (3) thermomechanical processing, and (4) room temperature deformation plus final age] were evaluated by tensile and stress rupture testing at 1200°F (650°C). Various levels of the four factors were assumed in order to construct the statistically-designed experiment, but the actual levels investigated were established in preliminary studies that preceded the statistical process development study.

Utilizing knowledge gained in the statistical process development study, four combinations of alloy and processing were selected, processed, and then evaluated by tensile testing before and after 100 hours of exposure at 1400°F (760°C). The two most promising combinations of alloy and processing were then selected for a detailed evaluation of physical and mechanical properties.

Ultrahigh tensile strengths with good ductilities were observed in the temperature range of 72°F (22°C) to 1300°F (705°C). Excellent resistance to creep was observed at 1000°F (540°C), but creep properties deteriorated at higher temperatures. The slow-bend Charpy fracture energy was reduced with increasing yield stress in the processing schedules investigated; however, in material with elongated grain structures, attractive Charpy fracture energies were observed considering the high level of yield stress attained. Variations in yield stress and grain shape had no significant effect on  $\hat{K}^*$  - the threshold stress intensity range for Mode I crack propagation. Thermal exposure at 1200°F (650°C) for 1500 hours had no significant effect on tensile properties or notch sensitivity; however, this exposure decreased Charpy slow-bend fracture energies. Exposure at 1400°F (760°C) for 1500 hours resulted in a reduction in tensile strength but did not influence notch sensitivity. The incorporation of  $\text{Al}_2\text{O}_3$  particles in the matrix of two alloys by the SAP technique produced no significant improvement in tensile or stress rupture properties.



## 2.0 INTRODUCTION

The purpose of this program was to develop, by powder metallurgy techniques, a nickel-base superalloy having mechanical properties superior to those of commercially-available alloys for compressor and turbine disc applications in jet engines. The program was initiated on 1 July 1969.

The upper temperature range for future disc materials is typically 1000°F (540°C) to 1400°F (760°C). It is required of disc materials that they have a high strength-to-density ratio, high creep strength, and a resistance to crack initiation and crack propagation. It is further required that the properties are not reduced by long-time thermal exposure. The specific minimum goals of this program were to develop a material with a 0.2 percent offset yield strength of 200 ksi (1380 MN/m<sup>2</sup>) and 10 percent elongation at 1200°F (650°C) in smooth bars, and retention of 100 percent of these properties after 100 hours exposure at 1400°F (760°C). It was planned, once these minimum goals were met, that the material would be evaluated extensively for tensile, creep, and stability. Also, as the program progressed, fracture resistance (which included both the energy for fracture and the resistance to crack propagation under cyclic loading) increased in importance in the requirements of disc materials and therefore was evaluated in the program.

The plan for this program was to take advantage of past disc alloy development by basing four alloy chemistries on the recently-developed disc alloy, Rene' 95<sup>(1)</sup>. The tensile yield strength advantage of this alloy is illustrated by the comparison with Inconel 718 and Astroloy shown in Figure 1. Alloy development in the present study was limited to the following modifications to Rene' 95: (1) variations in carbon, (2) addition of Al<sub>2</sub>O<sub>3</sub>, and (3) increase in  $\gamma'$  volume fraction. The four alloys studied and their designations were as follows: (1) Alloy A was Rene' 95 minus one weight percent Cr; the reduction in Cr was for increased stability to sigma formation so that the alloy's temperature range could be increased from 1200°F (650°C) to 1400°F (760°C); (2) Alloys A-1 and A-2 were Alloy A with reductions in C, and therefore carbides, and additions of Al<sub>2</sub>O<sub>3</sub> particles; and, (3) Alloy B was Alloy A modified so as to increase the calculated  $\gamma'$  volume fraction from 47 to 51 percent (higher  $\gamma'$  volume fractions are normally associated with increases in strength).

Most of the emphasis in the present program was directed toward processing. Strengthening mechanisms in disc alloys, as influenced by processing, are as follows: (1) grain size and shape, (2) dislocation density, and (3)  $\gamma'$  particle size. It was desired that: (1) the grain size be  $\sim 5\mu$  and elongated in a direction parallel to the maximum tensile stress; (2) a highly-stable dislocation substructure be formed (specifically, it was known that both the tensile strength and ductility of nickel-base superalloys could be increased by the formulation of dislocation substructures but that these dislocations normally are unstable, so that the creep strength is reduced); and, (3) a large percentage of the  $\gamma'$  be present as a fine-particle size (i.e.,  $\sim 500\text{\AA}$ ).

Powder metallurgy was selected over fusion metallurgy because of the increased control over the microstructure, and therefore strength, afforded by powder metallurgy. Powder metallurgy has recently gained importance in the development of superalloys, due to increased capabilities of powder vendors in producing high-purity powders. Advantages sought from powder metallurgy in this program were as follows: (1) improved alloy homogeneity (which, in turn, improves fabricability), (2) ability to introduce incoherent second-phase particles into the matrix, and (3) reduction in the grain size of the starting material as compared to ingot. The advantages sought from the incoherent second phase were not strengthening per se, but rather as a means of manipulating the microstructure. Thus, it was not anticipated that significant increases in strength would be derived directly from dislocation-particle interactions but that strengthening derived from the particles would be indirect (i.e., reduction in grain size and added stability to dislocation substructures for improved creep strength).

### 3.0 TECHNICAL PLAN

A flow chart of the program is illustrated in Figure 2. The approach was to produce powder of four alloys and consolidate these by extrusion. A statistical process development study was conducted to evaluate the effects on mechanical properties of four experimental factors: alloy composition, grain size, thermomechanical processing, and plastic deformation plus aging. Various levels of the four factors were assumed in order to construct the statistically-designed experiment; but, the actual levels used were established in preliminary studies conducted before the statistical process development study. Also, the preliminary studies established the response of each of the four alloys to various mechanical and thermal treatments. The four most promising alloy/process combinations were selected from the statistical process development study and evaluated by screening tests. Based on the results of the screening tests, the two best alloy/process combinations were selected and evaluated extensively for mechanical and physical properties.

## 4.0 EXPERIMENTAL WORK AND RESULTS

### 4.1 POWDER PRODUCTION AND CONSOLIDATION

Four alloys were studied in this program, and they were designated A, A-1, A-2, and B. The desired compositions of these alloys are given in Table I. Rene' 95 was selected as the base alloy for the program because of the strength advantage it offered over existing disc alloys (Figure 1). Alloy A was of the Rene' 95 chemistry except that the Cr content was reduced by one weight percent. Thermal exposure of Rene' 95 had revealed sigma precipitation at 1400°F (760°C) exposures but not at 1200°F (650°C). The Cr content was reduced for Alloy A to improve stability and minimize sigma precipitation.

Superalloys are typically heated to elevated temperatures for solutioning  $\gamma'$ . To retard grain growth during  $\gamma'$  solutioning, a second phase, (which is not solutioned at these temperatures) is included in the matrix. Carbides are normally used as the second phase for retarding grain growth; in atomized powders, the carbides are dispersed finely enough to act as pinning agents. However, even in a fine-grained material such as a powder metallurgy product, carbide instabilities could become a problem in long-time service exposures. Therefore, the carbon level of Alloy A (0.15 w/o) was reduced to two lower levels for Alloys A-1 and A-2, and the more stable oxide pinning agents were substituted for the carbides. In order to maintain a relatively constant amount of incoherent second-phase particles, Alloy A-1 was designed with 0.08 w/o C and 0.12 w/o oxygen ( $\sim 0.5$  v/o oxide), while Alloy A-2 was designed with  $< 0.02$  w/o C and 0.24 w/o oxygen ( $\sim 1$  v/o oxide). As will be described later, the oxygen concentration was adjusted by controlled oxidation of the powders; the oxide that forms is  $Al_2O_3$ . Alloy B was Alloy A modified to a higher  $\gamma'$  volume fraction (about a 10-percent increase). This was accomplished by a 1 w/o increase in the total Al + Ti + Cb content. The reason for increasing the  $\gamma'$  fraction is that the strength of superalloys generally increases as the volume fraction of  $\gamma'$  increases until the ductility becomes too low. Although the  $\gamma'$  volume fraction of Rene' 95 is near the maximum that can be utilized without loss in ductility in conventional materials, it was felt that an increase of  $\gamma'$  in a powder metallurgy product would be feasible because segregation problems are minimized and workability is enhanced.

#### 4.1.1 Melting

The four alloys were vacuum-induction melted and cast into about 100-pound ingots to serve as atomization remelt stock. Initially, Alloys A, A-1, and A-2 were cast by Cannon Muskegon of Muskegon, Mich. from the same heat, so that variations in chemistry could be limited to carbon. The limited capacity of the melting furnace permitted casting only enough metal from the split heat to conduct the planned work. Thus, when extrusion difficulties were encountered with the first series of alloys (to be discussed in Section 4.1.4), a second series of Alloys A and A-1 was vacuum melted. The second series was also melted by Cannon Muskegon, but the split-heat concept was

abandoned so that larger quantities of metal could be obtained. Alloy B was melted by Carpenter Technology of Reading, Pa. and was included in the program in the first series of alloys. Chemical analyses of the ingots that were used in this study (i.e., Alloys A-2 and B from the first series and Alloys A and A-1 from the second series) are given in Table II. These analyses indicated that the alloys were of the desired chemistries.

#### 4.1.2 Atomization

Ingots of the four alloys were converted to powder by Federal Mogul Corp. of Ann Arbor, Mich. using an argon atomization process. Powder for each alloy was separated into -100- and +100-mesh size fractions by screening under an argon atmosphere. Both particle size fractions were shipped and stored under an argon atmosphere; only -100-mesh powder was used in this investigation. Partial chemical analyses of these powders are given in Table III. Photomicrographs and scanning electron micrographs of these powders are illustrated in Figure 3. A screen analysis illustrating the particle size distributions for these powders is given in Figure 4. These powder studies revealed that the oxygen content was low, despite the relatively large percentage of -325-mesh powder and the fact that the powders contained the typical dendritic structures found in gas-atomized powders.

#### 4.1.3 Oxidation

The SAP technique was used to introduce oxide particles into the matrices of Alloys A-1 and A-2. In order to achieve the desired level of oxides, the degree of oxidation was determined as a function of time-temperature exposure conditions using approximately 150 grams of powder in Pt crucibles. The procedure was to determine the individual weight of five Pt crucibles with and without powder, to expose the five crucibles and powder in a box furnace, and remove one of the crucibles after 20, 40, 80, 160, and 320 minutes at the selected temperature. The weight of the crucibles and exposed powder was determined and the weight gain data calculated and plotted as illustrated in Figure 5. Based on the relationship between the weight gain data obtained at the first exposure temperature and that required to achieve target oxygen levels of Alloys A-1 and A-2, a second temperature was selected; and, the exposure procedure was repeated again until the desired level of oxidation was achieved in about two hours. In some instances, exposed powder was chemically analyzed and the oxygen contents compared to those calculated from weight gain data. In general, chemical analyses of loose powder indicated a lower level of oxygen than did the weight gain data.

The actual conditions for exposure of Alloys A-1 and A-2 were selected on the basis of weight gain data. The method used was to expose the powder in 25-pound batches so that two runs were made for each alloy. About twenty-five pounds of powder was spread to a depth of about one inch on a large Hastelloy X retort tray. Alloy A-1 was exposed for 1.3 hours at 850°F (455°C), and Alloy A-2 was exposed for 2.5 hours at 1125°F (605°C). After exposing the powder and before canning for extrusion, the powder of each alloy was blended in a twin-shell blender.

#### 4.1.4 Extrusion

The first attempt to consolidate the powder by extrusion was not completely successful; therefore, some of this work had to be repeated.

First Series - Initially, the approach was to extrude three small billets to aid in selection of the extrusion parameters for subsequent extrusion of four larger billets. The designs of these extrusion cans are given in Figure 6. The smaller billets each contained 1 pound of powder and each larger billet contained 50 pounds of powder; about forty pounds of consolidated powder was the minimum amount required for each of the four alloys.

The powder was canned by pouring the powder into the cans while mechanically tapping the cans. The density of the powder in the cans was about 63 percent of theoretical. After filling, the rear end closure [which contained a 0.062-inch (0.15-cm) diameter hole] was TIG welded to the body in a welding chamber filled with high-purity argon. The billets were then transferred to an electron beam welder, evacuated, and the 0.062-inch (0.15-cm) diameter hole welded. Finally, the billets were leak tested using a helium mass spectrometer.

The first series of alloys was extruded by Fansteel at Baltimore, Md. The three smaller billets were extruded with a vertical press through a 0.375-inch (1-cm) diameter die as follows:

Alloy	Temp.		Extrusion Ratio	Remarks
	°F	°C		
A-1	2050	1120	28:1	Extruded well
A-1	2150	1175	28:1	Extruded well
B	2050	1120	28:1	Stalled the press

Equipment difficulties prevented accurate determinations of extrusion constants or rates of extrusion. However, based on the maximum pressure capabilities of the vertical press, it was reasoned that the larger billets could be extruded on a horizontal extrusion press of larger capacity.

The large billets were extruded through a 1.1-inch by 1.1-inch (2.7-cm by 2.7-cm) square die at a ratio of 22:1. A summation of the extrusion parameters is given in Table IV. During the extrusion of Alloy A, about two-thirds of the billet passed through the die before the press stalled. The remaining one-third of the billet was machined and re-extruded at a rate comparable to those used in extruding Alloys A-2 and B. The first and second extrusions of Alloy A yielded about 2 feet (0.6 m) and 4 feet (1.2 m) of sound material, respectively. The macroscopic appearance of Alloy A-1 indicated that two-thirds of the extrusion was of good quality. However, radiography revealed that center line voids existed at intervals over the entire length of the extrusion so that no useable material was obtained for Alloy A-1. About 9 and 12 feet of sound material were obtained for Alloys A-2 and B, respectively.

Second Series - The second series of Alloys A and A-1 was extruded by James Hunt of Hyper-Form (Framingham, Mass.). His design of the extrusion can is shown in Figure 7. Major differences in the design of this extrusion can, as compared to that used in the first extrusion series, were: (1) the can was made from 321 stainless steel rather than mild steel (stainless steel has the advantage of being nearer to the strength of the powder core during extrusion), and (2) a heavier nose section was used (it was reasoned that the powder would be consolidated during the time that the nose of the billet was being extruded through the die). Of these two differences in the design of the extrusion cans, the second is thought to be the most important.

Canning procedures were the same as for the first series. The second series of alloys was extruded at Brush Beryllium (located at Elmore, Ohio) under the supervision of James Hunt. The extrusion cans were placed in carbon pots and covered during heatup, which prevented extensive oxidation of the cans and enabled excellent surfaces to be achieved on the extruded bars. From the summation of the extrusion parameters, which are given in Table IV, it is seen that the extrusion of the second series of Alloys A and A-1 was completely successful. Extruded bars from the two extrusion series are compared in Figure 8.

The as-extruded bar stock for each of the four alloys was evaluated by metallography, density, and chemical analyses. Photomicrographs in Figure 9 illustrate that: (1) the material was in the recrystallized condition as evidenced by the equiaxed grain shape; (2) the average grain size varied from about  $10\mu\text{m}$  for Alloys A and A-1 to about  $15\mu\text{m}$  for Alloys A-2 and B; (3) growth of the grains in Alloy A-2 was inhibited by the oxide stringers so that the grain size was related to the distance between oxide stringers; and (4) the material appeared to be fully dense. Comparison of the results from the density measurements of the extruded bar to calculated densities, or the density of cast-and-forged Rene' 95, revealed that the material was fully dense. These data and the results of grain size determinations by a line-intercept method<sup>(2)</sup> are given in Table V. Chemical analyses of the extruded bars in Table VI show that the alloys were within chemical specifications.

#### 4.2 PRELIMINARY STUDIES

These studies were first undertaken to determine information concerning working and heat-treating responses of the materials for use in the statistical design of the more detailed process development study. The following four types of preliminary studies were conducted using Alloys A-2 and B:

1. Rollability - to establish approximate working conditions
2. Grain Growth - to establish rolling and heat treating parameters so that as-extruded bars could be processed to two desired grain sizes
3. Thermomechanical processing - to identify the most promising types of processing schedules as evaluated by tensile and stress-rupture tests

4. Room temperature deformation and aging - to evaluate the temperature for solutioning  $\gamma'$  (which also influences grain size), to determine the strengthening potential of room temperature rolling, and to evaluate various final ages

#### 4.2.1 Rollability

Approximately 2-inch (5-cm) sections from extruded bar of Alloys A-2 and B were rolled as indicated in Table VII. After each rolling pass, or in some instances after every other pass, samples were cut from the sections for possible metallographic and x-ray studies. Rolling of Alloy A-2 at 72°F (22°C) and 2000°F (1095°C) resulted in longitudinal cracks which appeared to be related to the oxide stringers. Alloy A-2 rolled well at 2200°F (1205°C) (Section No. 5 in Table VII); by rolling first at 2200°F (1205°C), it was then possible to roll at 2000°F (1095°C) without severe cracking (Section No. 7). However, with Section No. 8 of Alloy A-2, initial rolling at 2200°F (1205°C) did not permit subsequent rolling at 72°F (22°C) or 1850°F (1010°C). Alloy B rolled well at all temperatures which were investigated except 1900°F (1040°C).

Metallographic examination of rolled material revealed that considerable grain growth occurred at 2200°F (1205°C), and that small reductions per rolling pass resulted in a variation in grain size from the surface to the center of the bar. This did not present a problem for Alloy B, because this alloy could be rolled at 2000°F (1095°C). However, in order to roll Alloy A-2 without cracking, it was necessary to roll initially at a temperature sufficiently high to produce grain growth. Also, the grain structures that were developed in Alloy A-2 were strongly duplexed (Figure 10); thus, subsequent processing to a predetermined equiaxed grain size was very difficult.

Because of the difficulties encountered with flat rolling of Alloy A-2, rod rolling was investigated and subsequently adopted as the sole forming method. Rod rolling greatly enhanced the rollability of Alloys A-2 and B, and 10-percent reductions in diameter (~ 20-percent reduction in area) per pass were accomplished without difficulty at temperatures as low as 1900°F (1040°C); however, in order to prevent cracking during rolling it was necessary to clad the rods. Presumably, the cladding prevented rapid cooling of the alloys by the unheated rolls.

From these studies it was found that Alloy B could be processed without difficulties, even though it contained a 10-percent increase in  $\gamma'$  as compared to Rene' 95. However, the addition of ~ 1 v/o of  $\text{Al}_2\text{O}_3$  for Alloy A-2 reduced fabricability such that rod rolling was adopted as the forming method for the program.

#### 4.2.2 Processing to Desired Grain Size

The objectives of these studies were to determine rolling and heat-treating schedules so that as-extruded bar could be reduced to any predetermined size and heat treated to provide either a 5 or 20 $\mu\text{m}$  grain size. This



permitted various TMP schedules to be conducted subsequently with either of two starting microstructures and ending the TMP at section sizes that were matched to the various TMP schedules. Hence, material from all TMP schedules ended with about the same diameter rod. This approach conserved material and also eliminated the effects of section size during final heat treatments of the processed rods.

To accomplish the objectives, sections of extruded bar from Alloys A-2 and B were reduced in diameter 25 to 50 percent by rod rolling at 2050°F (1120°C), and this was followed by 25- to 30-percent reductions at 1900°F (1040°C) and 2000°F (1095°C). Small samples from the rolled metal were heat treated from 1 to 16 hours in the temperature range of 2000°F (1095°C) to 2200°F (1205°C).

The rolling schedule selected for the remaining preliminary studies (i.e., TMP and room-temperature rolling plus final age) involved various reductions at 2050°F (1120°C) followed by 25- to 30-percent reduction at 1950°F (1065°C); reductions in diameter per pass were about 10 percent at both temperatures. After this rolling schedule, a 5 $\mu$ m grain size was achieved in all section sizes without difficulty by heat treating at 2050°F (1120°C) for 2 hours. In the sections of larger diameter, a 20 $\mu$ m grain size was achieved in Alloys A-2 and B by heat treating at 2150°F (1175°C) for 2 hours. Exaggerated grain growth or secondary recrystallization occurred with the smaller section sizes of Alloy A-2 after heat treating at 2150°F (1175°C) for 1 hour; any increase in either temperature or time increased the degree of exaggerated grain growth. When exaggerated grain growth occurred, it was frequently observed that large portions of the microstructure had small grains of about 10 $\mu$ m (Figure 10). The reason for exaggerated grain growth in smaller (but not larger) section sizes could be due to the development of a texture during the additional processing. Alloy B exhibited a greater resistance to exaggerated grain growth than did Alloy A-2, because of the differences in their  $\gamma'$  solution temperatures (which were approximately 2100°F (1150°C) and 2150°F (1175°C) for Alloy A-2 and Alloy B, respectively).

Since the extruded bar was to be rolled various amounts prior to heat treating for the desired grain sizes, it was desirable to evaluate the effect on properties of additional rolling at 2050°F (1120°C). This was accomplished by conducting the processing schedules illustrated in Figure 11. Tensile data revealed that additional rod rolling at 2050°F (1120°C) reduced the yield strength by about 10 ksi (690 MN/m<sup>2</sup>), or 5 percent, and that Alloy B was stronger and more ductile than Alloy A-2. The reason for the reduction in tensile properties with additional rolling is thought to be as follows: during additional rolling at 2050°F (1120°C),  $\gamma'$  particles at grain boundary triple points increased in size as rolling was continued; then, during heat treating for solutioning of  $\gamma'$ , the volume fraction of  $\gamma'$  that was solutioned varied indirectly with the extent of rolling. Thus, less extensive rolling at 2050°F (1120°C) was associated with a larger volume fraction of small  $\gamma'$  particles and higher strengths.

To summarize, processing schedules were established that permitted processing as-extruded bar to a predetermined size with either a 5 or 20 $\mu$ m grain size. It was difficult to achieve 20 $\mu$ m grains in small-diameter rod without exaggerated grain growth; fortunately, 20 $\mu$ m grains were required primarily in larger-diameter rods. The effect on yield strength from variations in hot-rolling reductions was  $\leq 5$  percent, which was not considered serious, and was adopted for the program because it conserved material.

#### 4.2.3 Thermomechanical Processing

There were two objectives to the thermomechanical processing (TMP) studies: (1) achievement of an elongated grain structure with an L/d ratio of about 4, and (2) evaluation of the mechanical properties of material with a dislocation substructure formed by warm rolling.

Initial attempts to achieve elongated grain structures in Alloys A-2 and B, by rod rolling at 2200°F (1205°C) followed by rolling at 2000°F (1095°C), were unsuccessful because the metal recrystallized during rolling at 2000°F (1095°C). A second attempt was successful and involved the following processing schedule: rod rolling two passes each of 10-percent reduction in diameter at 2200°F (1205°C), followed by fourteen rolling passes of 5-percent reduction at 1900°F (1040°C). This processing schedule resulted in grains about 80 $\mu$  in length by about 20 $\mu$ m in diameter. Heat treatments were conducted to determine the maximum temperature to which the material could be heated for  $\gamma'$  solutioning without recrystallization. The results of these studies indicated that heating to any temperature above 1900°F (1040°C) initiated recrystallization at the grain boundaries. Thus, the temperature selected for heat treating the elongated grain structure was 1900°F (1040°C).

The second objective of the TMP studies was to evaluate tensile and stress rupture properties of material having a dislocation substructure produced by warm rolling. To accomplish this, the processing schedules given in Figure 12 were conducted. Tensile data indicated that warm rolling prior to  $\gamma'$  solutioning heat treatments (specimen conditions I, II, III, and V in Figure 12) was not as effective in increasing 1200°F (650°C) tensile properties as was warm rolling after the  $\gamma'$  solutioning heat treatment (specimen condition IV). However, creep-monitored stress rupture data revealed that the dislocation substructure was unstable and exhibited higher creep rates in specimen condition IV as compared to material without warm rolling or material that was solution treated after rolling (specimen conditions I, II, III, and V). Specimen condition V appeared to be the best in terms of a balance between tensile and stress rupture or creep and was one of the types of schedules selected for the statistical study.

In summary, a processing schedule was identified that resulted in material with an elongated grain shape; however, it was necessary to increase the grain size of the starting material from  $\sim 20$  to  $\sim 100\mu$ m. Various types of TMP schedules were identified which resulted in attractive tensile and stress-rupture properties and served the basis for selecting TMP schedules for the statistical study.

#### 4.2.4 Room Temperature Deformation Plus Age

The aging response studies consisted of two parts: (1) evaluation of heat treatments not involving room-temperature rolling, and (2) evaluation of heat treatments of material that had been rolled to a 27-percent reduction in area at 72°F (22°C) prior to aging.

In order to relate aging treatments to properties in the absence of room-temperature deformation, the processing schedules illustrated in Figure 13 were conducted. It was surprising to find that cooling rates resulting from oil quenching and air cooling had little effect on tensile properties of specimen conditions AI and AVI. The presolution treatment of 1650°F (900°C)/24 hours did not influence tensile properties (specimen conditions AII and AIII of Figure 13). As evaluated by tensile yield strength, the best combination of  $\gamma'$  and grain size in Alloy A-2 resulted from heat treating at 2100°F (1150°C) (specimen condition AV). However, as the strength was increased by higher  $\gamma'$  solution temperatures, the ductility was decreased. Increasing the  $\gamma'$  partial solution temperature from 2100°F (1150°C) to 2150°F (1175°C) resulted in an increase in grain size, such that (even with the strengthening offered by solutioning additional  $\gamma'$ ) the net effect was a reduction in tensile yield strength.

The large number of thread failures in the stress-rupture tests prevented an analysis of stress-rupture properties. The reason for the large number of thread failures was never completely resolved, but the difference between the specimen's thread root diameter and the gage diameter was quite small. It is also difficult to interpret the exceptionally good creep or stress-rupture properties exhibited by specimen condition AIV, when consideration is given to the corresponding tensile data. The only explanation offered is that nonuniform grain growth occurred, and perhaps the average grain size of the tensile and stress-rupture specimens was different.

The processing schedules for the evaluation of aging treatments plus room-temperature rolling are illustrated in Figure 14. The room-temperature rolling to a 27-percent reduction in area resulted in large increases in yield and tensile strengths, but caused cracks to form on the surfaces of the rolled rods. These cracks were responsible for the thread failures observed in tensile tests of this test series. The large rolling reductions would be expected to increase the density of unstable dislocations, which explains the high creep rates and relatively short stress-rupture lives shown in Figure 14. The results of these aging studies show that the conventional Rene' 95 age (specimen condition I) produced combined tensile and stress-rupture properties as good as or better than those of the three experimental ages.

Thus, in this preliminary study, the temperature range for the best balance between amount of  $\gamma'$  solutioned and grain size was established. Rolling at room temperature followed by a final age resulted in significant increases in strength; rolling an ~ 27-percent reduction in area was too severe as evidenced by cracking. The conventional final age used for Rene' 95 resulted in as good or better properties than the other aging treatments investigated.

#### 4.3 STATISTICAL PROCESS DEVELOPMENT STUDY

In the statistical process development study (SPDS) it was desired to investigate the following number of levels of four metallurgical factors:

<u>Factor</u>	<u>No. of Levels</u>
Alloy Composition	4
Solution Temp (affects grain size and $\gamma'$ morphology)	3
TMP Schedule	9
72°F (22°C) Deformation Plus Final Age	4

Due to the large number of variables involved, the experiment was designed to a 1/12th replicate of a 4.3.9.4 factorial experiment to reduce the number of test conditions required. The design was derived by combining the normal fractional replication technique with the random balance design proposed by Thomas Budne<sup>(3)</sup>. The 36 experimental conditions to be evaluated were set down by first constructing a  $\frac{1}{2} \cdot 4 \cdot 3 \cdot 4$  fractional replicate followed by filling in this design with the nine levels of TMP. Finally, the nine levels of TMP were balanced against the remaining factors according to the random balance concept. The advantages of this design were:

1. Complete confounding between any two factors was avoided. This allowed definition of the interaction between any two variables.
2. The one-twelfth replicate reduced the 432 combinations to a reasonable number for evaluation; i.e., 36.
3. Analysis of the data was easily conducted with the aid of a computer.
4. The pitfalls of multiple regression of completely random variables were avoided.

The levels of the four factors selected for evaluation were as follows:

1. Alloy Composition: A, A-1, A-2, and B
2. Grain Size or Temperature for Solutioning  $\gamma'$

Note:  $T_s$  = temperature for complete  $\gamma'$  solutioning; most of the  $\gamma'$  is solutioned at  $T_s - 50^\circ\text{F}$  ( $30^\circ\text{C}$ ). Time at temperature was either 2 or 3 hours.

	Temperature		
	T <sub>S</sub> -100°F (55 °C)	T <sub>S</sub> -50°F (30 °C)	T <sub>S</sub>
Alloys A, A-1, and A-2	2050°F (1120°C)	2100°F (1150°C)	2150°F (1175°C)
Alloy B	2100°F (1150°C)	2150°F (1175°C)	2200°F (1205°C)

	Approximate Grain Size (μ)		
	T <sub>S</sub> -100°F (55 °C)	T <sub>S</sub> -50°F (30 °C)	T <sub>S</sub>
Alloys A, A-1, and A-2	5	10	20
Alloy B	10	20	25

### 3. TMP Schedule

Specimen Condition	Warm Rolling Conditions			Postrolling Heat Treatment		
	RA (%)	Temp		Temp		Time (Hr)
		°F	°C	°F	°C	
I	Recrystallized	---	---	---	---	---
II	20	1800	980	1800	980	1
III	10	1900	1040	1900	1040	0.5
IV	20	1900	1040	1900	1040	0.5
V	75	1900	1040	1900	1040	0.5
VI	20	1900	1040	1950	1065	0.5
VII	40	1900	1040	1950	1065	1
VIII	20	1950	1065	1950	1065	0.5
IX	20	2000	1095	2000	1095	0.5

### 4. Plastic Deformation Plus Final Age

% Reduction in Area at 72°F (22°C)

0  
8

Final Age

- a. 1400°F (760°C)/16 hr/AC
- b. 1200°F (650°C)/6 hr/AC + 1400°F (760°C)/50 hr/AC

The statistical process development study is summarized in Table VIII. The order of selection of the variables during processing is illustrated in Figure 15. Some of the processing schedules were less complex than others because some of the levels of the factors were zero. The following two examples for Alloy A, illustrate the use of Table VIII:

Condition 1:\*

- a. Roll as-extruded bar of Alloy A at 2050°F (1120°C) to 2000°F (1095°C).
- b. Heat treat - 2050°F (1120°C)/3 hr/oil quench
- c. Age - 1400°F (760°C)/16 hr/AC

Condition 2:

- a. Roll as-extruded bar of Alloy A at 2050°F (1120°C) to 2000°F (1095°C).
- b. Heat treat - 2150°F (1175°C)/2 hr/oil quench
- c. Roll 20% RA at 1800°F (980°C)/reheat to 1800°F (980°C)/1 hr/oil quench
- d. Roll 8% RA at 72°F (22°C)
- e. Age - 1200°F (650°C)/6 hr/AC  
1400°F (760°C)/50 hr/AC

Data from 1200°F (650°C) tensile and 1200°F/150 ksi (650°C/1030 MN/m<sup>2</sup>) for the 36 conditions of Table VIII are reported in Table IX. Note that six of the specimen conditions exhibited 0.2 percent yield stresses in excess of 200 ksi (1380 MN/m<sup>2</sup>). The average yield stress for specimen conditions 5, 10, and 23 was 215 ksi (1480 MN/m<sup>2</sup>), which is an increase of 40 to 45 ksi (275 to 310 MN/m<sup>2</sup>) over recrystallized material; e.g., specimen condition 1.

#### 4.3.1 Data Analyses

The data from the statistical process development study were analyzed independently by two methods: (1) a statistical analysis using a computer, and (2) an empirical metallurgical evaluation where "best data" were correlated to process variables.

The statistical analysis was conducted by E.L. Dunn of General Electric using the following regression model:

(See next page)

---

\*Initial processing was always conducted by rod rolling at 2050°F (1120°C) followed by 25 to 30 percent reduction in area at 1950°F (1065°C) to 2000°F (1095°C). In order to conserve material and economically produce rod of equal final diameter for all processing schedules, the amount of reduction at 2050°F (1120°C) was varied.

$$Y = \sum A_m X_m$$

In this study:

$Y = 1200^\circ\text{F}$  ( $650^\circ\text{C}$ ) tensile yield strength

or  $1200^\circ\text{F}$  ( $650^\circ\text{C}$ ) tensile elongation

or  $1200^\circ\text{F}$  ( $650^\circ\text{C}$ ) tensile reduction of area

or  $1200^\circ\text{F}/150 \text{ ksi}$  ( $650^\circ\text{C}/1030 \text{ MN/m}^2$ ) rupture life

$X_m$  = Presence of a TMP, an alloy, a room-temperature reduction, an age, or a solution temperature

$A_m$  = Fitted coefficients

The mechanics of the solution consisted of the following steps: (1) set up an equation for each data point (fit  $Y$  and  $X_m$  values in Model  $Y = \sum A_m X_m$ ); (2) assume difference between right- and left-hand sides of equation is error; i.e.,  $Y - \sum A_m X_m = \text{error}$ , and (3) by use of matrix algebra, solve the above equations to minimize  $(Y - \sum A_m X_m)^2$ .

The results of this statistical analysis are summarized in Table X, in which the level of the factors is listed in order of decreasing desirability. When levels are listed within parentheses or as "balance", this indicates that little or no distinguishable difference existed between these levels. These results can be summarized as follows: (1) Alloys A and B (without oxides) exhibited tensile and stress-rupture properties which were equal or better than those of Alloys A-1 and A-2 (with oxides); (2) of the three  $\gamma'$  solution temperatures investigated,  $T_s - 100^\circ\text{F}$  ( $55^\circ\text{C}$ ) resulted in the best balance between quantity of  $\gamma'$  solutioned and grain size; additional analyses indicated that  $T_s - 65^\circ\text{F}$  ( $36^\circ\text{C}$ ) would optimize stress-rupture properties; (3) TMP condition V was significantly different from the remaining TMP conditions and exhibited the most attractive tensile properties but the highest creep rate during the stress-rupture tests; (4) room-temperature deformation of 8% RA increased the yield stress but lowered stress-rupture properties; and, (5) final age (a) -  $1400^\circ\text{F}$  ( $760^\circ\text{C}$ )/16 hr/AC - resulted in better tensile and stress-rupture properties than did final age (b) -  $1200^\circ\text{F}$  ( $650^\circ\text{C}$ )/6 hr/AC +  $1400^\circ\text{F}$  ( $760^\circ\text{C}$ )/50 hr/AC. The observed interactions between TMP's I, II, and III with alloy composition, and between room-temperature deformation and final age (b), are not completely understood metallurgically, which is sometimes the outcome of a statistical analysis. It was decided to eliminate from further consideration levels of the factors that exhibited interactions causing decreased mechanical properties, because they also correlated to poorer properties even in the absence of interactions.

Analysis of the process development study through empirical metallurgical considerations of "best data" resulted in good agreement with the statistical analysis; therefore, discussion of this second analysis will be brief except where differences were observed. As for alloy composition, there

appeared to be a slight strength advantage with Alloy B and a slight ductility advantage with Alloy A. Oxides were not beneficial, and processing factors were much more strength determining than were alloy variations. Of the three solution temperatures investigated,  $T_S$ -100°F (55°C) resulted in the best combination of grain size and volume fraction of  $\gamma'$  solutioned, as judged by tensile and stress-rupture properties. Mechanical working [i.e., TMP or 72°F (22°C) deformation] increased the dislocation density, which improved tensile properties but increased the creep rates. A combination of TMP followed by 72°F (22°C) deformation (conditions 14 and 31) offered no advantage over either TMP (condition 5) or 72°F (22°C) deformation (condition 28) used singularly.

#### 4.3.2 Selection of Four Best Alloy/Process Combinations

The experimental plan was: (1) to determine the four best combinations of alloy and process as revealed by the analysis of the SPDS; (2) to conduct screening tests; and, (3) select two of the four materials for a more detailed evaluation. Accordingly, the four best alloy/process combinations for the screening tests were established and are given in Table XI. These four alloy/process combinations, and the materials processed according to them, were designated as S-1, S-2, S-3, and S-4. Materials S-1 and S-4 were Alloy A, and S-2 and S-3 were Alloy B. The designation of process variables (e.g., solution temperature, TMP, percent reduction in area, and final age) correspond to particular levels of factors evaluated in the SPDS. The subscript (M) for the TMP factor indicates that slight modifications were made as follows:

- S-1: (a) addition of a heat treatment of 24 hrs at 1650°F (900°C)
- S-2: (a) addition of a heat treatment of 24 hrs at 1650°F (900°C)  
(b) decrease in the reduction in area during TMP from 40 to 35 percent, so as to reduce the tendency for recrystallization during the postrolling heat treatment
- S-3: (a) addition of a heat treatment of 24 hrs at 1650°F (900°C)  
(b) omission of the post-TMP heat treatment: material was quenched directly from the rolls to improve the  $\gamma'$  morphology and to reduce recrystallization.
- S-4: (a) addition of a heat treatment of 24 hrs at 1650°F (900°C)

There were two reasons for the addition of the 24-hour heat treatment at 1650°F (900°C):

- (1) prior data indicate it improves creep strength<sup>(1)</sup>, and
- (2) it appeared that a higher combination of tensile and creep strength was achieved in the preliminary studies of the present work - where this treatment was used - than in the SPDS where this heat treatment was not used. The actual effects and mechanisms involved with this heat treatment are not completely understood.



To obtain material for the remainder of the test program, sufficient extruded bar stock was processed to provide ~ 35 feet (10m) of 0.35-inch (0.9 cm) diameter rod for each of the four alloy/process combinations according to the schedules illustrated in Figure 16.

Tensile screening tests at 72°F (22°C) and 1200°F (650°C) were conducted with these four materials in the as-processed conditions and after 100 hours of exposure at 1400°F (760°C). These data are given in Table XII and illustrate: (1) that excellent tensile properties were achieved, and (2) that the effect of thermal exposure was to reduce the yield strength by about 5 percent with only small reductions in ductility.

Stress-rupture tests were conducted at 1000°F (540°C) and 1200°F (650°C) for these four materials only in the as-processed condition. From the results of these tests (shown in Table XIII), it was observed that the stress-rupture or creep properties were very good at 1000°F (540°C) but decreased considerably at 1200°F (650°C). The behavior of S-3 was somewhat unexpected; i.e., it exhibited the shortest time to reach 0.2 percent creep at 1000°F/160 ksi (540°C/1100 MN/m<sup>2</sup>) but the longest stress-rupture life at 1200°F/150 ksi (650°C/1030 MN/m<sup>2</sup>). From these data, it was interpreted that S-3 had a high and extensive primary creep rate but a low secondary creep rate. In general, the stress-rupture or creep properties varied inversely with tensile strength, as was observed in the preliminary studies.

Materials S-1 and S-3 were finally selected for more extensive evaluation for the following reasons:

1. Tensile properties of S-1 and S-3 exceeded those of S-2 and S-4; S-1 and S-3 also surpassed the minimum tensile goals of the program.
2. Data from creep-monitored stress-rupture tests indicated that S-1 and S-3 had sufficient creep properties at 1000°F/160 ksi (540°C/1100 MN/m<sup>2</sup>) to meet the long-range creep goals of the program at 1000°F (540°C). Also, it was anticipated that S-3 had a high primary creep rate, but a low secondary creep rate. If the high primary creep rate was associated only with the first loading cycle, this initial deformation could be accommodated in jet engines by design.
3. Fracture resistance data were nonexistent for the four screening test materials, but the elongated grain shape of S-1 made this material of special interest for fracture-resistance evaluation.

#### 4.3.3 Processing of Additional Material

After it was established that materials S-1 and S-3 were to be further evaluated, it was necessary to process additional material for fracture-toughness testing because of the larger specimen size required; i.e., 0.5-inch (1.3-cm) diameter rod was required as compared to the 0.35-inch (0.9-cm)

diameter rod used in tensile and creep testing. Accordingly, extruded bars of Alloys A and B were processed to obtain additional 0.5-inch (1.3-cm) diameter S-1 and S-3 material. In an attempt to achieve the same microstructure in the two different diameter rods, the amount of initial hot rolling at 2050°F (1120°C) was varied. With the exception of this variation in hot rolling, the processing schedules were the same for the two different diameter rods for each of S-1 and S-3. The influence of this variation in hot rolling was determined by tensile tests conducted with specimens from both the 0.35-inch (0.9-cm) and 0.5-inch (1.3-cm) diameter rods. The results from these tensile tests (Table XIV) revealed that the yield stresses of the 0.5-inch (1.3-cm) diameter rods were about 2 percent lower than the 0.35-inch (0.9-cm) diameter rods.

#### 4.4 EVALUATION OF TWO BEST ALLOY/PROCESS COMBINATIONS

Materials S-1 and S-3 were evaluated by tensile, creep, and fracture-resistance testing. Tensile testing included notched and unnotched tests for S-1 and S-3 in the as-processed condition and after various thermal exposures. Creep testing was conducted only with as-processed material, but fracture-resistance testing was conducted with S-1 and S-3 before and after thermal exposure. Drawings of the specimens and a discussion of the test procedures are given in the Appendix. In addition to the mechanical testing, material conditions S-1 and S-3 were evaluated by metallography and phase analysis to determine the microstructural effects of long-time exposure at elevated temperature. Also, material conditions S-1, S-2, S-3, and S-4 were evaluated by replication and transmission electron microscopy.

##### 4.4.1 Tensile Test Results

Unnotched tensile tests of as-processed 0.35-inch (0.9-cm) diameter rod were conducted over the 72°F (22°C) to 2000°F (1095°C) temperature range for the S-1 and S-3 material conditions. The data from these tests are given in Table XV, and the yield strengths and ductilities are compared to cast-and-forged Rene' 95 in Figure 17. The influence of temperature on the 0.2 percent yield stresses of S-1 and S-3 were typical of wrought nickel-base superalloys in that: (1) the strength decreased rapidly in the temperature range of 1300°F (705°C) to 1600°F (870°C), and (2) the change in strength in the temperature range of 800°F (425°C) to 1200°F (650°C) was slight. S-1 exhibited the greatest improvement in yield strength and was about 45 ksi (310 MN/m<sup>2</sup>) stronger than Rene' 95. The change in ductility with temperature for the two materials was different (Figure 17); this is thought to be related to the large elongated grain structure of S-1 as compared to the small equiaxed grains of S-3. In 1200°F (650°C) tensile tests, the fracture of S-1 was predominantly by transgranular shear; in S-3, fracture often initiated in the center of the specimen by a mixture of intergranular and transgranular crack propagation in a plane perpendicular to the tensile axis, and final failure occurred by propagation of the crack to the surface by transgranular shear. The observed fracture modes in S-1 and S-3 are both typical of tensile fracture in round test bars of ductile materials.

Unnotched tensile tests were also conducted at 72°F (22°C) and 1200°F (650°C) for S-1 and S-3 after thermal exposure at 1200°F (650°C) and 1400°F (760°C) for 1500 hours; data are given in Table XVI and compared to unexposed S-1 and S-3 in Figure 18. The data for 1200°F (650°C) exposure were within experimental scatter of data for unexposed material (exposed S-1 was slightly higher in strength) and, therefore, reveal that this thermal exposure had no noticeable effect on tensile properties. However, the exposure at 1400°F (760°C) for 1500 hours reduced the 1200°F (650°C) tensile yield stresses of S-1 and S-3 by 16.3 and 13.2 percent, respectively.

Notched tensile tests were also conducted at 72°F (22°C) and 1200°F (650°C) for unexposed S-1 and S-3 and at 1200°F (650°C) after exposure at 1400°F (760°C) for 1500 hours (Table XVII). These notched specimens had a stress concentration of  $K_t = 3.5$ . The ratios of the notched strength to the ultimate tensile strength for unexposed S-1 and S-3 were 1.2 and 1.1, respectively; therefore, these materials were not notch sensitive. The effect of the thermal exposure at 1400°F (760°C) was to reduce the notch strength for S-1 and S-3 by 3.7 and 6.1 percent, respectively. However, the ratios of the notched strength to the ultimate tensile strength for exposed S-1 and S-3 were 1.3 and 1.2, respectively, and therefore were also not notch sensitive.

#### 4.4.2 Creep Test Results

A total of 30 creep tests was conducted for material conditions S-1 and S-3 in the temperature range of 1000°F (540°C) to 1400°F (760°C). The results from these tests are given in Table XVIII and are compared to Rene' 95 in Figure 19. The creep strengths of S-1 and S-3 were similar at 1000°F (540°C) and 1400°F (760°C); but, at intermediate temperatures, S-3 was somewhat more creep resistant than S-1. At high levels of stress and at lower Larson-Miller parameters, material conditions S-1 and S-3 exhibited creep properties superior to cast-and-forged Rene' 95. However, above a test temperature of about 1000°F (540°C), Rene' 95 has a creep strength superior to S-1 and S-3.

#### 4.4.3 Fracture Resistance

Fracture-resistance testing in this study consisted of both slow-bend tests of precracked Charpy bars (SBPC) and  $\hat{K}^*$  testing as described in the Appendix. Both tests employed the conventional vee-notched Charpy bars, except that the specimen used in  $\hat{K}^*$  testing was increased to 5 inches (12.7 cm) in length. In both tests, a fatigue crack was first initiated and then propagated at progressively-decreasing stress-intensity factors in order to provide a sharp crack tip. The SBPC test was used to measure the energy required for fracture, and  $\hat{K}^*$  was taken as a measure of the threshold stress-intensity range required for Mode I (which is the opening mode as contrasted to a shearing or tearing mode) crack propagation. The energy measured in the SBPC tests was designated as  $W_{\mu}/A$  and was that energy required for crack instability.  $\hat{K}^*$  is a measure of the materials resistance to crack propagation under cyclic loading.

SBPC tests were conducted at 1000°F (540°C) and 1200°F (650°C) for as-processed S-1 and S-3 material conditions and at 1200°F (650°C) for S-1 and S-3 exposed at 1200°F (650°C) for 1500 hours. These data are compared to cast-and-forged Rene' 95 in Table XIX and show that S-1 and S-3 have lower SBPC fracture energies than Rene' 95. This is not too surprising considering the higher yield strengths of S-1 and S-3 as compared to Rene' 95 (Figure 17). The fact that S-1 had both a higher yield stress and fracture energy than S-3 was attributed to the elongated grain shape in the former. The variation in fracture energies between 1000°F (540°C) and 1200°F (650°C) was within the data scatter band of these tests for both S-1 and S-3. Aging at 1200°F (650°C) for 1500 hours resulted in a large reduction in the fracture energy; i.e., the fracture energy in S-1 was reduced by a factor of two.

The data for material conditions S-1 and S-3 tested at 1000°F (540°C) to determine  $\hat{K}^*$  are given in Figure 20. The value of  $\hat{K}^*$  for both materials was  $9.5 \pm 1$  ksi  $\sqrt{\text{in.}}$  ( $10.5 \text{ MNm}^{-3/2}$ ), which is approximately the same as observed with conventional Rene' 95. These data indicate that  $\hat{K}^*$  was not strongly influenced by grain shape or yield stress.

#### 4.4.4 Light Microscopy

Photomicrographs of the four best alloy/process combinations (i.e., S-1, S-2, S-3, and S-4) are given in Figure 21. These show that S-1 had an elongated grain shape with a L/D ratio of about 5 and a uniform distribution of coarse  $\gamma'$ . The microstructures of S-2, S-3, and S-4 were similar to each other in that they exhibited a  $\gamma$  grain size of about  $5\mu\text{m}$  with particles of  $\gamma'$  approximately  $2\mu\text{m}$  in diameter, which were located at  $\gamma$  grain boundaries. These  $\gamma'$  particles were formed during recrystallization of the metal below the solvus. The grain shape of S-2 and S-4 appeared equiaxed; S-3 had slightly elongated grains. In all four of these materials, fine  $\gamma'$  was present which was too small to be resolved by light microscopy.

The microstructures of S-1 and S-3 were also studied by light microscopy after various thermal exposures; but, due to magnification limitations, it was not possible to determine the effects of exposure on microstructures. Thus, in order to study the smaller  $\gamma'$  particles and the effects of thermal exposure, replication electron microscopy studies were conducted.

#### 4.4.5 Replication Electron Microscopy Evaluations

The four best alloy/process combinations (i.e., S-1, S-2, S-3, and S-4) were studied by replication electron microscopy in the as-processed condition and after various thermal exposures. Electron micrographs of these four materials in the as-processed condition are illustrated in Figure 22, and reveal that the size and distribution of the  $\gamma'$  was different for each of the four material conditions. The observed  $\gamma'$  sizes and distributions will subsequently be related to the thermomechanical processing schedules used in processing these materials. The extruded bars were first processed to similar microstructures, which served as the starting condition for the processing schedules that were conducted with the four best alloy/process combinations.

This initial microstructure exhibited  $\gamma$  grains of about  $5\mu\text{m}$  with particles of  $\gamma'$  of about  $2\mu\text{m}$  at  $\gamma$  grain boundaries. The  $\gamma$  grains also contained fine intra-granular  $\gamma'$  precipitate. The processing of this initial structure to form the four material conditions is summarized in Figure 16.

In material condition S-1, two distinct sizes of  $\gamma'$  were formed, as observed in the electron micrograph of Figure 22a. About 30 percent of the observed  $\gamma'$  volume fraction was  $\leq 0.1\mu\text{m}$  and the remaining 70 percent was  $\sim 0.3\mu\text{m}$ . A uniform dispersion of MC carbides of about  $1\mu\text{m}$  diameter was also observed in S-1 as well as in materials S-2, S-3, and S-4. The observed  $\gamma'$  morphologies for S-1 will now be discussed in terms of the processing schedule for this material (Figure 16). The initial heat treatment solutioned all of the  $\gamma'$  and increased the  $\gamma$  grain size to about  $200\mu\text{m}$ . During quenching from this solution treatment, a general precipitation of background  $\gamma'$  occurred, and the heat treatment of  $1650^\circ\text{F}$  ( $900^\circ\text{C}$ ) for 24 hours resulted in a general coarsening of  $\gamma'$ . During rolling at  $1900^\circ\text{F}$  ( $1040^\circ\text{C}$ ), some of the  $\gamma'$  was solutioned, and the remaining  $\gamma'$  would be expected to increase in size. The postrolling heat treatment at  $1900^\circ\text{F}$  ( $1040^\circ\text{C}$ ) would be expected to result in some coarsening to the  $\gamma'$ ; some recrystallization appeared to occur at the grain boundaries which had the effect of increasing the spacings among the  $\gamma'$  particles. During quenching, that portion of  $\gamma'$  that was solutioned at  $1900^\circ\text{F}$  ( $1040^\circ\text{C}$ ) was probably retained in solution and was then precipitated during the aging heat treatment at  $1400^\circ\text{F}$  ( $760^\circ\text{C}$ ) for 16 hours.

The electron micrograph in Figure 22b reveals the  $\gamma'$  morphologies observed in material S-2. The  $\gamma'$  was present as four different particle sizes. Qualitatively, the percentage of the total  $\gamma'$  volume fraction, and the approximate size for each of these particles, was as follows: (1) 20% of  $\leq 0.1\mu$  (2) 40% of  $0.3\mu\text{m}$ , (3) 15% of  $1\mu\text{m}$ , and (4) 25% of  $\geq 2\mu\text{m}$ . These different  $\gamma'$  sizes will now be related to the processing of S-2 (Figure 16). The initial heat treatment did not solution all of the  $\gamma'$ , the unsolutioned  $\gamma'$  are the largest particles in the electron micrograph (Figure 22b). During cooling from this partial  $\gamma'$  solution treatment,  $\gamma'$  would precipitate and subsequently would be coarsened both by the  $1650^\circ\text{F}$  ( $900^\circ\text{C}$ )/24-hour heat treatment and during rolling at  $1900^\circ\text{F}$  ( $1040^\circ\text{C}$ ). The diameter of this  $\gamma'$  was about  $0.3\mu\text{m}$  and was the third largest in the electron micrograph. During the second rolling pass and the postrolling heat treatment, partial recrystallization is thought to have occurred which would form the second largest of the observed  $\gamma'$  particle sizes. Quenching from the postrolling heat treatment supersaturated  $\gamma$  with  $\gamma'$ , and fine  $\gamma'$  precipitated during the  $1400^\circ\text{F}$  ( $760^\circ\text{C}$ )/16-hour heat treatment.

There were three  $\gamma'$  particle sizes in material S-3 (Figure 22c); and, of the observed  $\gamma'$  volume fraction, 20% was  $\leq 0.1\mu$ , 60% was  $\sim 0.3\mu\text{m}$ ; and, 20% was  $\geq 2\mu\text{m}$ . These observations will now be related to the processing of material S-3 (Figure 16). Initially, a presolution heat treatment of  $1650^\circ\text{F}$  ( $900^\circ\text{C}$ )/24

hours was employed. The microstructural effects of this heat treatment are not understood, but there is evidence that it improves the creep strength of Rene' 95 when followed by a partial solution treatment 2000°F (1095°C)/1 hr/AC and aging at 1100°F (590°C)/64 hrs + 1350°F (730°C)/64 hrs<sup>(1)</sup>. In the processing of S-3, it is thought that this heat treatment coarsened the finer  $\gamma'$ , which was then solutioned during the subsequent heat treatment at 2100°F (1150°C). The largest  $\gamma'$  particles in Figure 22c were not solutioned; and, during cooling from this  $\gamma'$  solutioning temperature, fine  $\gamma'$  was probably precipitated. During the prerolling heat treatment, the intermediate  $\gamma'$  particle size was formed. The material was quenched directly from the rolls which supersaturated the matrix with  $\gamma'$ . The smallest  $\gamma'$  particles were then precipitated during the 1400°F (760°C)/16-hour heat treatment. Note that  $\gamma$  zones void of the intermediate size  $\gamma'$  were formed during the prerolling heat treatment, because of the driving force for small precipitate particles to be solutioned and reprecipitated on larger particles.

In material S-4, two  $\gamma'$  sizes were observed (Figure 22d); of these, 75 percent were  $\leq 0.1\mu\text{m}$  and 25 percent were  $\geq 2\mu\text{m}$ . In the processing of S-4, the presolution heat treatment of 1650°F (900°C)/24 hours was also used; [the effects of which are thought to have been eliminated by the subsequent partial solutioning heat treatment at 2050°F (1120°C)]. Complete  $\gamma'$  solutioning did not occur at 2050°F (1120°C), and the large isolated  $\gamma'$  particles remained. Quenching from 2050°F (1120°C), followed by heat treating at 1400°F (760°C)/16 hours, formed the fine  $\gamma'$  particles.

In summary, the four best alloy/process combinations were observed to exhibit different  $\gamma'$  morphologies; these observations are given qualitatively below:

Material Condition	Percent of $\gamma'$ at indicated size (approx)			
	$\leq 0.1\mu\text{m}$	$0.3\mu\text{m}$	$1\mu\text{m}$	$\geq 2\mu\text{m}$
S-1	30	70	---	---
S-2	20	40	15	25
S-3	20	60	---	20
S-4	75	---	---	25

Materials S-1 and S-3 were also studied after thermal exposures at 1200°F (650°C) for 1500 hours and at 1400°F (760°C) for 100 and 1500 hours. The effects of these thermal exposures on the as-processed microstructures of S-1 and S-3 are illustrated in Figures 23 and 24, respectively.

Exposing S-1 at either 1200°F (650°C) for 1500 hours, or at 1400°F (760°C) for 100 hours, resulted in a slight coarsening of the smaller  $\gamma'$  particles. Increasing the severity of the exposure to 1500 hours at 1400°F (760°C) increased the size of both  $\gamma'$  particle sizes and resulted in the formation of  $\text{M}_{23}\text{C}_6$ .

Exposing S-3 either at 1200°F (650°C) for 1500 hours, or at 1400°F (760°C) for 100 hours, also resulted in a slight coarsening of the finest  $\gamma'$  particles. Exposure at 1400°F (760°C) for 1500 hours resulted in: (1) a coarsening of the smallest  $\gamma'$  particles, (2) elimination of the denuded zones around the largest  $\gamma'$  particles, (3) formation of  $M_{23}C_6$ , and (4) the apparent precipitation of an undetermined phase within the larger  $\gamma'$  particles. X-ray analyses (to be discussed in Section 4.4.7) indicated that sigma formed in both S-1 and S-3 after thermal exposure at 1400°F (760°C) for 1500 hours. However, platelets of sigma were not observed by electron microscopy.

#### 4.4.6 Transmission Electron Microscopy Evaluations

Thin foils of material conditions S-1, S-2, S-3, and S-4 were studied by transmission electron microscopy. For purposes of comparison, a foil of Alloy A in the recrystallized condition was also included in this study (material condition 1 of Tables VIII and IX). Selected electron micrographs of these materials are illustrated in Figure 25 for the recrystallized condition and in Figure 26 for the four best alloy/process combinations. Although many additional features were observed, these electron micrographs represent the primary observations.

As expected, the recrystallized condition exhibited a low dislocation density (Figure 25). A portion of four grains is shown in the micrograph of this material. There was evidence of  $\gamma'$  in three of these grains;  $\gamma'$  is not always observed due to the high degree of coherency. It was also observed that the grain boundaries were very clean, i.e., free of precipitates.

During processing of materials S-1, S-2, S-3, and S-4, the dislocation density was much higher than the recrystallized material; however, the grain boundaries exhibited a low density of precipitate for all material conditions. This observation is in contrast to the presence of carbide precipitates frequently observed at grain boundaries in wrought nickel-base superalloys.

Large areas of S-1 exhibited subgrains of about 0.5 $\mu$ m (Figure 26a). Some of these subgrains had boundaries that were dislocation tangles, whereas others were similar to high-angle grain boundaries; these observations indicate that considerable rearrangement or polygonization of the substructure occurred during the 16 rolling passes which were conducted at 1900°F (1040°C). During this extensive rolling, it is possible that subgrains formed, increased in size, and reformed again. A limited number of recrystallized regions existed in S-1, as supported by the observation that regions in the substructure were free of dislocations.

A very common observation in S-2 was a relatively large grain, about 2 $\mu$ m, growing into a region of subgrains that had an average size of about 0.25 $\mu$ m. This observation agrees well with the observations made by replication electron microscopy that considerable recrystallization had occurred during the second rolling pass at 1900°F (1040°C) and during the postrolling heat treatment.

Nearly all of the substructure in S-3 consisted of about  $0.2\mu\text{m}$  diameter subgrains. These had extensive dislocation tangles at their boundaries and are thought to have formed during rolling at  $1900^{\circ}\text{F}$  ( $1040^{\circ}\text{C}$ ). Material S-3 exhibited the highest dislocation density of the materials investigated and had very few regions that were dislocation free.

Material S-4 exhibited the greatest variations in substructure and contained regions of both high- and low-dislocation density. The dislocations were present as tangles or networks, and only a limited number of cells or subgrains were observed. The regions of low-dislocation density are assumed to be due to nonuniform deformation, rather than to recrystallization; because, the dislocations were formed in S-4 by processing at room temperature and the highest postrolling thermal exposure was  $1400^{\circ}\text{F}$  ( $760^{\circ}\text{C}$ ).

#### 4.4.7 Phase Analysis Results

Phase analysis determinations were conducted by x-ray diffraction using material conditions S-1 (Alloy A) and S-3 (Alloy B) in the as-processed condition and after various thermal exposures. Based on the chemistry of the alloys and past experience, it was evident that  $\gamma'$  precipitate,  $\text{Ni}_3(\text{Al}, \text{Ti}, \text{Cb})$ , was present in a  $\gamma$  matrix. Both are solid solution strengthened by the various alloying elements. In preparation for phase analysis, portions of S-1 and S-3 were dissolved electrolytically in a solution of 100 ml HCl and 900 ml  $\text{CH}_3\text{OH}$ . The  $\gamma$  and  $\gamma'$  were dissolved, and the carbides and borides settled out as sludge which was collected by filtration. This sludge was then scanned by x-ray diffraction through  $2\theta$  to  $160$  degrees  $2\theta$ .

The results, summarized in Table XX, revealed that the phases present in as-processed S-1 and S-3 were very similar and that new phases were formed during thermal exposure. The probable compositions of the phases are also given in Table XX. Excluding  $\gamma'$ , the most abundant second phase in the as-processed materials was MC carbides.  $\text{M}_6\text{B}_2$  was also present in very small amounts but was not always detected.

The most abundant new phase that formed during exposure was  $\text{M}_{23}\text{C}_6$ . Exposure at  $1200^{\circ}\text{F}$  ( $650^{\circ}\text{C}$ ) for 1500 hours was sufficient to form small amounts of  $\text{M}_{23}\text{C}_6$ ; increasing the severity of the exposure to  $1400^{\circ}\text{F}$  ( $760^{\circ}\text{C}$ ) for 1000 and 1500 hours resulted in considerable amounts of  $\text{M}_{23}\text{C}_6$ . The exposure at  $1400^{\circ}\text{F}$  ( $760^{\circ}\text{C}$ ) for 1500 hours caused small amounts of sigma to form. This phase was not observed after the less severe exposures. There was an indication that  $\text{M}_6\text{C}$  may have formed in S-1 after exposure at  $1400^{\circ}\text{F}$  ( $760^{\circ}\text{C}$ ) for 1500 hours; but, if present, it was in very small amounts.



## 5.0 DISCUSSION

The four factors studied in this investigation were alloy chemistry, grain size, TMP, and 72° F (22° C) deformation plus final age. It was shown that a slight improvement in strength could be achieved by a 10-percent increase in the  $\gamma'$  volume fraction as was done with Alloy B. However, this chemical modification to Rene' 95 had a much smaller effect than did the variations in microstructure achieved by processing. The influence of oxides on tensile and stress-rupture properties was not significant, and the desired goal of  $\gamma$  grain growth prevention by oxides during solutioning treatments was not achieved. This observation was in contrast to earlier studies of consolidated powder of Rene' 77, in which oxides did inhibit grain growth<sup>(4,5)</sup>. However, it is significant to note that excellent properties were observed with oxide bearing material (i.e., Alloys A-1 and A-2). The point is that an improvement in properties was not observed; and, therefore, there exists no justification at present for their use.

The effects of the remaining three factors (grain size, TMP, and cold work plus age) can best be discussed in terms of grain size, dislocations (both density and arrangement or substructure), and  $\gamma'$  size and distribution. For a given superalloy chemistry, the mechanical properties are strongly influenced by these three factors. Qualitatively, for 1000°F (540°C) to 1400°F (760°C) applications, the following microstructure is envisioned to exhibit the best properties: (1) a grain size of  $\sim 5\mu\text{m}$ , and preferably with an elongated grain shape aligned in the direction of maximum tensile stress; (2) a dislocation substructure; and (3) a large volume fraction of very fine  $\gamma'$  (i.e.,  $\sim 0.05\mu$ ).

In this study, elongated grain shapes were achieved in material S-1, but this required a substantial increase in grain size to  $> 100\mu\text{m}$ . Also, during the numerous rolling passes required to achieve the elongated grain shape, much of the  $\gamma'$  was severely coarsened. Thus, much of the strength of S-1 was derived from the dislocation substructure, which proved to be unstable in creep at elevated temperatures. Therefore, the tensile strength and ductility were excellent, but creep properties were adversely affected due to the high density of unstable dislocations and the coarse  $\gamma'$ . The elongated grain shape of S-1 was beneficial to the slow-bend Charpy fracture energy but did not have a significant effect on  $\hat{K}^*$ .

In material condition S-2, two rolling passes at 1900°F (1040°C) were used to increase the dislocation density, and a postrolling heat treatment was employed in an attempt to stabilize the dislocations. The latter heat treatment resulted in partial recrystallization and, therefore, reduced the strengthening contribution from dislocations. The postrolling heat treatment increased the volume fraction of fine  $\gamma'$ ; however, most of the total volume fraction of  $\gamma'$  particles were relatively large and reduced the  $\gamma'$  strengthening effect. The grain size of material S-2 was favorable, but the grains were not elongated. This material condition had the lowest tensile strength; but, based on the results of creep-monitored stress-rupture tests (Table XIII), S-2 exhibited the best creep properties of the four material conditions.

Material condition S-3 was given one rolling pass at 1950°F (1065°C) for increasing the dislocation density, followed by quenching directly out of the rolls. This treatment resulted in a high density of unstable dislocations. The high-temperature exposure of this rolling schedule coarsened much of the  $\gamma'$ , and only a small fraction of the total  $\gamma'$  volume fraction was present as fine  $\gamma'$ . The grain size was favorable at about 5 $\mu$ m, but these grains were not elongated. This material had excellent tensile properties, but the high density of unstable dislocations and the small volume fraction of fine  $\gamma'$  adversely influenced creep. The slow-bend Charpy fracture energy was decreased in proportion to the increase in yield stress. The  $K^*$  of S-3 was not influenced by this variation in yield stress.

Material S-4 had the proper balance between grain size and volume fraction of fine  $\gamma'$ , because the dislocations were produced by room-temperature deformation. However, the dislocations were unstable because the 1400°F (760°C) age was the highest temperature that the metal was heated to after the room-temperature deformation.

Thus, in no instance in the present study, was the optimum-envisioned microstructure achieved. It was demonstrated that large variations in properties can be achieved in a given alloy chemistry by processing. Processing schedules were identified that resulted in simultaneous increases in both tensile and creep properties at temperatures up to 1000°F (540°C).

The minimum 0.2 percent yield stress goal of the program [200 ksi (1380 MN/m<sup>2</sup>) at 1200°F (650°C)] was exceeded by about 10 percent, but the goal of 98 percent retention of the as-processed strength after exposure at 1400°F (760°C) for 100 hours was not achieved; rather, about 94 percent of this strength was retained. It appears that such reductions in strength from extended exposures at 1400°F (760°C) are inevitable in these alloy systems due to coarsening of the fine  $\gamma'$ .

The primary deficiency of the high-strength materials developed in this program was their poor creep strength at temperatures above 1000°F (540°C). The most substantial increase in strength over the recrystallized condition resulted from increases in the dislocation density. These dislocations proved to be unstable during creep tests at elevated temperatures; thus, tensile and creep strengths varied inversely. For further improvements in disc alloys, future work should be directed toward stabilization of dislocations. Approaches that might be taken to stabilize dislocations and improve creep strength are:

1. Process consolidated powder of an alloy containing a fine incoherent second phase; perhaps a second phase smaller, and with a more uniform distribution, than the oxides investigated in this program would be beneficial. Alternately, precipitation of a phase from solid solution onto dislocations could improve creep and should therefore be considered.

2. Process by either forging or flat rolling, both of which require less time for working the metal as compared to rod rolling, which was used in this program. The resulting shorter time at elevated temperatures will reduce the degree of  $\gamma'$  coarsening, which is expected to improve creep strength.
3. Develop alloys with high creep strengths in the recrystallized condition. Variations in alloy chemistry can increase creep strength by: (a) increasing the antiphase boundary energy of the  $\gamma'$  to make dislocation shearing of  $\gamma'$  more difficult; (b) decreasing the stacking-fault energy, which in turn improves the creep strength by causing cross-slip to be more difficult; and (c) solid solution strengthening by increasing the refractory metal content.

As for fracture resistance, improvements in the slow-bend fracture energy can be achieved by elongated grains. Further improvements in fracture resistance might also be derived from alloy development. The mechanism causing the observed reduction in fracture energy, resulting from thermal exposure at 1200°F (650°C) for 1500 hours, was not studied, due to insufficient time and funds. However, this mechanism should be studied because of its importance in application of these materials in jet engines.

## 6.0 SUMMARY OF RESULTS

1. Processing variables that influence grain size, grain shape, dislocations, and  $\gamma'$  were determined that increased the yield strength of recrystallized material by 45 ksi (310 MN/m<sup>2</sup>) over the temperature range of 72°F (22°C) to 1300°F (705°C) with no loss in ductility. These increases in strength are thought to be additive to the strength achieved by changes in alloy compositions.
2. Full advantage of the observed improvement in properties was shown to be limited to the temperature range of 72°F (22°C) to 1000°F (540°C), because the largest of these improvements in tensile properties resulted from increases in dislocation density which adversely affected creep at temperatures in excess of 1000°F (540°C). Attempts to stabilize these dislocations through heat treatment were only partially successful.
3. The slow-bend Charpy fracture energy was reduced by increasing the yield stress by the processing schedules investigated; however, improvement of both yield stress and fracture energy was achieved when the equiaxed grain structure was replaced by an elongated grain structure.
4. Variations in yield stress and grain shape had no significant effect on the stress range necessary to initiate crack propagation.
5. Thermal exposure at 1200°F (650°C) for 1500 hours had no significant effect on properties except fracture energy, which was decreased by as much as one-half. Exposure at 1400°F (760°C) for 1500 hours reduced the tensile yield stresses by about 15 percent but did not influence notch sensitivity (the materials did not become notch sensitive).
6. The incorporation of Al<sub>2</sub>O<sub>3</sub> into the matrix of two alloys by the SAP technique resulted in no significant effect on the tensile, stress-rupture, or fracture resistance properties.
7. In order to utilize the large strengthening potential of TMP in nickel-base superalloys at temperatures above 1000°F (540°C), future efforts must be directed at stabilizing dislocation substructures.

### ACKNOWLEDGEMENTS

The author wishes to express his appreciation to N.H. Berling and the various service groups at M&PTL for doing the experimental work.

Thanks are also extended to Drs. R.E. Allen and C.A. Bruch for their suggestions and criticisms.

A special thanks is due E.L. Dunn for construction and analysis of the statistical work in this program.

APPENDIX  
TEST SPECIMENS AND PROCEDURES

All mechanical testing was conducted in air.

TENSILE TESTS

Drawings of unnotched and notched tensile specimens are given in Figures 27 and 28, respectively. Tensile tests were conducted with Baldwin Universal tensile testing machines equipped with strain pacers. An initial strain rate, based on a gage length of 0.7 inch (1.8 cm), of 0.005/min. was used until yielding occurred. After yielding, the elongation rate was increased to a higher, but constant, rate until fracture. Offset-yield-strength values were calculated from load-strain curves obtained from each test.

The test temperatures were measured by a thermocouple which touched the specimen in the center of the gage section.

STRESS-RUPTURE TESTING

The stress-rupture testing was conducted with Tatnall rupture stations. The stress-rupture specimens (Figure 27) were held at temperature for 2.5 to 3 hours before the load was applied. The load was transferred to the specimen by a lever with a 10:1 loading advantage. The load was applied by a crank assembly in approximately 30 seconds.

Once failure occurred, a dashpot controlled the rate at which the load descended. A microswitch was then activated which stopped the timer and shut-off all power to this stress-rupture station.

Four thermocouples were used to assure temperature control within the gage limits of the specimen to the following limits:  $\pm 5^{\circ}\text{F}$  ( $2^{\circ}\text{C}$ ) for the first 24 hours and  $\pm 3^{\circ}\text{F}$  ( $1^{\circ}\text{C}$ ) after the first 24 hours. One thermocouple, which touched the test specimen at the center of the gage section, was used for control. The output of this thermocouple was checked manually each day with a Medistor Model A-75 potentiometer to assure accuracy. The output of the other three thermocouples was continuously recorded. One of the thermocouples touched the specimen in the center of the gage section and the other two thermocouples were located at opposite ends of the gage section.

CREEP TESTING

The design of the creep specimens used in this study was the same as that used for the tensile and stress-rupture specimens (Figure 27), with the exception that the gage length was increased from 0.65 to 1.0 inch (1.6 to 2.5 cm). Creep data were obtained using either optical or electronic measuring

techniques. For tests of anticipated short duration (200 hrs), the electronic system was used. The optical procedure was used on tests of anticipated longer duration (over 200 hrs). The temperature was controlled, monitored, and controlled as previously described for stress-rupture testing.

The electronic system, a continuously-recording method, provided the frequency of measurement required to adequately define creep behavior in short-time tests. One limitation of the electronic system is that it may be subject to a small amount of electronic "drift" when operated for extended periods.

Optical creep measuring techniques have several advantages over electronic systems. The platinum strip extensometers, which indicate specimen extension, were fastened directly to the test specimen. These were read directly by a cathetometer, sighting the extensometer through a small window in the furnace. This eliminated small errors associated with a mechanical transfer system needed to transmit the specimen motion to an LVDT outside the furnace as used in the electronic recording system. Also, by being fully contained in the furnace, the optical extensometer is subjected only to temperature variations inside the furnace, and is not affected by the possibly greater temperature fluctuations in the laboratory. For longer test durations, it is free of the "drift" experienced by electronic systems. The limitation of the system is that a minimum of technicians should be used to keep down the "scatter" in readings due to differences in operator interpretation of a reading. After the multiple readings to define the early stages of creep, the readings were made once or twice a day as necessary to properly monitor the creep rate being observed.

Loading curves were determined by loading in increments to develop the load-strain relationship. The optical system can also produce an unloading curve, which serves as a check on elastic deformation. However, the electronic system usually does not result in acceptable data on unloading a specimen.

After full load was applied, the test was considered to be at time zero. The creep datum as reported was any deformation which occurred after this time plus any plastic deformation as determined from the loading curve.

#### SLOW-BEND TESTING OF PRECRACKED CHARPY BARS

Standard vee-notched Charpy bars (Figure 29) were precracked in fatigue by cyclic testing in three-point bend loading at room temperature. A fatigue cycle of zero-tensile-zero at 1725 cycles/minute was used. The crack tip was sharpened by stepping down the stress during propagation of the fatigue crack. The following stresses are typical of those used to grow the indicated crack lengths:

Stress		Total Fatigue Crack Length*	
ksi	MN/m <sup>2</sup>	in.	cm
50	344	0.025	0.06
30	206	0.045	0.11
25	172	0.075	0.19
* Does not include the depth of the vee-notch			

The total crack length (vee-notch plus fatigue crack) was between 0.45 and 0.55 of the Charpy bar's thickness.

The precracked specimen was tested in three-point bending by using a Baldwin Universal testing machine. The ratio of the bending support span to the specimen thickness was four. During the bend test, a strain pacer was used to provide a loading rate of 3000 pounds/minute (13,200 N/minute). A load-deflection curve was obtained as illustrated in Figure 30. The energy required to reach crack instability (i.e., Wu in Figure 30) was taken as a measure of the material's fracture energy. This energy was determined as follows:

1. Measure the area (Ao) under the load-deflection curve (a planimeter was used) to the point of crack instability, which is the cross-hatched area in Figure 30.
2. Record the strain and load magnifications used in determining the load-deflection curve.
3. Determine the uncracked area of the Charpy bar prior to slow-bend testing; this was done after the specimen was tested.
4. Calculate the fracture resistance, Wu, as follows:

$$Wu = \frac{(Ao) (Strain Mag.) (Load Mag.)}{Uncracked Area}$$

$$Wu = \frac{(in.^2) (in./in.) (lbs / in.)}{in.^2} = in.-lbs / in.^2$$

$$Wu = \frac{m^2 (m/m) (N/m)}{m^2} = Nm / m^2$$



Values of fracture energy obtained by the above procedure were used to rank materials as to relative fracture toughness. It is anticipated that this method works best with materials exhibiting high levels of yield stress and low values of  $K_{Ic}$ . It is important to realize that this technique did not give true values of  $K_{Ic}$  or fracture toughness.

#### $\hat{K}^*$ TEST PROCEDURE FOR MODIFIED CHARPY SPECIMENS

$\hat{K}^*$  was determined by high-cycle-fatigue testing a modified Charpy specimen with nominal dimensions of 0.394-inch (1 cm) width x 0.394-inch (1 cm) height x 5-inch (12.7 cm) length. A 45° notch was machined in the center of the specimen to a depth of 0.079-inch (0.2 cm), and the notch radius was then sharpened by EDM techniques to produce a 0.087-inch (0.22 cm) deep notch with a 0.003-inch (0.008 cm) radius. The machined test specimen was then precracked by high-cycle-fatigue loading at room temperature, to produce a sharp crack and extend length (a) to within 0.45 to 0.55 times the total thickness (w) of the specimen.

All precracking and fatigue tests were performed on a Sonntag SFOIU Universal fatigue machine which operated at 30 cps, and was equipped with a 4-point pure bending test fixture with a specimen-free span length of 3 inches (7.5 cm). The A-ratio for all precracking and fatigue testing was 0.95.

The heating source for the elevated temperature tests was a Lepel 5 KW high-frequency generator equipped with a West S.C.R. temperature controller that was operated from a Type K thermocouple spot welded to the test sample at the top of the notch. A second thermocouple was also attached in a similar manner and was used to continuously record specimen temperature.

A telescope with a calibrated Vernier scale was used to monitor and measure crack extension of the sample during precracking and testing.

All precracking was performed at room temperature, and stress values were calculated using the formula for single-edge-cracked plate specimen in pure bending from ASTM STP-410 page 13, where:

$$K_I = 6 M a^{\frac{1}{2}} / B W^2 [1.99 - 2.47 (a/w) + 12.97 (a/w)^2 - 23.17 (a/w)^3 + 24.80 (a/w)^4]$$

It has been noted in previous work that the precracking technique can influence later  $\hat{K}^*$  results if certain precautions are not followed and a final sharp crack is not obtained. To obtain a sharp crack, an initial stress [20 ksi (138 MN/m<sup>2</sup>) for these tests] was selected and the test was run until approximately 0.010 inch (0.025 cm) of crack growth had occurred. Based on the new crack length and the crack growth rate, a new stress value and machine load was calculated, and subsequent precracking steps were performed. Precracking steps were adjusted such that the following conditions were met:

1. Stress was not decreased in increments greater than 2 ksi ( $13.8 \text{ MN/m}^2$ ).
2. The final overall crack length (a) was within 0.45 to 0.55 times the specimen thickness (w), and the final crack lengths as measured on both sides of the sample were within 10 percent.
3. The final rate of crack growth in precracking is critical in producing a sharp crack. For these materials, crack growth rates less than  $5 \times 10^{-8}$  in/cycle ( $12.7 \times 10^{-8}$  cm/cycle) were achieved by running the test for 100,000 cycles with less than 0.005 inch (0.013 cm) crack extension.

All  $\hat{K}^*$  tests were conducted at  $1000^\circ\text{F}$  ( $540^\circ\text{C}$ ). Stress values were calculated from the (a) dimensions measured on the sides of the sample. The true stress was recalculated after failure, using the quarter-point method to measure the average crack length on the failed surface.

Failure was arbitrarily defined as any measurable crack growth that occurred within  $2.5 \times 10^6$  cycles. If a test exceeded  $2.5 \times 10^6$  cycles, it was considered a runout. A test sample that either failed or ran out could be retested by precracking at room temperature and fatigue tested at temperature, providing the new precracking did not extend the crack length beyond 0.55 times the specimen thickness. An S/N plot of the data was then made and the maximum  $R^*$  that did not produce failure was defined as the  $\hat{K}^*$  value for that material.

#### REFERENCES

1. C. S. Wukusick, and R. W. Smashey, "Ultra-High Strength Superalloys", General Electric AEG-TIS Report No. R68AEG457, October 31, 1968.
2. J. E. Hilliard, "Grain-Size Estimation", General Electric Report No. 62-RL-3133M, December 1962.
3. T. A. Budne, "Random Balance", Industrial Quality Control, V. 15, Nos. 10-12, April-June, 1959.
4. R. E. Allen, and C. D. Calhoun, "A Study of Rene' 77 and Rene' 77 + 1 w/o  $Al_2O_3$  Consolidated from Powder", General Electric TIS Report No. R70AEG456, April 1971.
5. C. D. Calhoun, "The Effects of Oxide Dispersions and Post Heat Treatment Warm Working on the Mechanical Properties of U-700", AEG-TIS Report No. R71AEG232, June 10, 1971.

Table I. Desired Composition and Limits of Consolidated Powders.

Element	Weight Percent			
	Alloy A	Alloy A-1	Alloy A-2	Alloy B
C	$0.15 \pm 0.02$	$0.08 \pm 0.02$	0.02 max.	$0.15 \pm 0.02$
O	0.02 max.	$0.12 \pm 0.02$	$0.24 \pm 0.03$	0.02 max.
N	0.015 max.	Same as Alloy A		0.015 max.
Cr	$13.0 \pm 0.75$	"	"	$12.0 \pm 0.75$
Co	$8.0 \pm 0.25$	"	"	$7.5 \pm 0.25$
Ni	Balance	"	"	Balance
Ti	$2.5 \pm 0.2$	"	"	$2.7 \pm 0.2$
Al	$3.5 \pm 0.2$	"	"	$3.9 \pm 0.2$
Cb	$3.5 \pm 0.2$	"	"	$3.9 \pm 0.2$
Ti + Al + Cb	$9.5 \pm 0.2$	"	"	$10.5 \pm 0.2$
Mo	$3.5 \pm 0.2$	"	"	$3.2 \pm 0.2$
W	$3.5 \pm 0.2$	"	"	$3.2 \pm 0.2$
Zr	$0.05 \pm 0.02$	"	"	$0.05 \pm 0.02$
B	$0.01 \pm 0.005$	"	"	$0.01 \pm 0.005$
Mn	0.15 max.	"	"	Same as Alloy A
Fe	1.00 max.	"	"	"
Si	0.20 max.	"	"	"
P	0.015 max.	"	"	"
S	0.015 max.	"	"	"
Pb	0.002 max.	"	"	"
Bi	0.002 max.	"	"	"
Sn	0.002 max.	"	"	"
Ag	0.002 max.	"	"	"
Cu	0.150 max.	"	"	"

Table II. Chemical Analyses of Ingots.

Element	Weight Percent			
	Alloy A	Alloy A-1	Alloy A-2	Alloy B
C	0.16	0.08	0.005	0.14
O	0.0053	0.0029	0.0023	---
N	0.0060	0.006	0.006	---
Cr	13.1	12.9	13.0	11.9
Co	8.1	8.0	8.0	7.6
Ni	51.8	52.5	52.3	52.3
Ti	2.5	2.5	2.5	2.8
Al	3.6	3.5	3.6	3.8
Cb	3.6	3.6	3.6	3.9
Ti + Al + Cb	9.7	9.6	9.7	10.5
Mo	3.4	3.4	3.4	3.2
W	3.5	3.4	3.4	3.4
Zr	0.05	0.05	0.05	0.04
B	0.012	0.011	0.012	0.0016
Mn	<0.15	<0.15	<0.15	0.006
Fe	<0.20	<0.20	<0.20	0.84
Si	<0.10	<0.10	<0.10	0.04
P	<0.015	<0.015	<0.015	<0.001
S	0.007	0.007	0.007	0.0012
Pb	<0.001	<0.001	<0.001	<0.0002
Bi	<0.001	<0.001	<0.001	<0.0001
Sn	0.0015	0.0013	0.001	0.0005
Ag	<0.0005	<0.0005	<0.0005	0.0002
Cu	0.01	0.01	0.01	0.0015

Table III. Partial Chemical Analysis of As-Received, -100-Mesh Powders<sup>(1)</sup>.

Alloy	C	O (ppm)	N (ppm)	H (ppm)	Nominal Al + Ti + Cb
A	0.17	101	25	1	9.5
A-1	0.09	67	7	1	9.5
A-2	0.003	85	4	1	9.5
B	0.15	133	5	3	10.5
<sup>(1)</sup> Reported as weight percent.					

Table IV. Summation of Extrusion Parameters.

Alloy	Reduction Ratio	Temp		Time at Temp (hr)	Extrusion Rate		Extrusion Constant		Useable Material		Yield (%)
		°F	°C		in/min	m/min	TSI	MN/m <sup>2</sup>	ft	m	
<u>FIRST SERIES</u>											
A <sup>(1)</sup>	22:1	2100	1150	3.0	60, 700	1.5, 17.8	30	414	2, 4	0.6, 1.2	20, 80
A-1	22:1	2100	1150	3.2	360	9.2	29	400	0	0	0
A-2 <sup>(2)</sup>	22:1	2100	1150	3.5	600	15.2	26	358	9	2.7	65
B <sup>(2)</sup>	22:1	2150	1175	4.0	880	22.4	25	345	12	3.6	90
<u>SECOND SERIES</u>											
A <sup>(2)</sup>	16:1	2050	1120	4.0	175	4.4	27	358	12	3.6	90
A-1 <sup>(2)</sup>	16:1	2050	1120	3.5	175	4.4	27	358	12	3.6	90

(1) The press stalled after about 65% of this billet had been extruded. The remaining portion of the billet was extruded at a later date.

(2) Material used in this investigation

Table V. Density and Average Grain Size of Extruded Bars.

Alloy	Density				Grain Size ( $\mu\text{m}$ )
	Calculated		Measured		
	(lbs/in. <sup>3</sup> )	(g/cm <sup>3</sup> )	(lbs/in. <sup>3</sup> )	(g/cm <sup>3</sup> )	
A	0.294	8.16	0.300	8.32	10
A-1	---	---	0.299	8.29	7
A-2	---	---	0.298	8.25	16
B	0.292	8.10	0.294	8.16	17
Density of Cast-and-Forged Rene' 95: 0.296 lbs/in. <sup>3</sup> (8.20 g/cm <sup>3</sup> ).					



Table VI. Chemical Analyses of Extruded Bars<sup>(1)</sup>.

Element	Weight Percent			
	Alloy A	Alloy A-1	Alloy A-2	Alloy B
C	0.15	0.09	0.003	0.16
O	0.0119	0.095	0.22	0.01
N	0.0026	0.0028	0.001	0.0014
Cr	12.88	12.86	12.4	11.8
Co	8.28	8.28	8.1	7.6
Ni	Bal.	Bal.	Bal.	Bal.
Ti	2.43	2.43	2.5	2.7
Al	3.55	3.4	3.2	3.9
Cb	3.49	3.56	3.6	4.0
Ti + Al + Cb	9.47	9.39	9.3	10.6
Mo	3.44	3.48	3.3	3.1
W <sup>(2)</sup>	2.97	2.94	2.9	2.8
Zr	0.07	0.05	0.04	0.03
B	0.0098	0.010	0.005	0.0047
Mn	0.01	0.01	0.003	0.001
Fe	0.31	0.27	0.14	0.3
Si	0.06	0.04	0.14	0.08
P	0.0008	0.0011	0.002	0.002
S	0.0054	0.0042	0.0037	0.0012
Pb	0.0001	0.0001	0.0006	0.0004
Bi	<0.00002	<0.00002	<0.0001	<0.0001
Sn	0.0001	0.0001	0.0002	0.0005
Ag	<0.0001	0.0002	0.0005	0.0002
Cu	0.008	0.006	0.01	0.008
<p>(1) Analyses by Ledoux and Co.</p> <p>(2) Results for W analyses are thought to be low by ~ 0.5 weight percent based on additional analyses conducted by General Electric and on results of ingot analyses (Table II).</p>				

Table VII. Summation of Data From Flat Rollability Studies.

Alloy	Section No.	Temp		Number of Rolling Passes	Total Percent Reduction In Thickness	Rating Of Rollability
		°F	°C			
A-2	1	72	22	2	13	Poor
A-2	3	2000	1095	1	6	Poor
A-2	5	2200	1205	14	50	Good
A-2	7	2200	1205	7	30	Good
A-2	7*	2000	1095	13	50	Fair
A-2	8	2200	1205	7	30	Good
A-2	8+	72	22	3	3	Poor
A-2	8+	1850	1010	2	11	Poor
B	2	72	22	4	19	Fair
B	9	1900	1040	9	20	Fair
B	4	2000	1095	11	48	Good
B	6	2200	1205	14	50	Good
<p>* Section No. 7 was rolled 30 percent at 2200°F (1205°C) followed by an additional 50 percent at 2000°F (1095°C).</p> <p>+ Section No. 8 was rolled 30 percent at 2200°F (1205°C), cut in half and rolled at 72°F (22°C) and 1850°F (1010°C) as indicated.</p>						

Table VIII. Statistical Design of Process Development Study<sup>(1)</sup>.

TMP	RA at RT (%)	Final Age	Alloys											
			A			A-1			A-2			B		
			Temperature			Temperature			Temperature			Temperature		
			T <sub>S</sub> -100	T <sub>S</sub> -50	T <sub>S</sub>	T <sub>S</sub> -100	T <sub>S</sub> -50	T <sub>S</sub>	T <sub>S</sub> -100	T <sub>S</sub> -50	T <sub>S</sub>	T <sub>S</sub> -100	T <sub>S</sub> -50	T <sub>S</sub>
I	0	a	1						19					
		b												
	8	a				10						28		
II	0	a												
		b						11						29
	8	a												
III	0	a		3						21				
		b												
	8	a					12						30	
IV	0	a												
		b	4						22					
	8	a												
V	0	a			5						23			
		b												
	8	a						14						32
VI	0	a												
		b		6						24				
	8	a												
VII	0	a				16	15					34		
		b												
	8	a	7						25					
VIII	0	a												
		b			8					26				
	8	a												
IX	0	a					18	17						35
		b											36	
	8	a		9						27				
		b												

(<sub>1</sub>) TMP Schedule on page 16.

Table IX. Tensile and Stress Rupture Data from Statistical Process Development Study.

Specimen <sup>(1)</sup> Condition	Alloy	1200° F (650° C) Tensile						Stress Rupture 1200°F/150 (ksi) (650°C/1030 MN/m <sup>2</sup> )		Grain Size (μm)
		0.2% YS		UTS		El (%)	RA (%)	Time (hr)	El (%)	
		ksi	MN/m <sup>2</sup>	ksi	MN/m <sup>2</sup>					
1	A	182	1250	228	1570	7	11.4	306 <sup>(2)</sup>	0.13	8
2		188	1290	217	1490	3	4.6	2	1.7	30
3		181	1250	226	1560	6	10	0.3	TF	33
4		187	1290	227	1560	11	15	37	4.9	10
5		214 <sup>(3)</sup>	1470	238	1640	13	27.3	50.4	14.5	L/d ~ 100/20
6		190	1310	235	1620	8.5	11.4	120	2.4	33
7		198	1360	235	1620	8.5	11.2	98	5	7
8		183	1260	228	1570	8.5	12	FOL	0.6	42
9		193	1330	238	1640	7.5	8.6	208	3	23
10	A-1	203 <sup>(3)</sup>	1400	244	1680	6	9.2	18	TF	8
11		177	1220	223	1530	6	4.5	28	2.6	95
12		176	1210	193	1330	2.5	4.6	95	TF	> 300
13		186	1280	186	1280	1.5	3.2	3.5	1.5	---
14		215 <sup>(3)</sup>	1480	248	1710	10	17.2	70.6	11	L/d ~ 500/100 (Some Recrystallation)
15		199	1370	243	1670	7	11.3	69	2.6	30
16		183	1260	232	1600	8.5	10	261	2.2	10
17		195	1330	238	1640	6.5	8.6	124	3.2	11
18		183	1260	233	1600	8.5	13.2	261 <sup>(2)</sup>	0.47	55
19	A-2	180	1240	216	1490	5.5	7.4	12	TF	6
20		192	1320	195	1340	TF	---	---	TF	20/55
21		(4)	(4)	159	1090	0.8	2	---	TF	37/>300
22		183	1260	225	1550	6	8.6	22	2.5	10
23		217 <sup>(3)</sup>	1490	256	1760	6	10.5	26	13.5	L/d ~ 100/20
24		(4)	(4)	163	1120	1.5	2.4	7	1.5	8/>300
25		212 <sup>(3)</sup>	1460	247	1700	6	10	67	5.5	7
26		185	1270	231	1590	5.5	8	1	1	29
27		(4)	(4)	110	756	---	---	---	---	>300
28	B	211 <sup>(3)</sup>	1450	251	1730	4.5	8	209 <sup>(2)</sup>	3	6
29		Cracked during processing				---	---	---	---	---
30		(4)	(4)	147	1010	0	0.8	---	1	20/>300
31		195	1340	214	1470	6	7.2	67	5.5	10
32		Cracked during processing				---	---	---	---	---
33		188	1290	205	1410	1.5	6	Visibly Cracked		20/225
34		194	1340	234	1610	8.5	12	147	4.5	7
35		187	1290	212	1460	3	6	Visibly Cracked		13/150
36		176	1210	222	1530	8.5	14	0.6	TF	23/58
<p>(1) For processing schedule, go to Table VIII and use the number corresponding to the specimen condition number.</p> <p>(2) Unloaded without a failure.</p> <p>(3) Exceeded minimum program goal.</p> <p>(4) Failed prior to 0.2% YS.</p>										

Table X. Results from Statistical Analysis of Process Development Study<sup>(1)</sup>.

Factor	Response			
	0.2% YS	% El	% RA	Stress-Rupture
Alloy	(A, A-2, B) A-1	A (A-1, B) A-2	(A, B) A-1, A-2	(A, A-1, B) A-2
Partial Sol'n. Temp.	(T <sub>s</sub> -100) (T <sub>s</sub> ) (T-50)	Not Sign.	Not Sign.	(T <sub>s</sub> -100) (T <sub>s</sub> -50) T <sub>s</sub>
TMP	V (VII, VIII, IX) Bal.	Bal. (I, II, III) <sup>(2)</sup>	Bal. (I, II, III) <sup>(2)</sup>	Bal. (V)
72°F (22°C) Deformation	8, 0	(3)	(3)	0, 8
Final Age	a, b	(3)	(3)	a, b
<sup>(1)</sup> Variables are given in order of decreasing desirability; those within parentheses are equivalent. Taking effects of alloy on % El as an example, Alloy A was best, A-1 and B were equivalent and A-2 was the worst. <sup>(2)</sup> TMP I, II, III interact with Alloy (Alloy A helped, Alloy A-1 lowered). <sup>(3)</sup> Interaction 8, b lower than balance.				

Table XI. Four Best Alloy/Process Combinations.

Material Designation	Alloy	$\gamma'$ Partial Solution Temp	TMP	% RA at RT	Final Age
S-1	A	$T_s^{(1)}$	$V_{(M)}$	0	a
S-2	B	$T_s - 100^\circ\text{F} (55^\circ\text{C})$	$VI_{(M)}$	0	a
S-3	B	$T_s - 100^\circ\text{F} (55^\circ\text{C})$	$VIII_{(M)}$	0	a
S-4	A	$T_s - 100^\circ\text{F} (55^\circ\text{C})$	$I_{(M)}$	8	a
$^{(1)}T_s$ for Alloy A = $2150^\circ\text{F} (1175^\circ\text{C})$ $T_s$ for Alloy B = $2200^\circ\text{F} (1205^\circ\text{C})$					

Table XII. Tensile Screening Test Results for Four Best Alloy/Process Combinations.<sup>†</sup>

Material Designation	Alloy	Test Temp		Unexposed						Exposed 1400°F (760°C)/100 hrs					
				0.2% YS		UTS		RA	El	0.2% YS		UTS		RA	El
		°F	°C	ksi	MN/m <sup>2</sup>	ksi	MN/m <sup>2</sup>	%	%	ksi	MN/m <sup>2</sup>	ksi	MN/m <sup>2</sup>	%	%
S-1	A	72	22	251	1730	286	1970	15	12	238	1640	270	1860	15	11
S-2	B	72	22	219	1510	280	1930	17	16	207	1420	264	1820	14	10
S-3	B	72	22	229	1580	293	2020	14	10	215	1480	277	1910	9	8
S-4	A	72	22	230	1580	280	1930	18	12	217	1490	272	1870	14	11
S-1	A	1200	650	222†	1530	239	1650	24	13	208†	1430	225	1550	19	12
S-2	B	1200	650	198	1360	229	1580	12	11	191	1310	228	1570	14	10
S-3	B	1200	650	214†	1470	248	1710	13	10	196	1350	234	1610	14	8
S-4	A	1200	650	207†	1430	247	1700	10	7	199	1370	235	1620	6	5
NASA Min. Requirement	---	1200	650	200	1380	---	---	--	10	200	1380	---	---	--	10

† Data are average of two tests.

‡ Exceeded minimum program goal.

Table XIII. Creep-Monitored Stress Rupture Data for Four Best Alloy/Process Combinations.

Material Designation	Alloy	Temperature		Stress		Approx. Time for 0.2% Creep, hrs	Unloaded Without Failure Time (hrs)/El (%)	Time to Failure (hrs)
		°F	°C	ksi	MN/m <sup>2</sup>			
S-1	A	1000	540	160	1100	> 137	137/0.12	---
S-2	B	1000	540	160	1100	> 137	137/0.04	---
S-3	B	1000	540	160	1100	~ 15	137/0.23	---
S-4	A	1000	540	160	1100	> 160	160/0.09	---
S-1	A	1200	650	150	1030	2	---	50 <sup>(1)</sup>
S-2	B	1200	650	150	1030	8	---	90 <sup>(1)</sup>
S-3	B	1200	650	150	1030	1	---	123 <sup>(1)</sup>
S-4	A	1200	650	150	1030	---	---	98
(1) Average of two tests.								



Table XIV. Comparison of 1200°F (650°C) Tensile Data for 0.35- to 0.5-Inch (0.9- to 1.3-cm) Diameter Rods<sup>(1)</sup>.

Material Condition	Rod Diameter		0.2% YS		UTS		RA %	EL %
	in.	cm	ksi	MN/m <sup>2</sup>	ksi	MN/m <sup>2</sup>		
S-1	0.35	0.9	222	1530	239	1650	24	13
S-1	0.5	1.3	218	1500	236	1630	22	14
S-3	0.35	0.9	214	1470	248	1710	13	10
S-3	0.5	1.3	209	1430	246	1690	14	9
<sup>(1)</sup> Data are average of two tests.								

Table XV. Tensile Data From Evaluation of Two Best Alloy/Process Combinations.

Material Condition	Alloy	Test Temp		0.2% YS		UTS		EL %	RA %
		°F	°C	ksi	MN/m <sup>2</sup>	ksi	MN/m <sup>2</sup>		
S-1	A	72	22	250	1720	282	1940	14	12
S-1	A	800	425	231	1600	262	1810	14	17
S-1	A	1000	540	228	1570	259	1790	10	16
S-1	A	1100	600	234	1540	263	1810	10	15
S-1	A	1200	650	227	1560	248	1710	13	21
S-1	A	1300	705	213	1470	228	1570	14	26
S-1	A	1400	760	157	1080	191	1320	22	34
S-1	A	1600	870	50	344	88	605	34	42
S-1	A	1800	980	16	110	31	214	52	48
S-1	A	2000	1095	1.8	12.4	6.6	45.5	178	82
S-3	B	72	22	241	1660	300	2070	11	18
S-3	B	800	425	210	1450	272	1870	14	16
S-3	B	1000	540	218	1500	274	1890	10	13
S-3	B	1100	600	215	1480	274	1890	10	11
S-3	B	1200	650	212	1460	255	1760	10	12
S-3	B	1300	705	200	1380	236	1630	8	12
S-3	B	1400	760	150	1030	190	1310	6	8
S-3	B	1600	870	71	490	100	689	14	13
S-3	B	1800	980	17	117	36	248	29	19
S-3	B	2000	1095	1.7	12	6.6	45	132	55

Table XVI. Tensile Data for Two Best Alloy/Process Combinations After Thermal Exposure<sup>(1)</sup>.

Material Condition	Exposed at 1200°F (650°C) for 1500 Hours							
	Test Temp		0.2%YS		UTS		El %	RA %
	°F	°C	ksi	MN/m <sup>2</sup>	ksi	MN/m <sup>2</sup>		
S-1	72	22	264	1820	289	1990	14	18
S-1	1200	650	230	1580	244	1680	15	23
S-3	72	22	296	2040	241	1660	8	10
S-3	1200	650	210	1450	251	1730	10	14
		Exposed at 1400°F (760°C) for 1500 Hours						
S-1 <sup>(2)</sup>	1200	650	175	1210	221	1520	14	20
S-1 <sup>(2)</sup>	1200	650	206	1420	226	1560	14	22
S-3	1200	650	184	1270	228	1570	9	11
<sup>(1)</sup> Data from tests at 1200°F (650°C) are average of two tests; 72°F data are single test results. <sup>(2)</sup> Data given for both tests due to large difference in yield stresses, the reason for this difference is not known.								

Table XVII. Notched Tensile Data for Two Best Alloy/Process Combinations<sup>(1)</sup>.

Material Condition	Alloy	Test Temp		Notch Strength		Smooth Bar UTS		NS/UTS
		°F	°C	(ksi)	(MN/m <sup>2</sup> )	(ksi)	MN/m <sup>2</sup> )	
				As-Processed				
S-1	A	72	22	348	2400	282	1940	1.23
S-1	A	1200	650	298	2050	248	1710	1.2
S-3	B	72	22	311	2140	300	2060	1.04
S-3	B	1200	650	294	2020	255	1760	1.15
		Exposed at 1400°F (760°C) for 1500 Hours						
S-1	A	1200	650	287	1980	223	1540	1.29
S-3	B	1200	650	276	1900	228	1570	1.21
(1) Notched specimens have $K_t=3.5$ ; data are average of two tests.								

Table XVIII. Creep Data for Two Best Alloy/Process Combinations.

Material Condition	Test Temperature		Stress		Secondary Creep Rate $\text{hr}^{-1} \times 10^6$	Time (hr) to Plastic Creep of			Test Duration, hr	Final % Creep	
	$^{\circ}\text{F}$	$^{\circ}\text{C}$	ksi	$\text{MN}/\text{m}^2$		0.1%	0.2%	0.5%		Extensometer	Measured (After Test)
S-1	1000	540	160	1100	0.63	10	1100	---	2808	0.28	0.17
S-1	1000	540	170	1170	1.5	105	590	---	2617	0.46	0.73
S-1	1000	540	180	1240	1.8	1	60	1510	2090	0.61	0.61
S-1	1000	540	190	1310	6.4	8	35	315	384	0.52	0.44
S-1	1100	595	100	689	3.8	76	210	910	938	0.50	0.36
S-1	1100	595	115	790	7.5	32	108	590	598	0.50	0.46
S-1	1200	650	50	344	1.1	290	1200	---	2451	0.34	0.35
S-1	1200	650	60	414	6.0	55	210	---	624	0.45	0.28
S-1	1200	650	90	620	17.0	1	17	159	313	0.91	1.1
S-1	1200	650	130	695	---	< 1	< 1	8	116	19.1	18.6
S-1	1300	705	25	172	8.7	53	128	435	476	0.53	0.59
S-1	1400	760	10	69	2.7	30	120	930	1154	0.56	0.67
S-1	1400	760	20	138	---	5	20	82	164	0.68	0.68
S-1	1400	760	40	276	---	< 1	1	6	100	5.87	6.10
S-1	1400	760	90	620	---	< 1	< 1	< 1	2 <sup>(1)</sup>	---	38.5
S-3	1000	540	160	1100	0.73	6	105	---	2809	0.45	0.31
S-3	1000	540	170	1170	0.7	82	1270	---	2645	0.30	0.21
S-3	1000	540	180	1240	0.33	1800	---	---	2159	0.10	0.41
S-3	1000	540	190	1310	5.2	< 1	6	170	291	0.58	0.37
S-3	1100	595	130	695	1.4	64	630	---	2036	0.40	0.42
S-3	1100	595	145	1000	12.0	1	11	165	185	0.52	0.35
S-3	1200	650	80	550	10.0	17	90	365	502	0.64	0.66
S-3	1200	650	90	620	2.9	105	445	1100	1152	0.53	0.56
S-3	1200	650	100	689	9.2	73	210	540	678	0.71	0.71
S-3	1200	650	130	695	67.0	< 1	8	49	117	1.08	1.16
S-3	1300	705	30	207	5.2	60	160	650	725	0.54	0.50
S-3	1400	760	10	69	6.4	75	235	590	602	0.52	0.62
S-3	1400	760	20	138	25.0	5	21	82	306	1.23	1.30
S-3	1400	760	50	344	---	< 1	1	3	50 <sup>(1)</sup>	---	24.0
S-3	1400	760	90	620	---	< 1	< 1	< 1	5 <sup>(1)</sup>	---	14.5

<sup>(1)</sup> Failed.

Table XIX. Slow-Bend Fracture Energies of Two Best Alloy/Process Combinations<sup>(1)</sup>.

Material Condition	Test Temp		Exposure	Charpy Fracture Energy (Wu/A)	
	°F	°C		(in.-lb/in. <sup>2</sup> )	N/m
S-1	1000	540	None	138	24,200
S-1	1200	650	None	138	24,200
S-1	1200	650	1200°F(650°C)/1500 hrs	66	11,500
S-3	1000	540	None	73	12,800
S-3	1200	650	None	77	13,500
S-3	1200	650	1200°F(650°C)/1500 hrs	50	8,700
Conventional Rene' 95	1200	650	None	≈ 190	33,200
(1) Data are average of two tests.					

Table XX. X-Ray Analyses of Phases in Two Best Alloy/Process Combinations as Influenced By Thermal Exposure<sup>(1)</sup>.

Material Condition	Phases Present in Addition to $\gamma'$			
	As-Processed	1200°F/1500 hrs 650°C/1500 hrs	1400°F/1000 hrs 760°C/1000 hrs	1400°F/1500 hrs 760°C/1500 hrs
S-1	MC (S) $M_3 B_2$ (Wk)	MC (S) $M_3 B_2$ (Wk) $M_{23} C_6$ (V Wk)	MC (S) $M_6 B_2$ (Wk) $M_{23} C_6$ (S)	MC (S) $M_6 B_2$ (V Wk) $M_{23} C_6$ (S) $M_6 C$ (V Wk) Sigma (V Wk)
S-3	MC (S)	MC (S) $M_{23} C_6$ (Wk)	MC (S) $M_{23} C_6$ (S) $M_3 B_2$ (V Wk)	MC (S) $M_{23} C_6$ (S) Sigma (Wk)
<p>PROBABLE COMPOSITION OF ABOVE PHASES<sup>(2)</sup></p> <p>MC - (Cb, Ti, Mo, Zr, W)C; Cb rich</p> <p><math>M_{23} C_6</math> - <math>Cr_{21} (Mo, W)_2 C_6</math></p> <p><math>M_6 C</math> - (Mo, W, Ni, Co, Cr)<sub>6</sub> C</p> <p><math>M_3 B_2</math> - (Mo, Ti, Cr, Ni)<sub>3</sub> B<sub>2</sub>; small quantities of Cr and Ni</p> <p>Sigma - (Cr, Mo)<sub>x</sub> (Ni, Co)<sub>y</sub>; x and y vary from 1 to 7</p>				
<p><sup>(1)</sup> W radiation was used. Relative indications of phases present are given by S (strong), Wk (weak) and V Wk (very weak).</p> <p><sup>(2)</sup> Probable compositions based in part on prior work; e.g., see C.T. Sims, J. Metals, Oct., 1966.</p>				

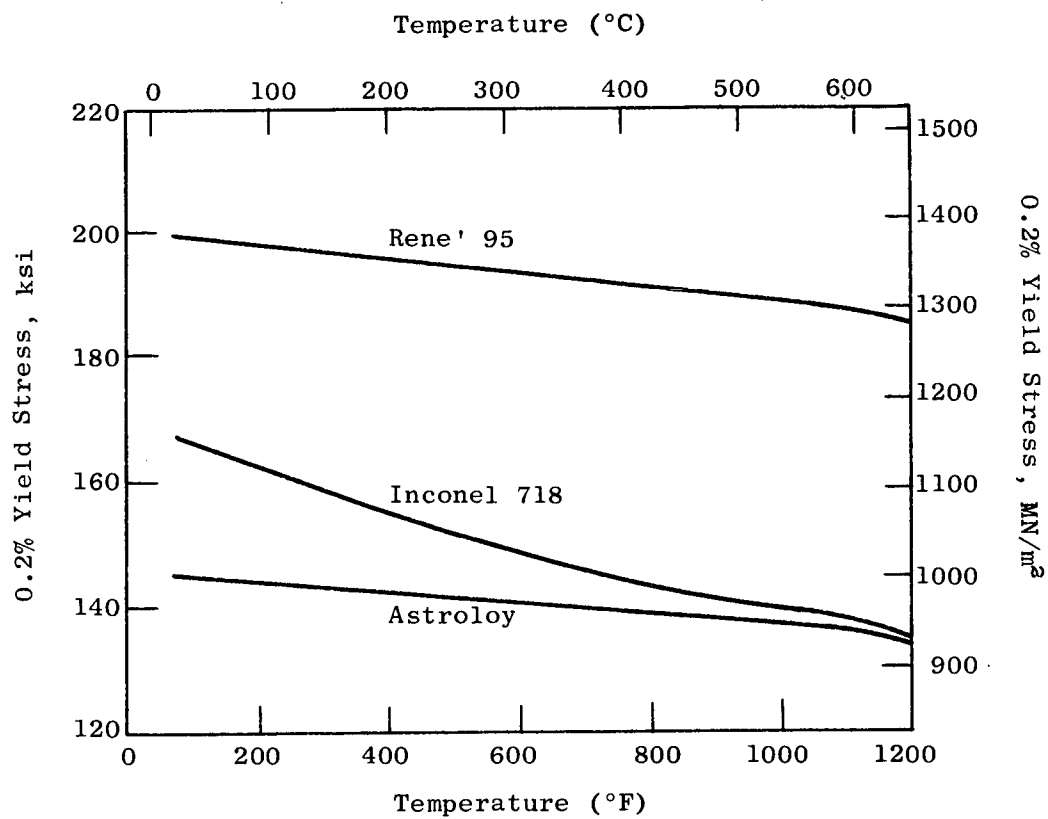


Figure 1. Strength Advantage of Rene' 95 Over Inconel 718 and Astroloy.



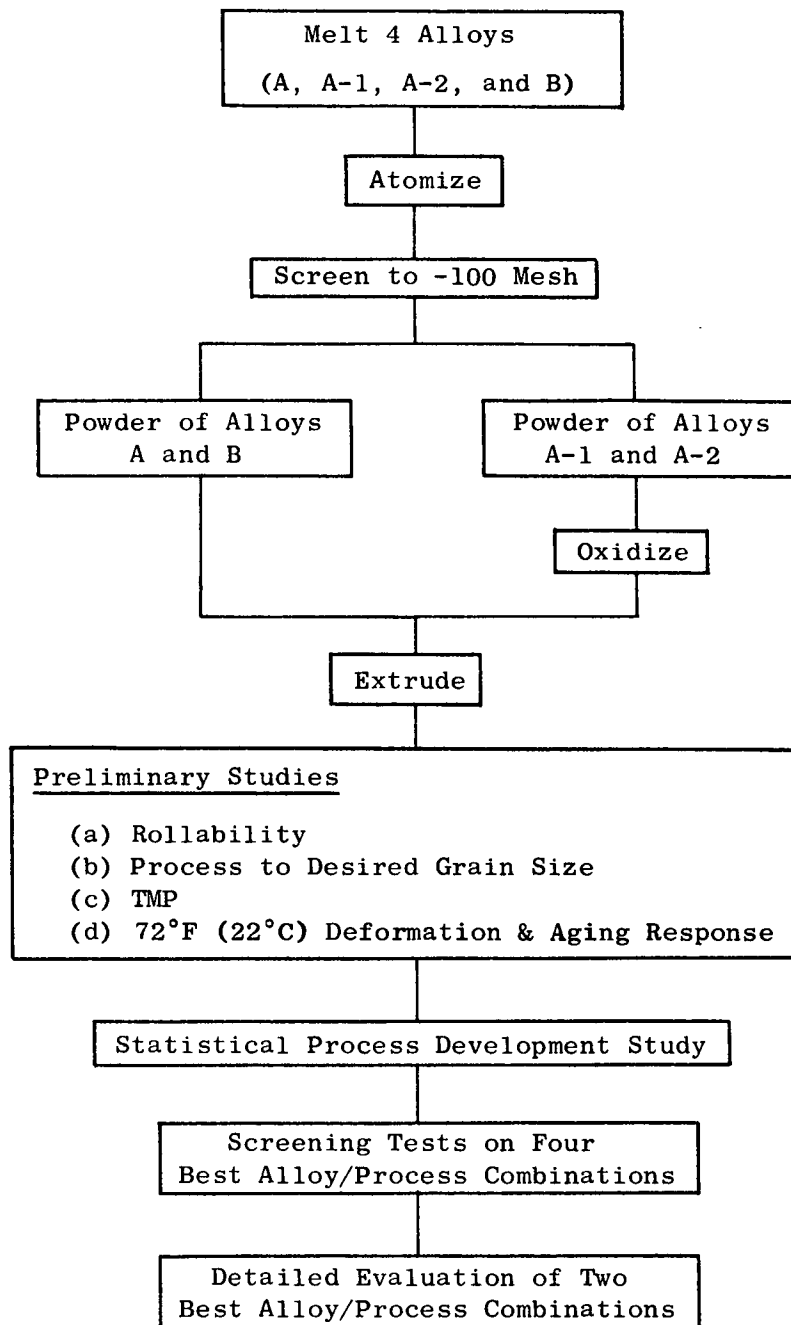
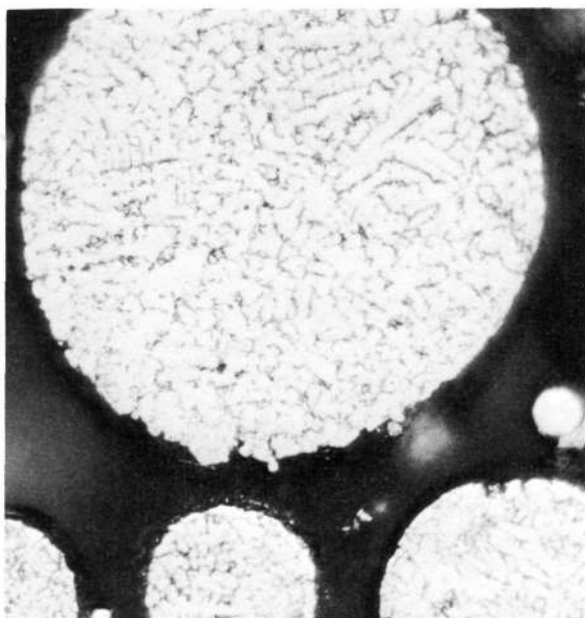


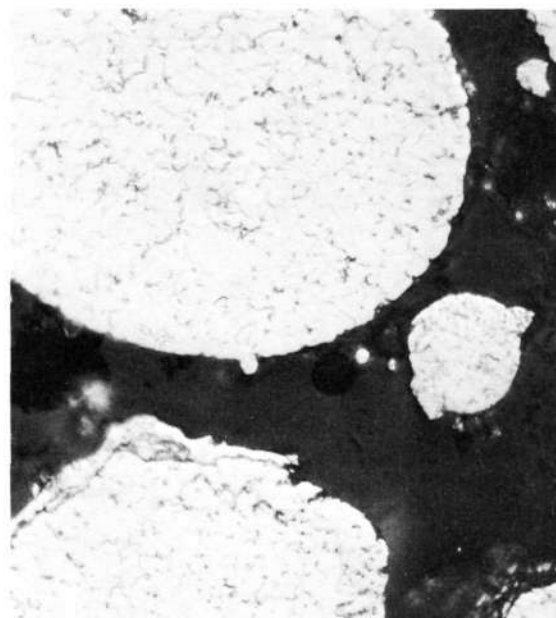
Figure 2. Program Flow Chart.



B11337

500X

a. Alloy B

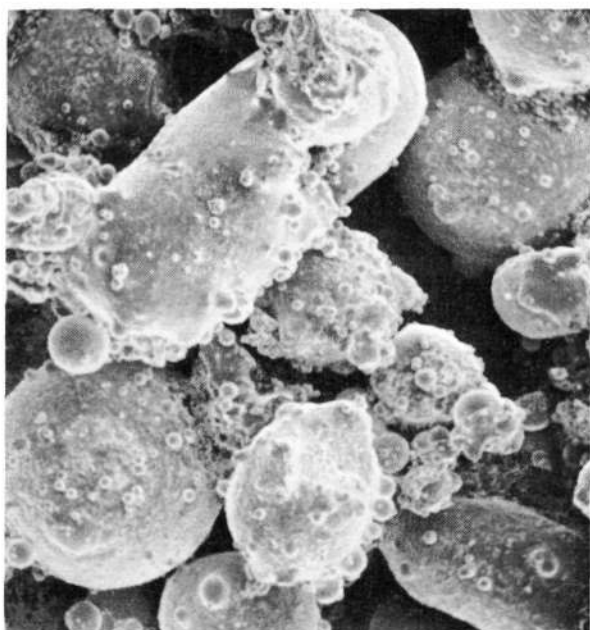


F1451

500X

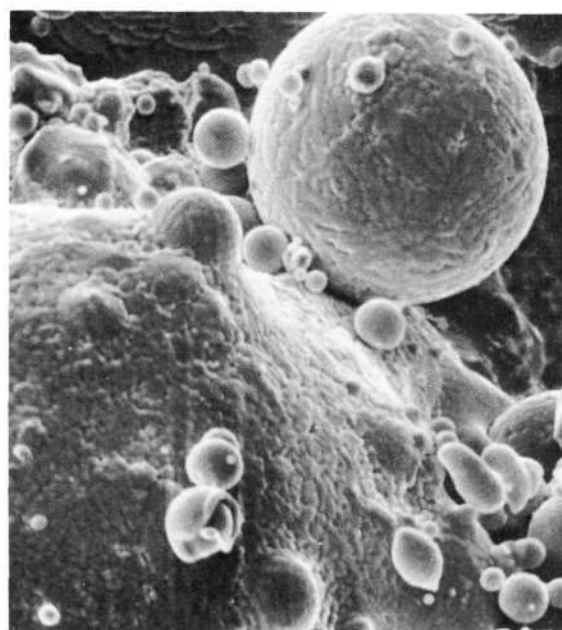
b. Alloy A-2

Light Microscopy



200X

c. Alloy A



1000X

d. Alloy A

Scanning Electron Microscopy

Figure 3. Representative Micrographs of Gas-Atomized Powder Used in this Investigation.

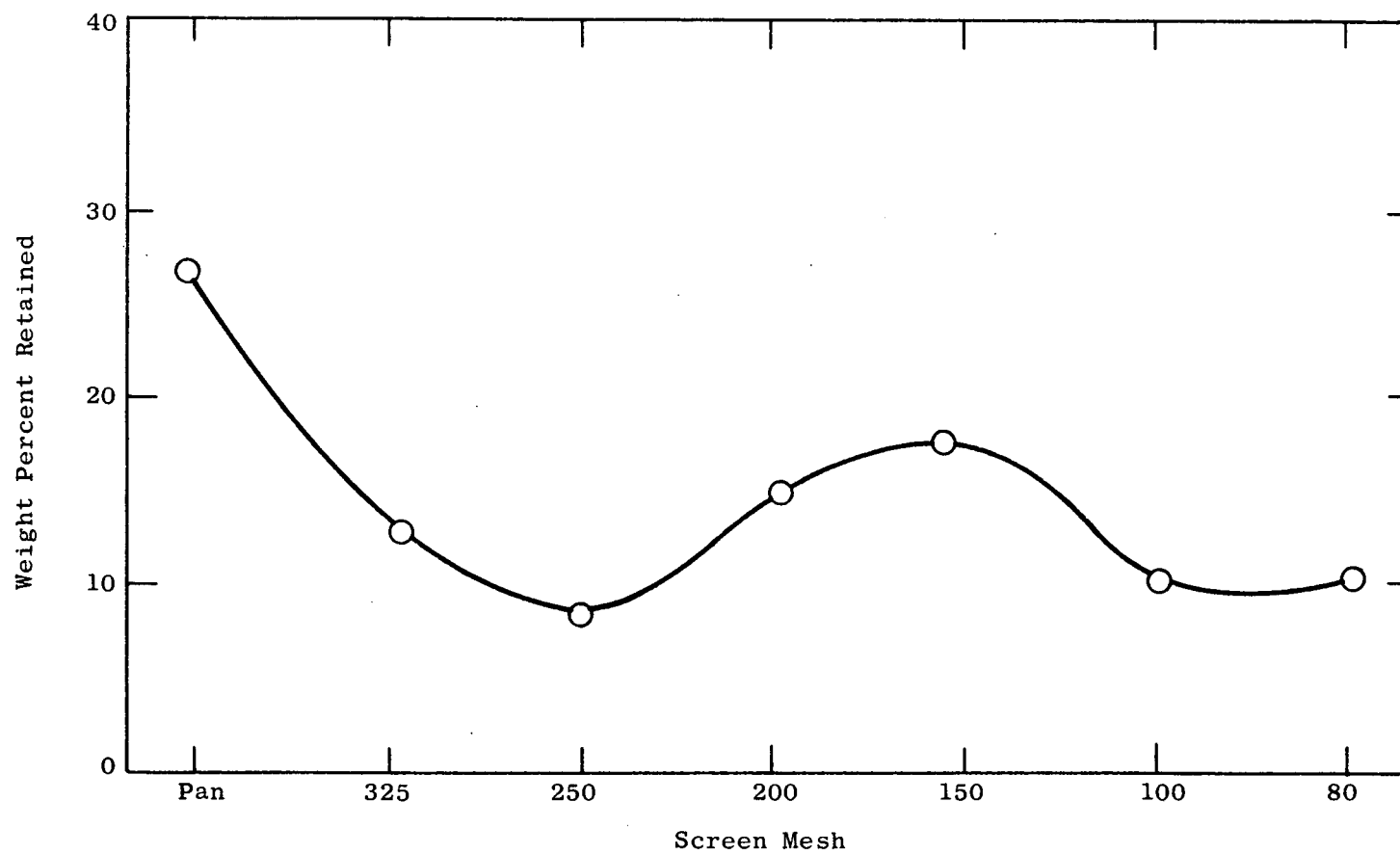


Figure 4. Representative Particle Size Distribution of Powder Used in this Investigation.

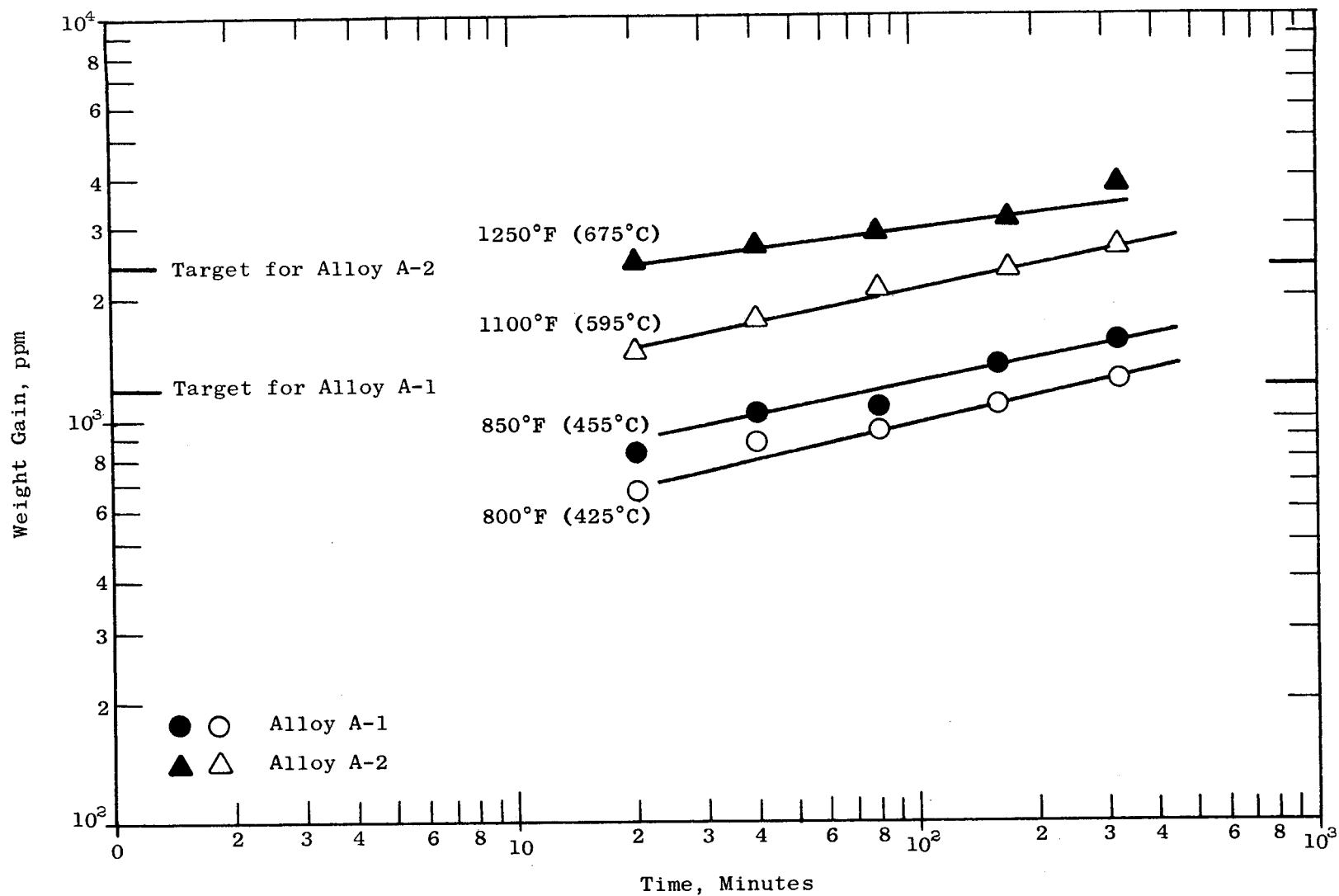
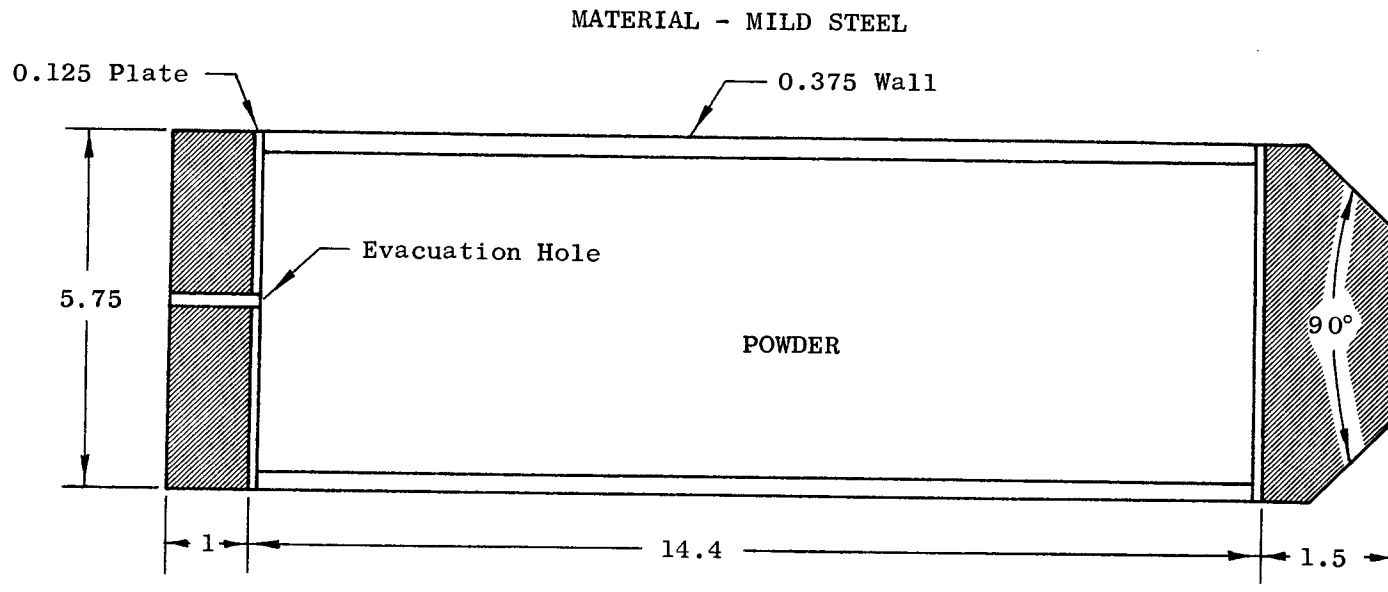


Figure 5. Oxidation Data from Air Exposure of -100 Mesh Powders of Alloys A-1 and A-2.



All Dimensions in Inches

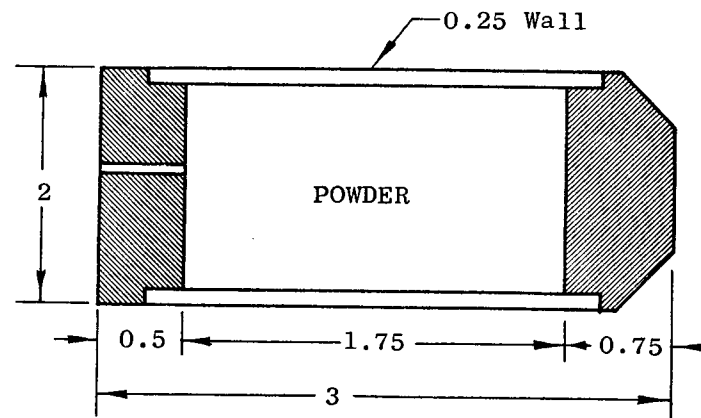


Figure 6. Schematic Drawing of Extrusion Cans Used for the First Extrusion Series.

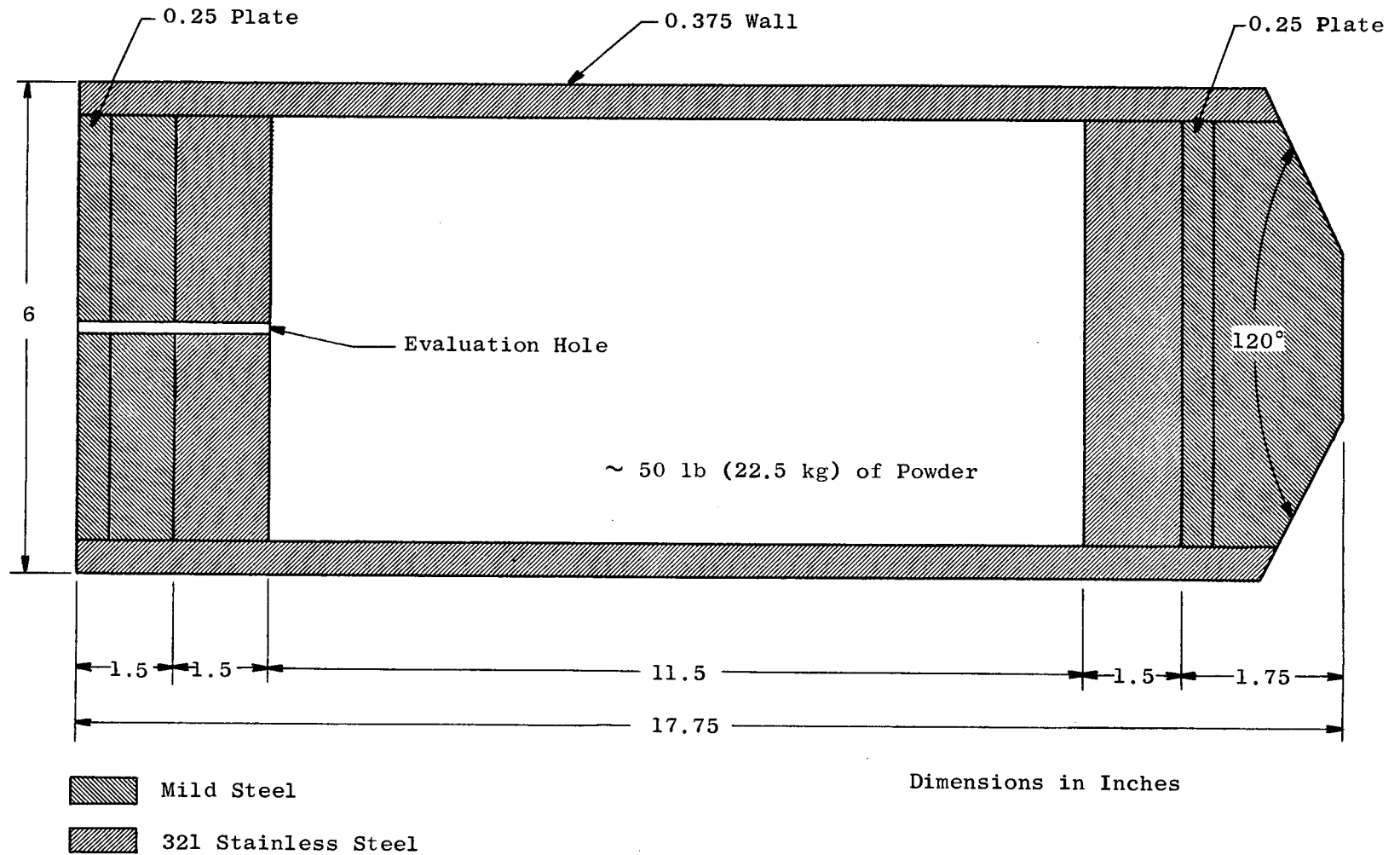


Figure 7. Schematic Drawing of Extrusion Can Used for Second Extrusion Series.

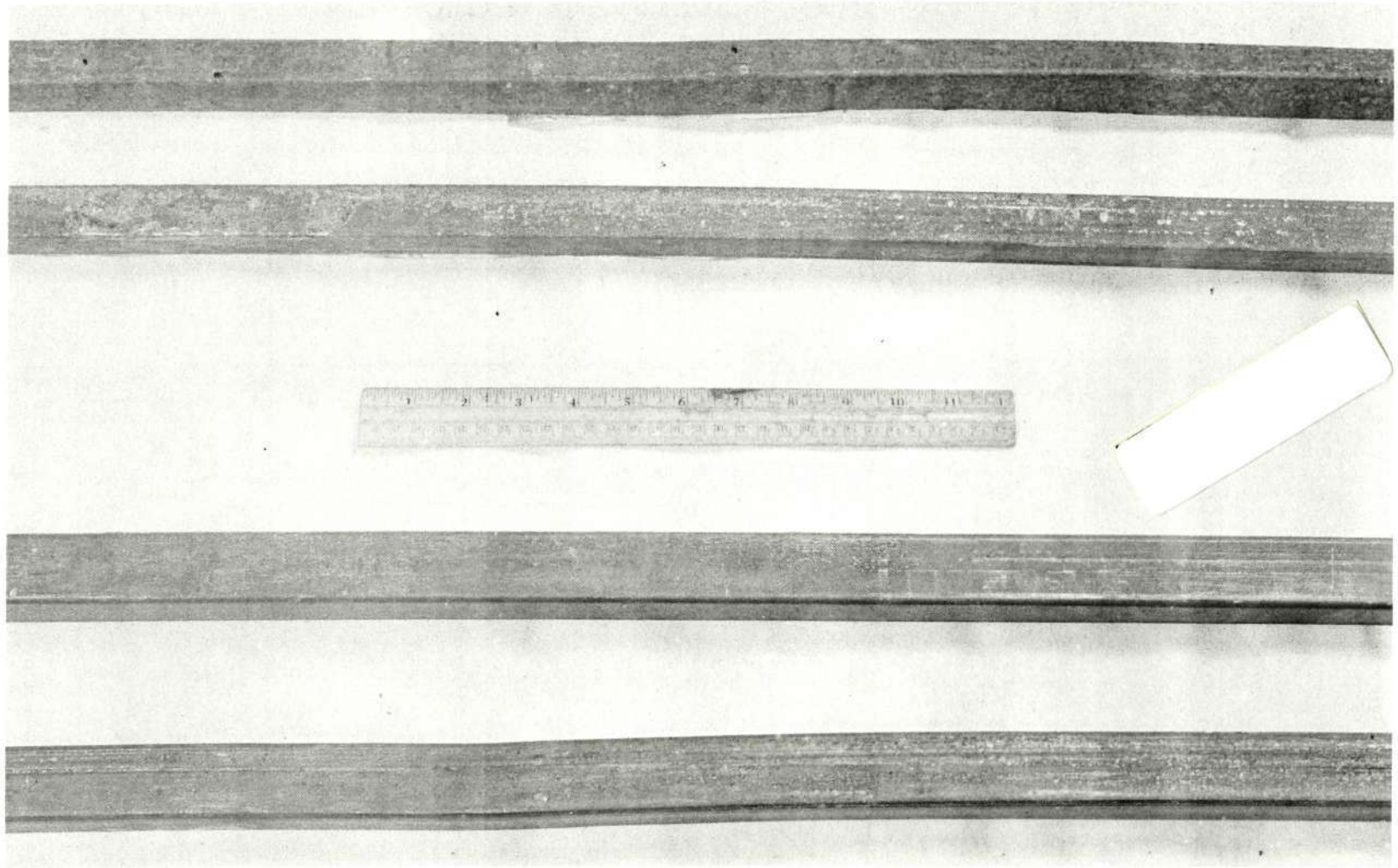


Figure 8. Photograph of Sections from Extruded Bars. Top Two Bars are from the First Extrusion Series and Bottom Two are from the Second Extrusion Series.



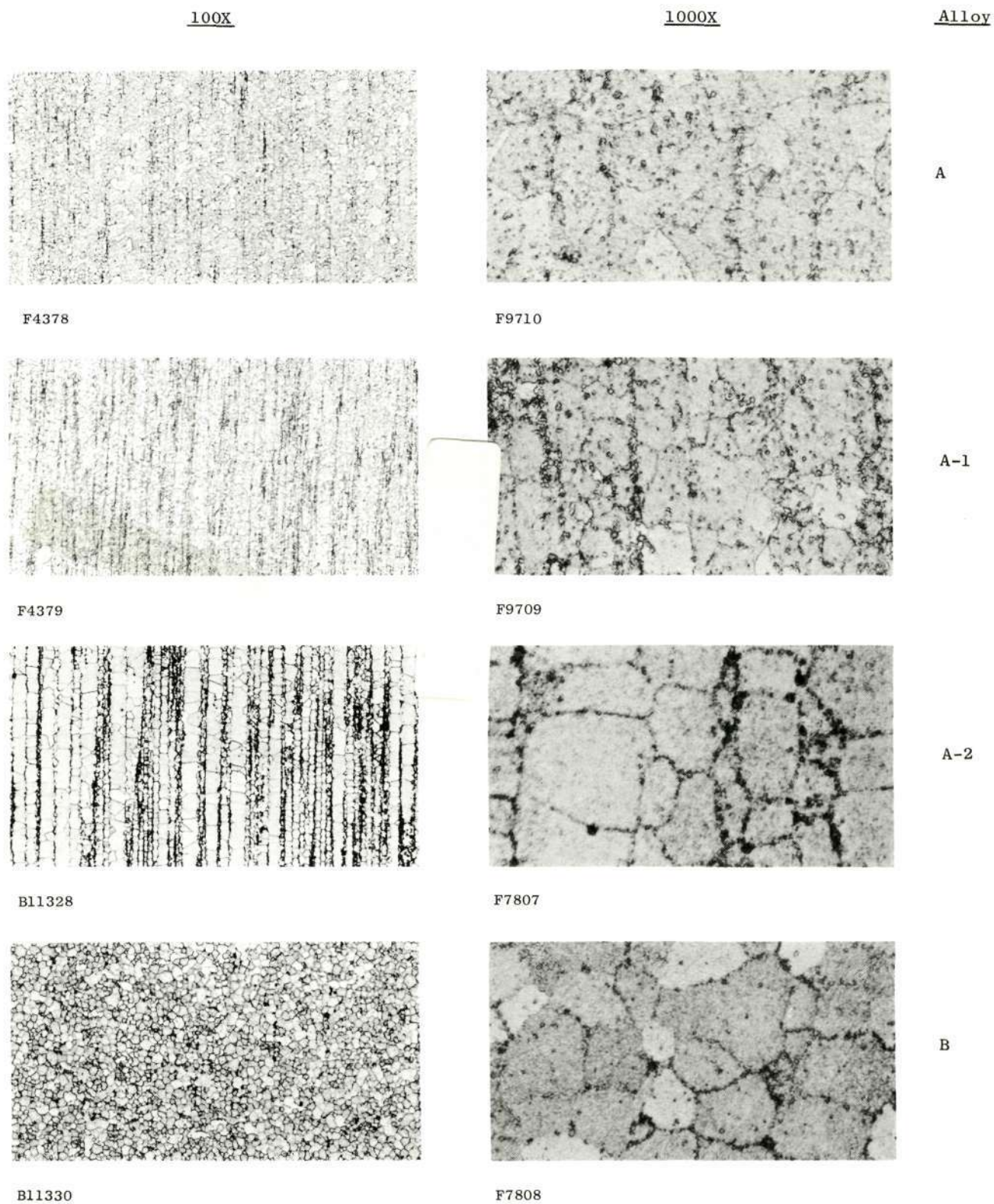


Figure 9. Photomicrographs of As-Extruded Microstructures; Extrusion Direction is Vertical.





F4838

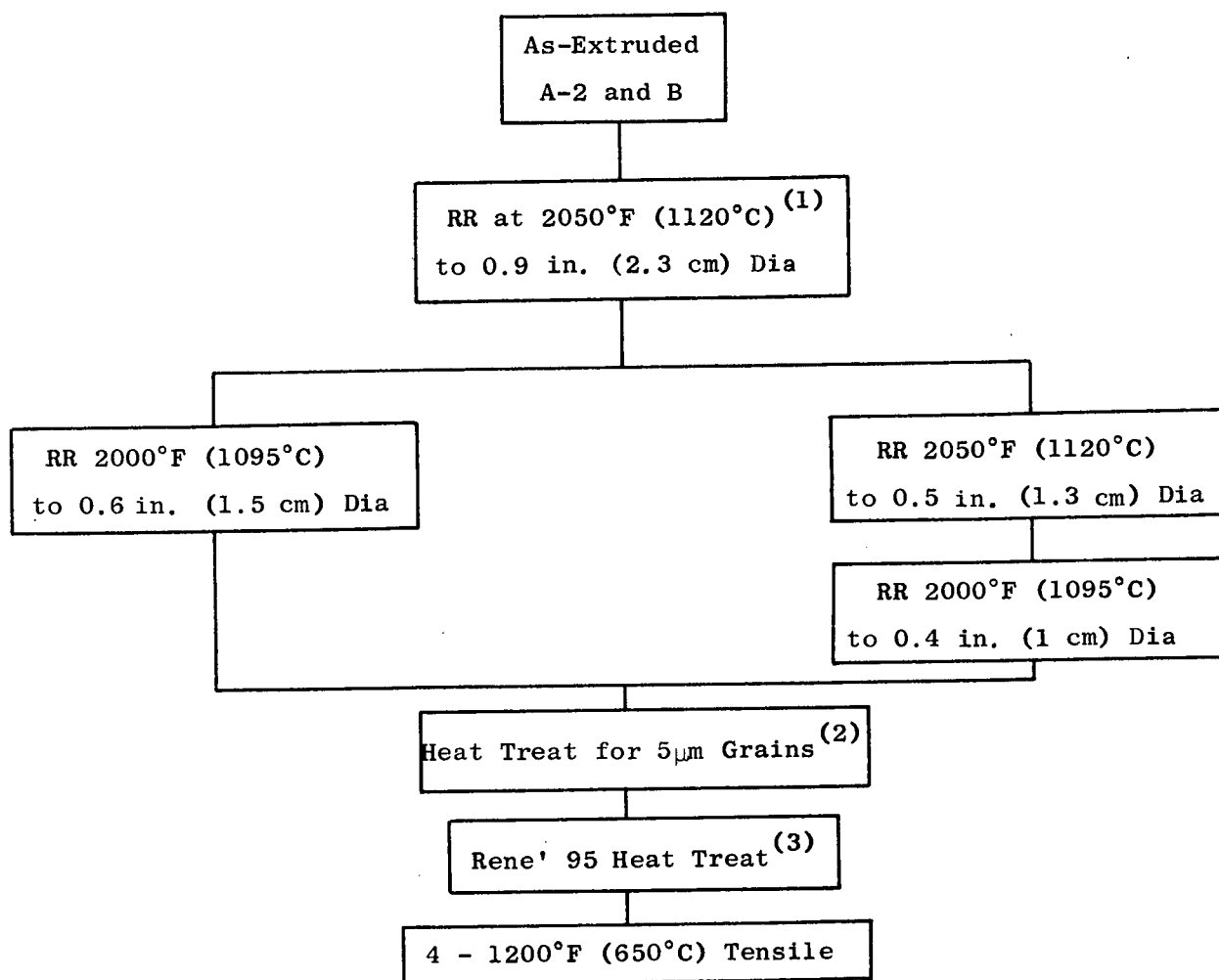
a. Alloy A-2, with Oxides



F0937

b. Alloy B, without Oxides

Figure 10. Examples of Duplex Grain Structures that Formed when Attempting to Achieve Equiaxed Grain Growth (100X).



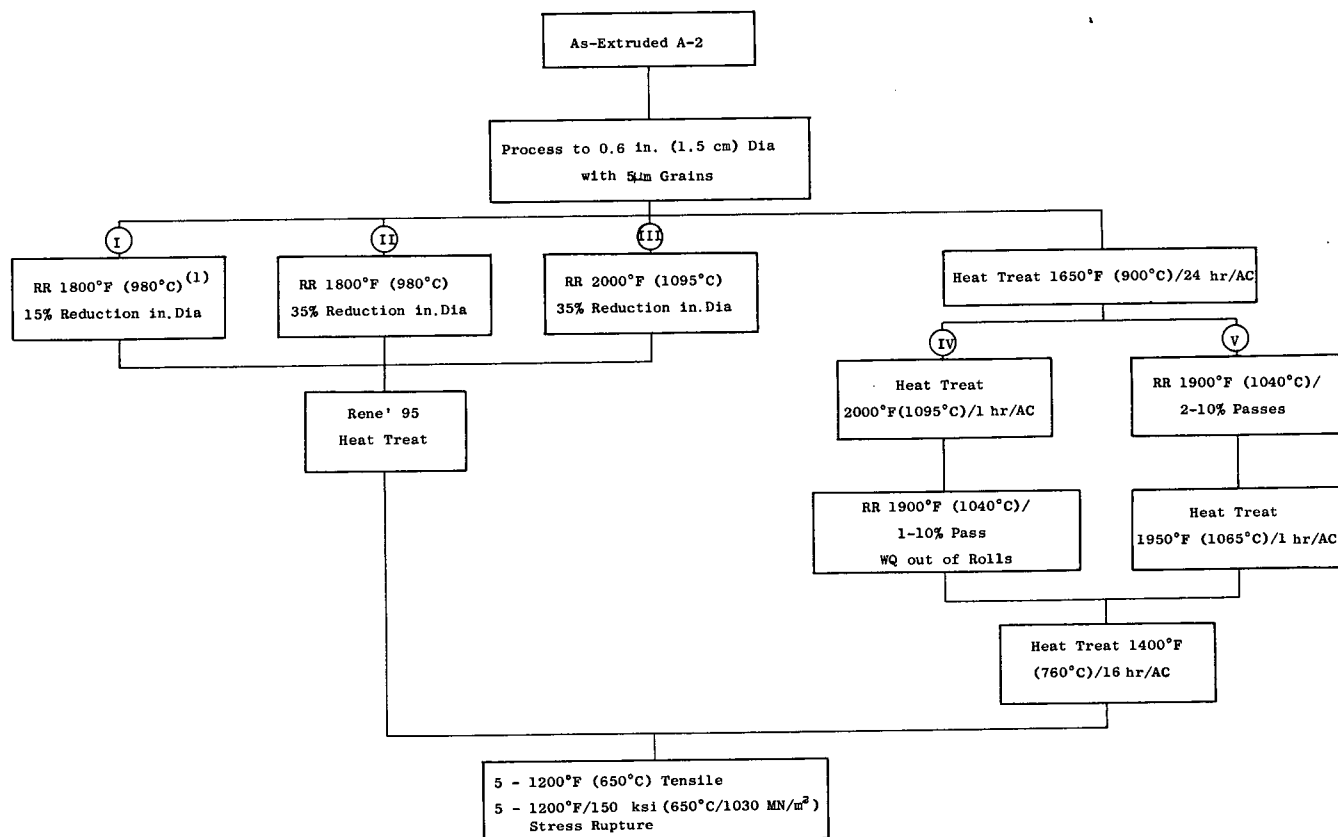
Alloy	Side of Flow Chart	0.2 YS		UTS		Elongation, %	RA, %
		ksi	MN/m <sup>2</sup>	ksi	MN/m <sup>2</sup>		
A-2	Left	180	1240	216	1490	9	13
A-2	Right	170	1170	209	1440	9	11
B	Left	187	1290	212	1460	12	19
B	Right	174	1200	226	1550	15	14

(1) RR - Rod Rolled

(2) 2050°F (1120°C)/3 hr/AC

(3) 1650°F (900°C)/24 hr/AC, 2000°F (1095°C)/1 hr/OQ, 1400°F (760°C)/16 hr/AC

Figure 11. Preliminary Study 2 - Processing to Desired Grain Size - Effect of Variations in Rolling Reduction at 2050°F (1120°C) on Properties.



Specimen Condition	1200°F (650°C) Tensile						Stress Rupture		
							1200°F/150 ksi (650°C/1030 MN/m <sup>2</sup> )		
	0.2 YS		UTS		Elongation,	RA, %	Time,	Elongation,	Grain
	ksi	MN/m <sup>2</sup>	ksi	MN/m <sup>2</sup>	%		hr	%	Size, μm
I	188	1290	224	1540	10	14	212 <sup>(2)</sup>	1.7	5
II	189	1300	228	1570	11	17	175	3.7	4
III	179	1230	234	1610	14	17	208 <sup>(2)</sup>	0.35	6
IV	195	1340	246	1700	11	14	157	4.1	10
V	190	1310	236	1630	12	17	210 <sup>(2)</sup>	0.2	8

(1) RR - Rod Rolled.

(2) Unloaded Without Failure.

Figure 12. Preliminary Study - TMP - Preformed to Relate Dislocation Substructures formed by TMP to Properties.

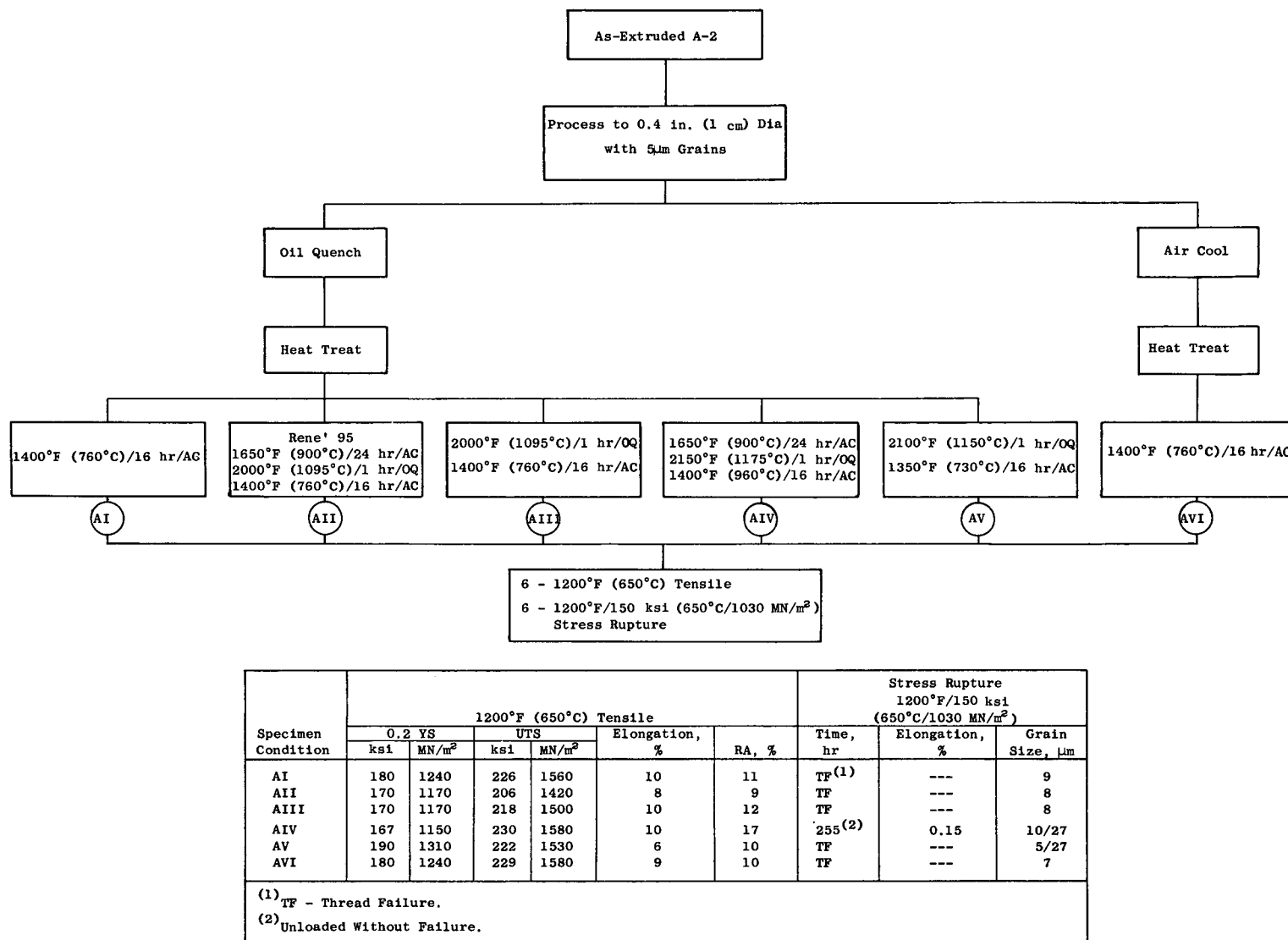
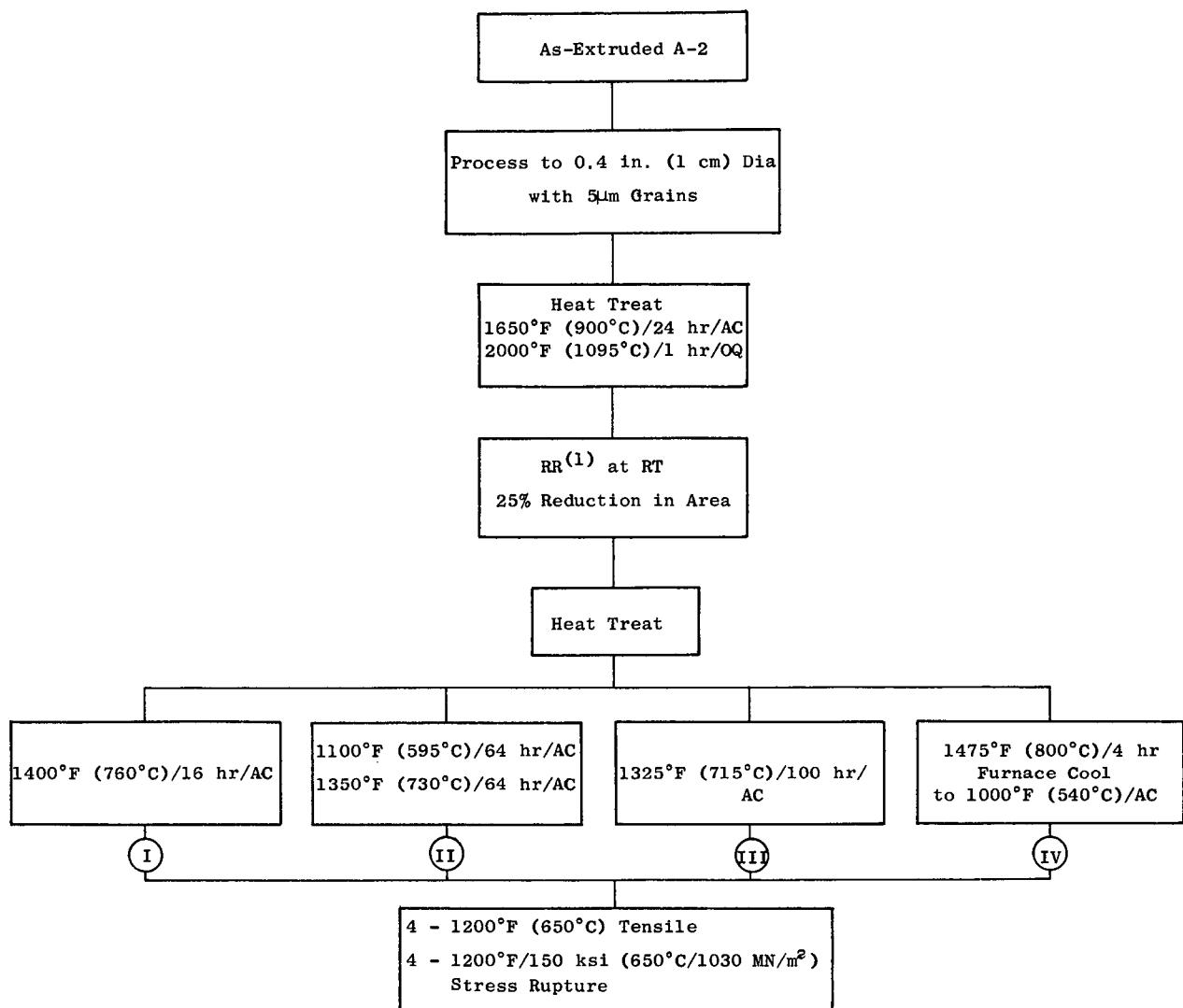


Figure 13. Preliminary Study 4 - Aging Response - Performed to Relate Aging Treatments to Properties.



Specimen Condition	1200°F (650°C) Tensile						Stress Rupture 1200°F/150 ksi (650°C/1030 MN/m <sup>2</sup> )		
	0.2 YS		UTS		Elongation, %	RA, %	Time, hr	Elongation, %	Grain Size, μm
	ksi	MN/m <sup>2</sup>	ksi	MN/m <sup>2</sup>					
I	214	1460	>236	>1630	TF <sup>(2)</sup>	---	>186	6.4	6
II	225	1550	259	1790	8	12	133	4.0	12
III	215	1480	>232	>1600	TF	---	TF	---	8
IV	Cracked Specimen						83	6	8

(1) RR - Rod Rolled

(2) TF - Thread Failure

Figure 14. Preliminary Study 4 - Aging Response - Performed to Relate Aging Treatments Plus Room Temperature Deformation to Properties.

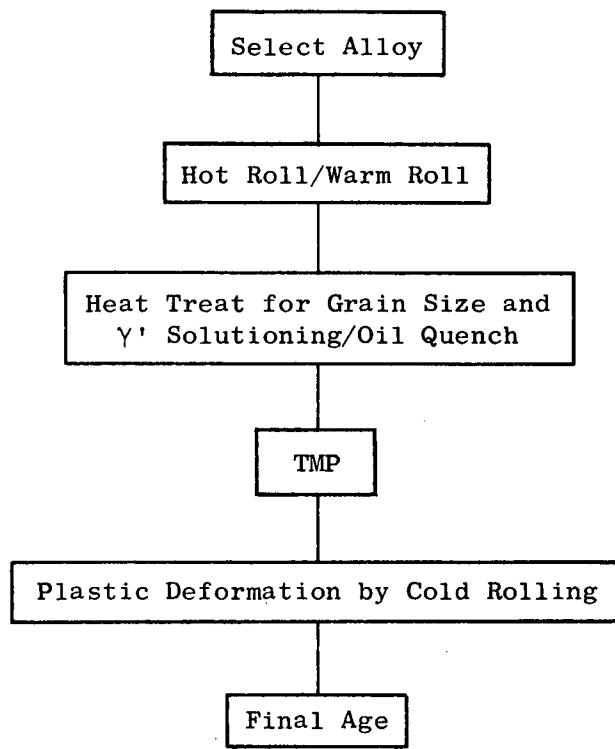


Figure 15. Processing Flow Diagram.

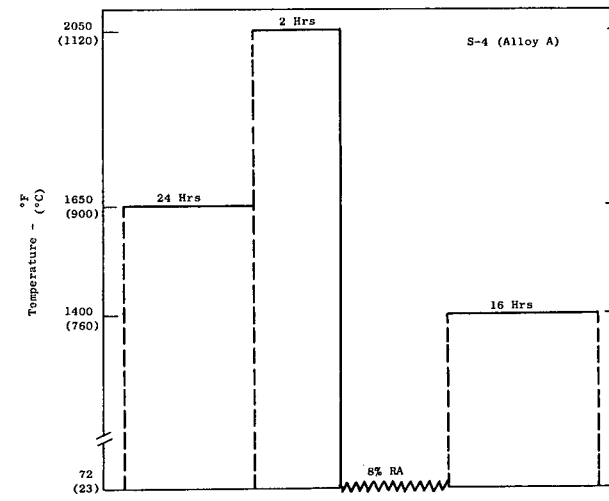
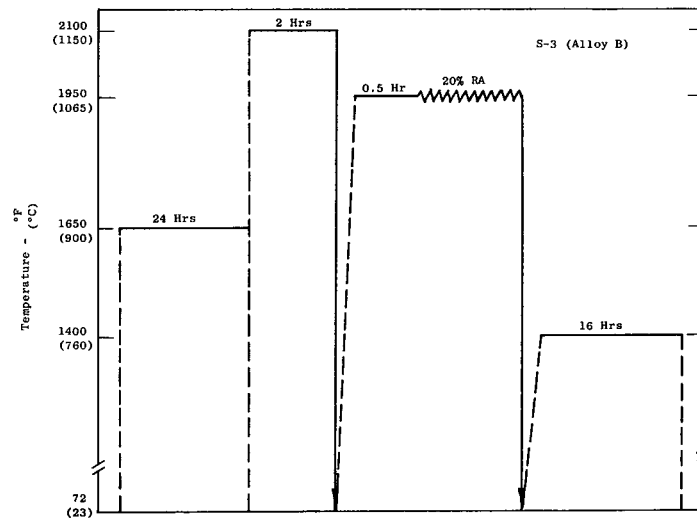
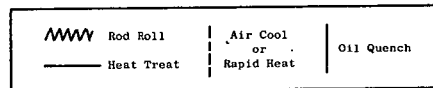
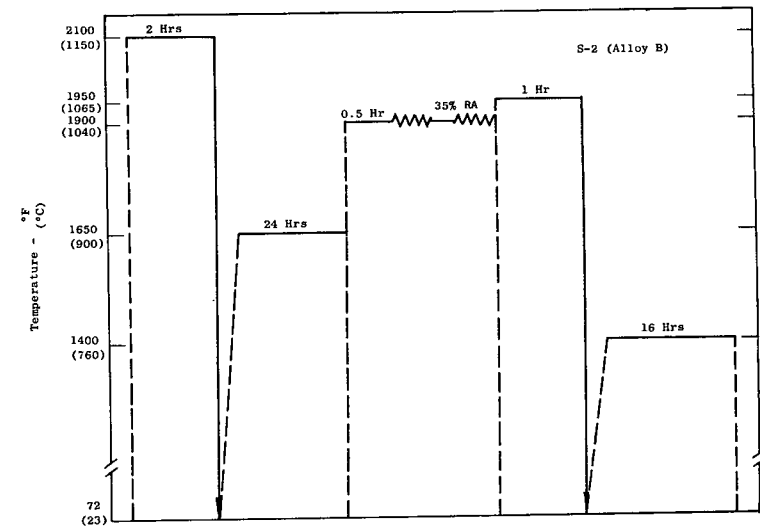
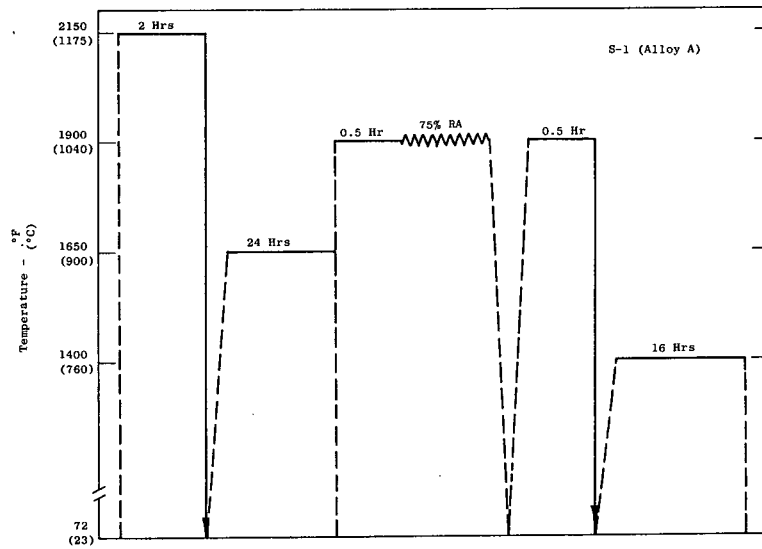


Figure 16. Schematic Diagrams of Processing Schedules Selected from Statistical Process Development Study.

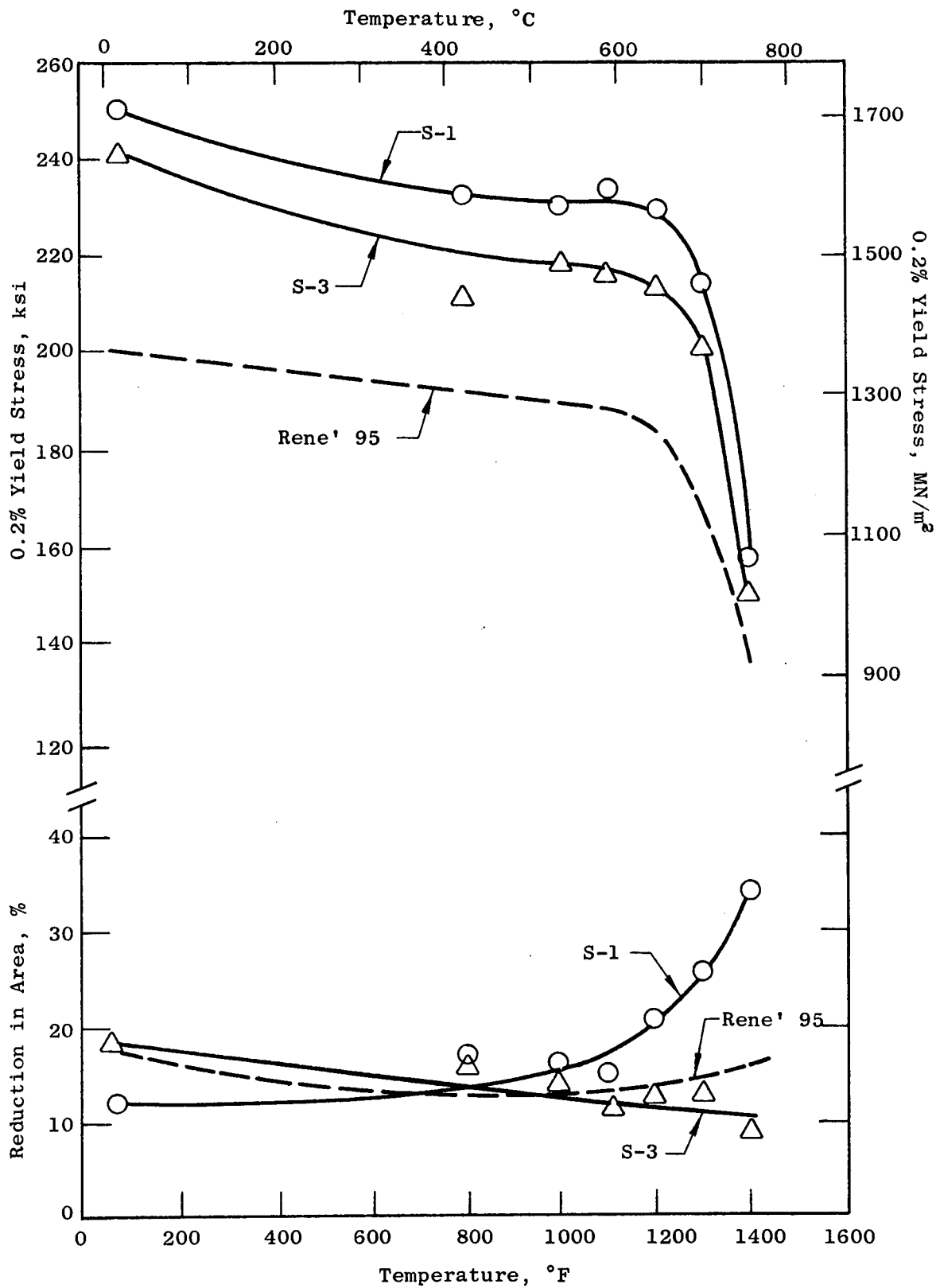


Figure 17. Tensile Data for Two Best Alloy/Process Combinations Compared to Cast-and-Forged Rene' 95.



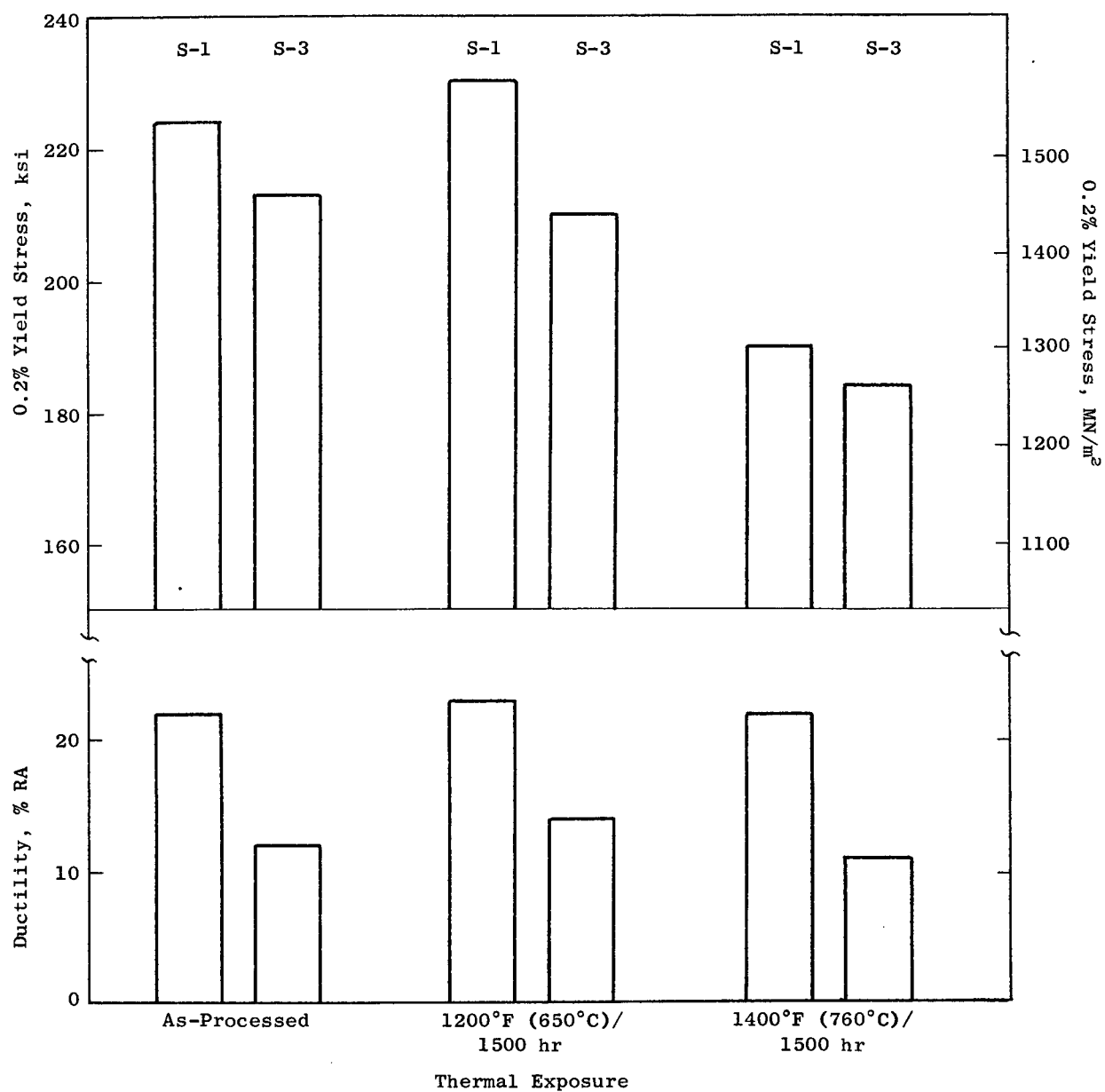


Figure 18. Tensile Data [1200°F (650°C)] for Two Best Alloy/Process Combinations As-Processed and After Thermal Exposure.

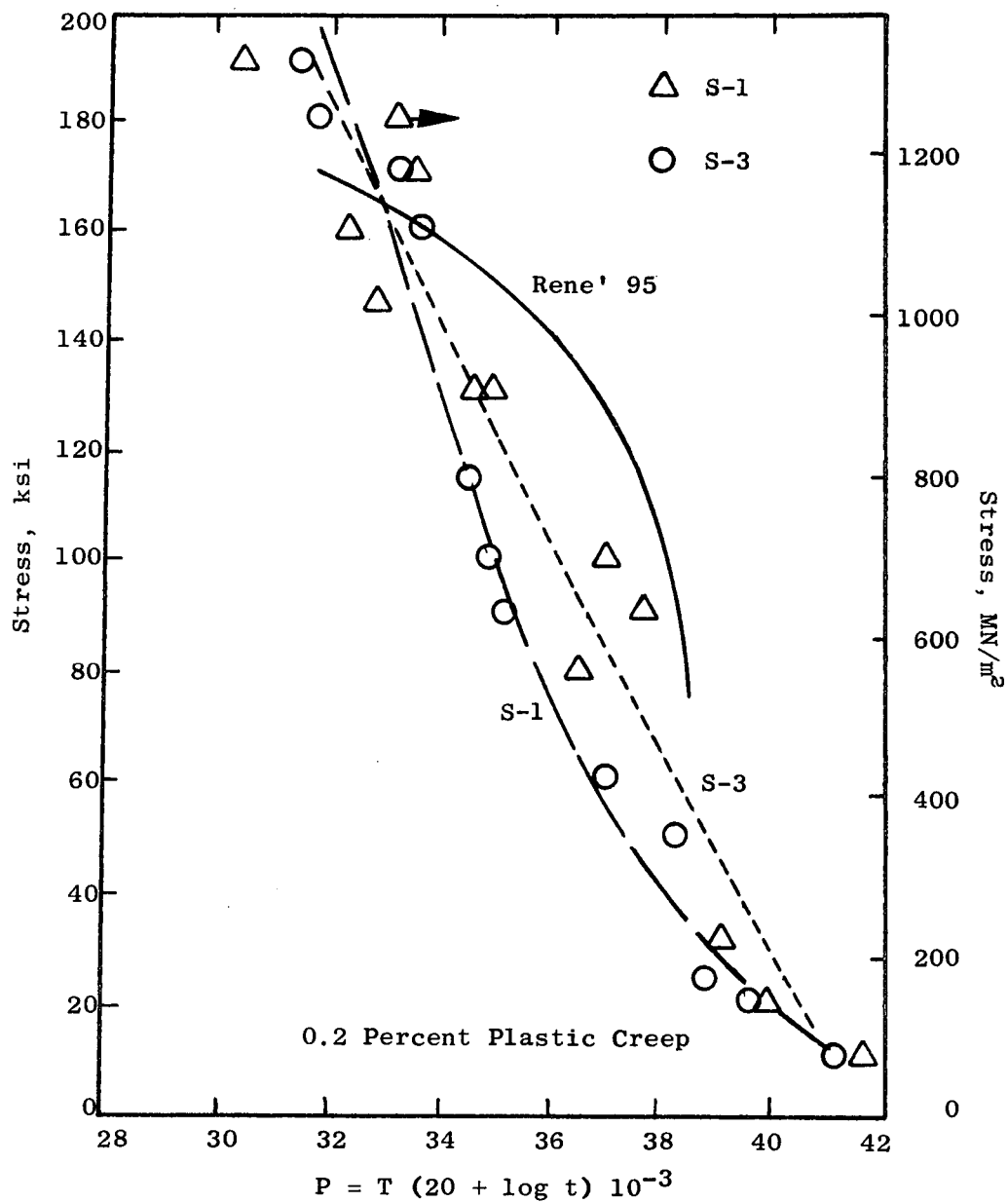


Figure 19. Comparison of the Creep Properties of Two Best Alloy/Process Combinations to Cast and Forged Rene' 95.

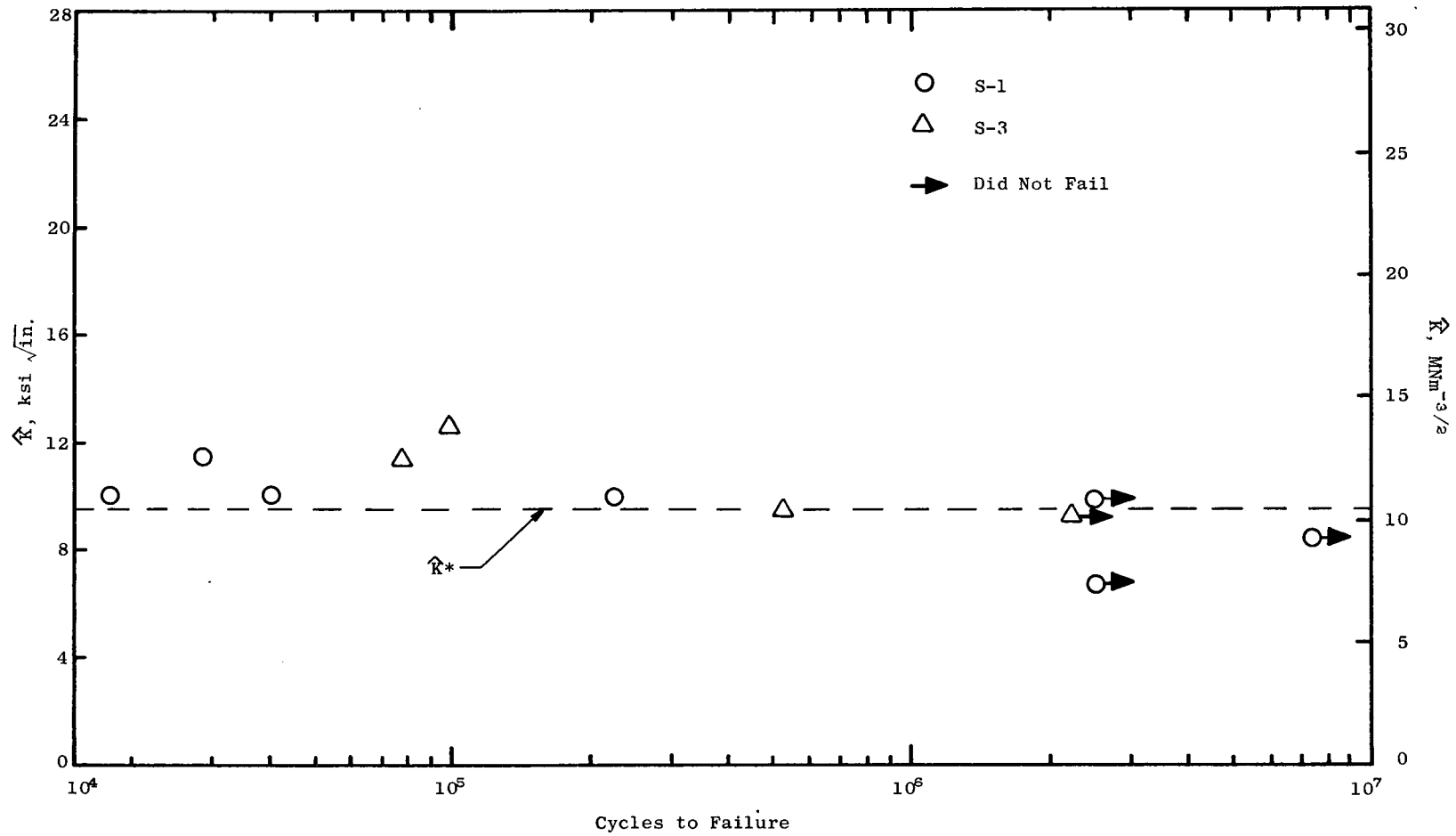


Figure 20. Test Results from  $K^*$  Testing at 1000°F (540°C) of Two Best Alloy/Process Combinations.  $K^*$  is the Threshold Stress Intensity Factor Range for Mode I Crack Propagation.


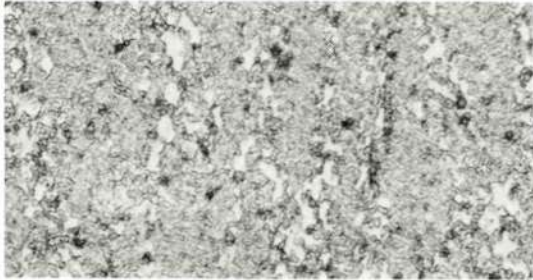
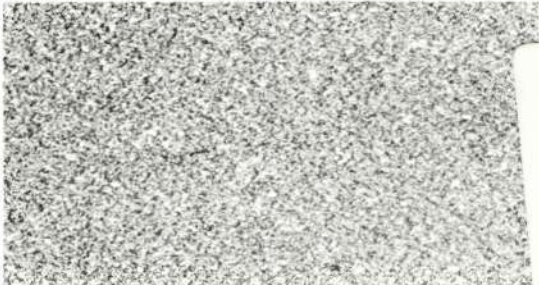
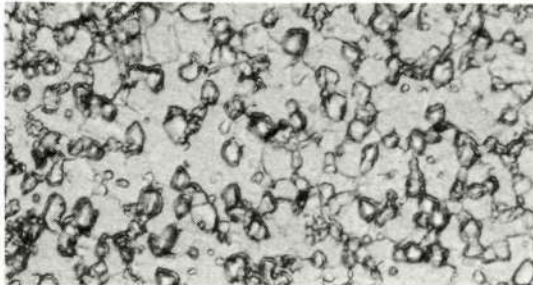
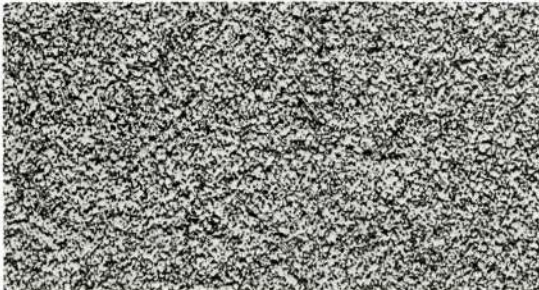
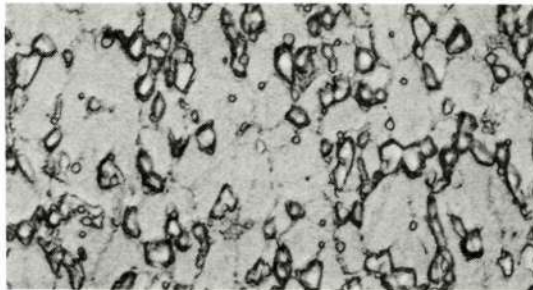
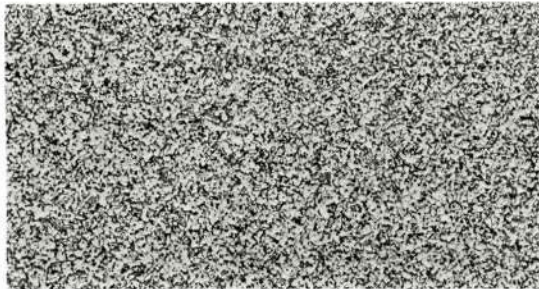
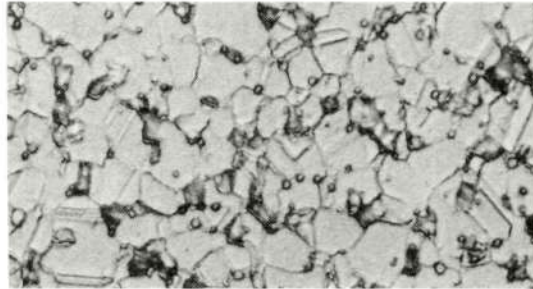
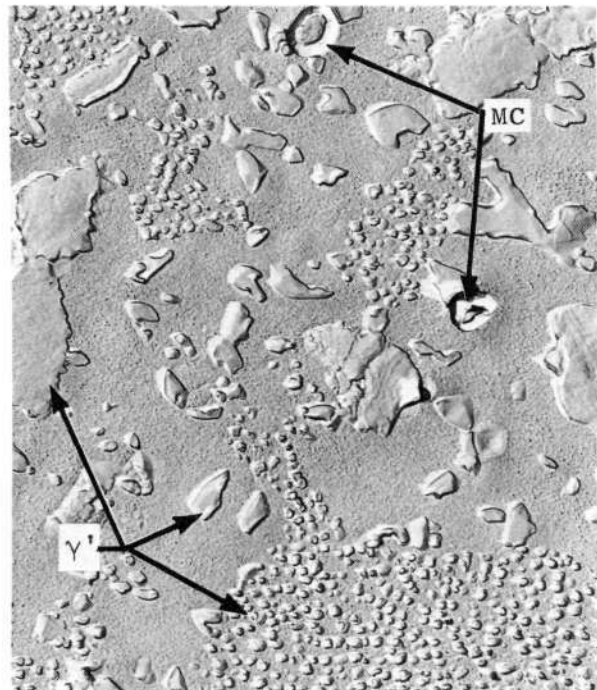
<u>100X</u>	<u>1000X</u>	<u>Material Designation</u>
		S-1
F7799	G0355	
		S-2
F9691	F8182	
		S-3
F8178	G0355	
		S-4
F8179	F8180	

Figure 21. Photomicrographs of Four Best Alloy/Process Combinations.



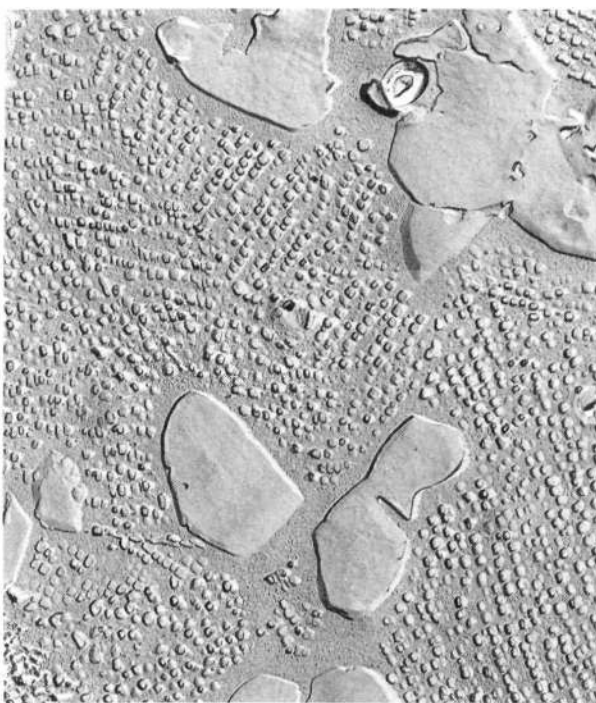
213-1

a. S-1



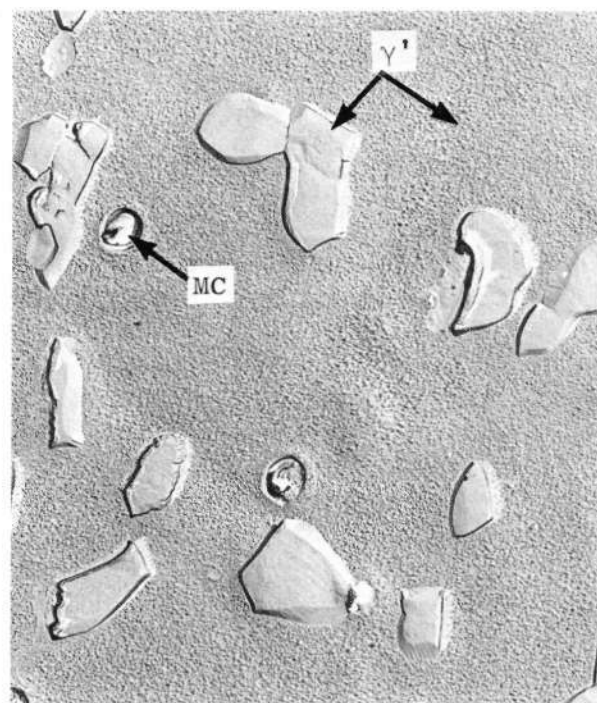
211-11

b. S-2



211-17

c. S-3

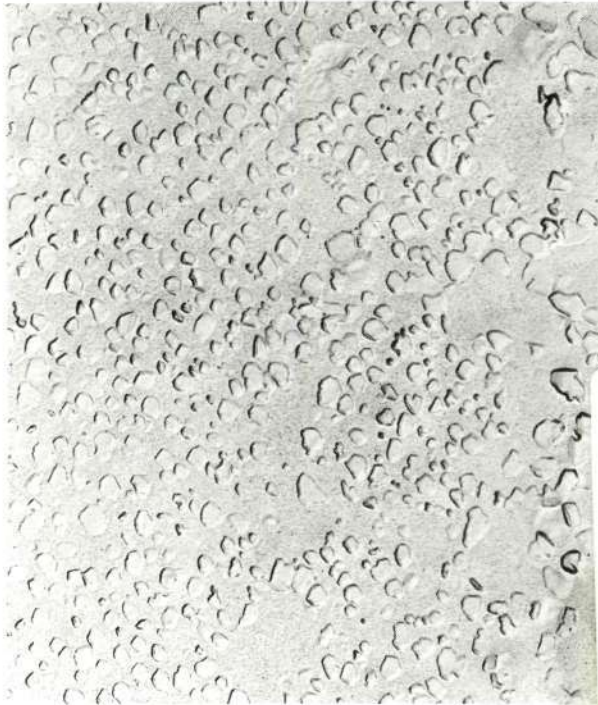


211-9

d. S-4

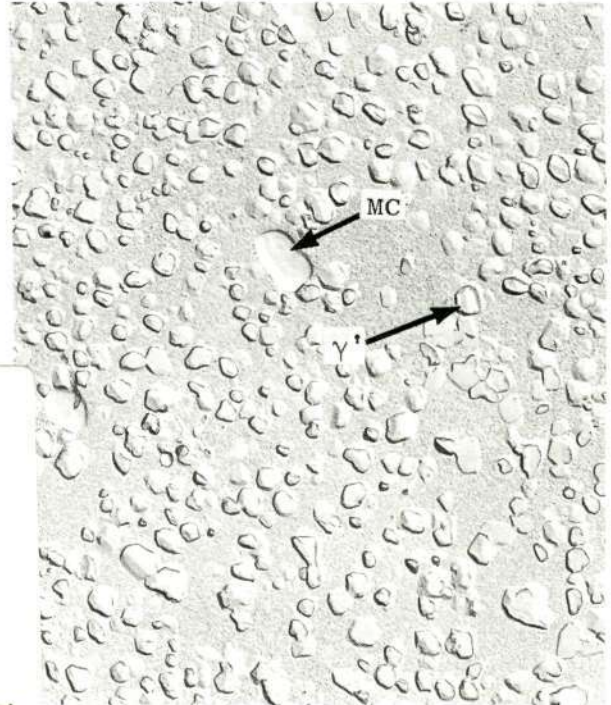
Figure 22. Electron Micrographs of Four Best Alloy/Process Combinations (5000X).





213-1

a. As-Processed



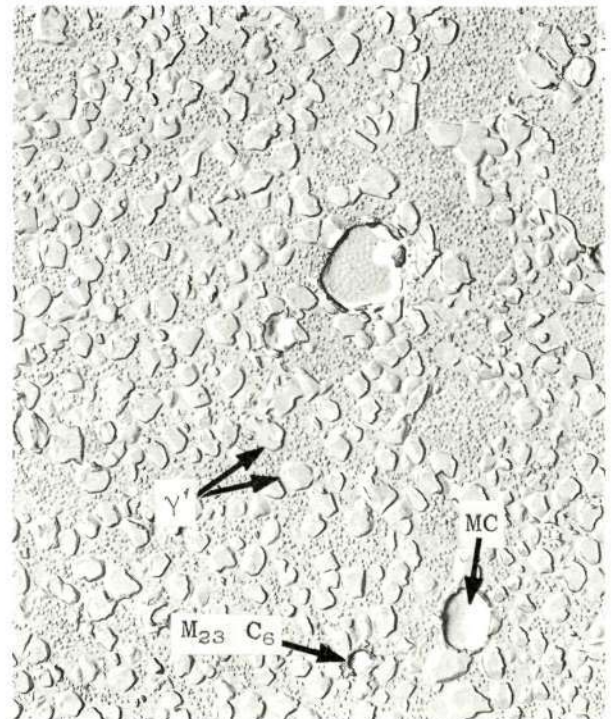
221-8

b. 1200°F/1500 Hours (650°C)



224-2

c. 1400°F/100 Hours (760°C)

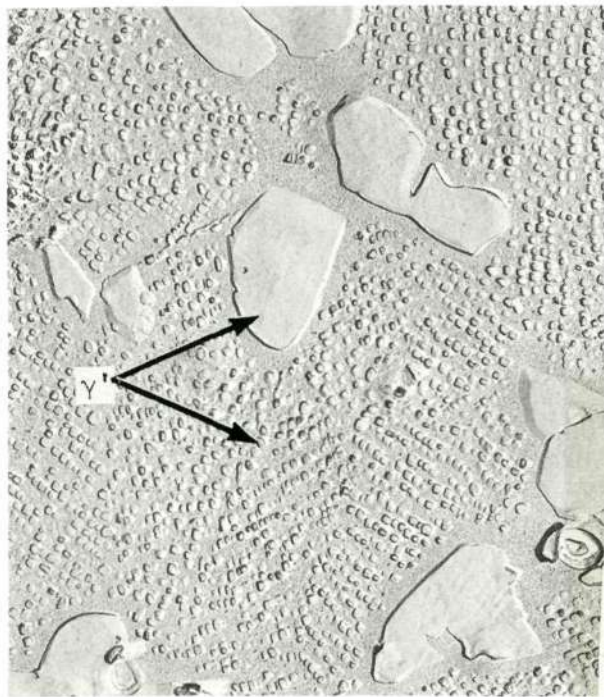


221-14

d. 1400°F/1500 Hours (760°C)

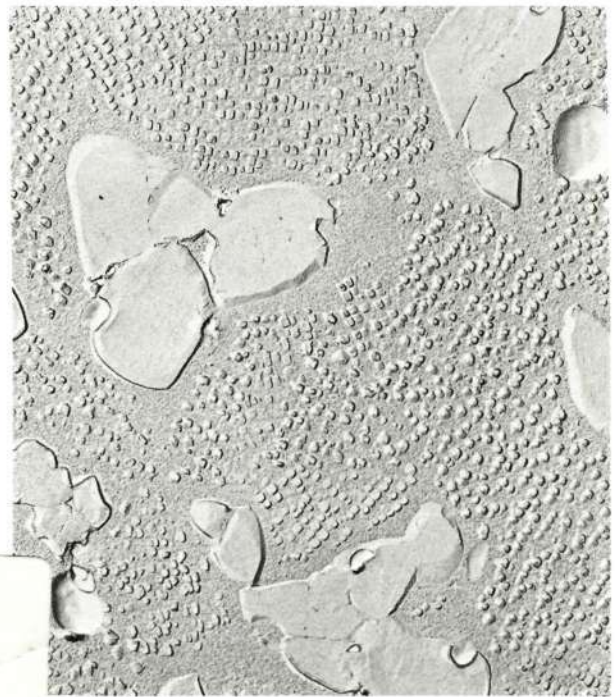
Figure 23. Electron Micrographs Illustrating the Influence of Thermal Exposure on the Microstructure of Material Condition S-1 (5000X).





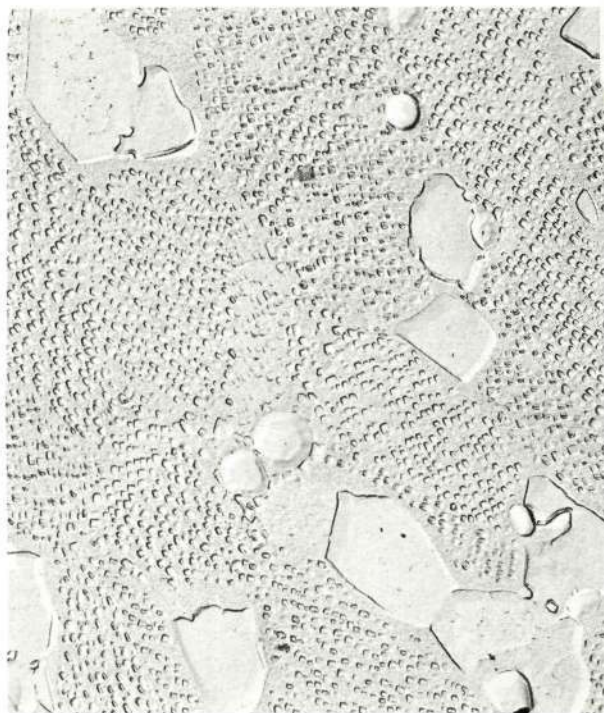
211-18

a. As-Processed



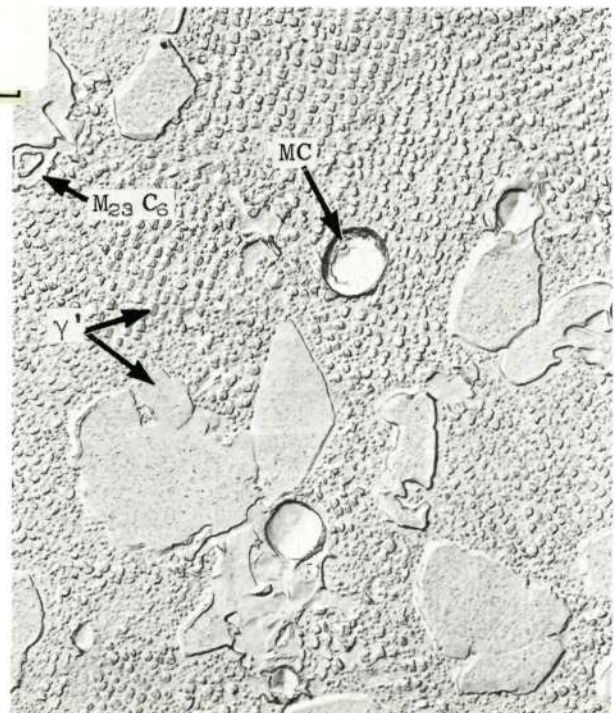
21-11

b. 1200°F/1500 Hours (650°C)



221-5

c. 1400°F/100 Hours (760°C)



221-16

d. 1400°F/1500 Hours (760°C)

Figure 24. Electron Micrographs Illustrating the Influence of Thermal Exposure on the Microstructure of Material Condition S-3 (5000X).

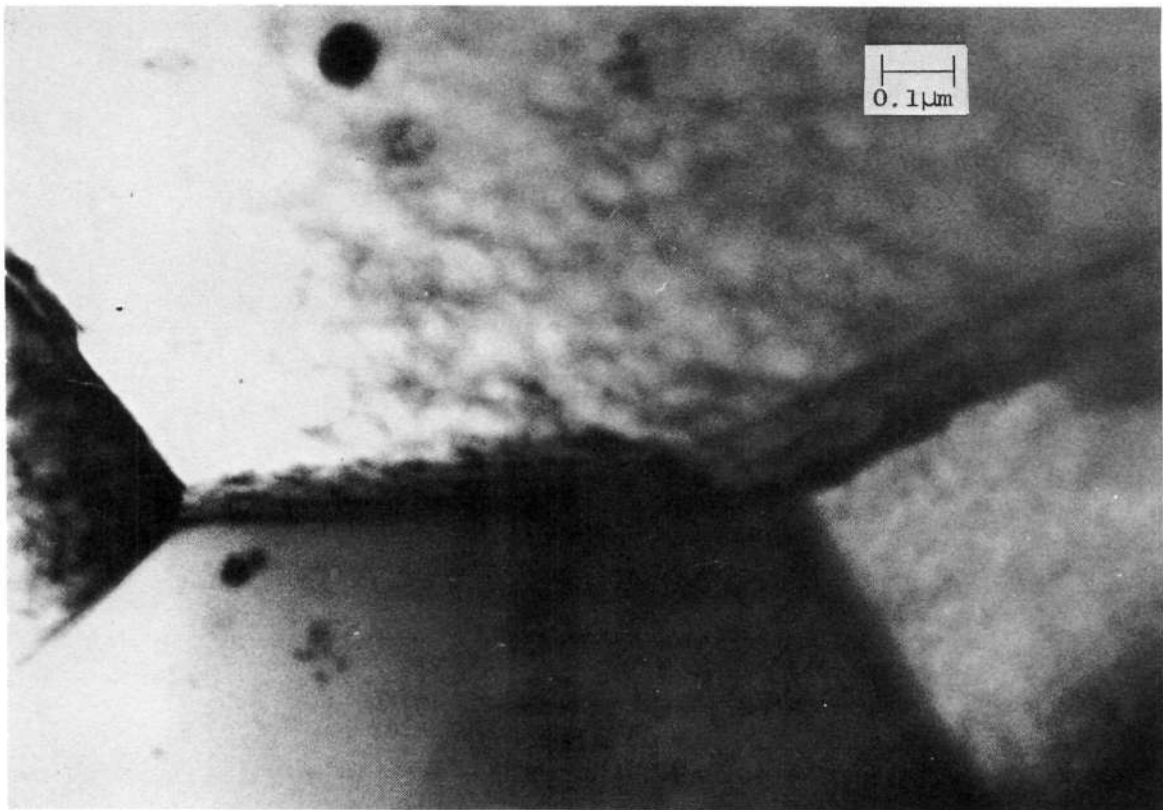


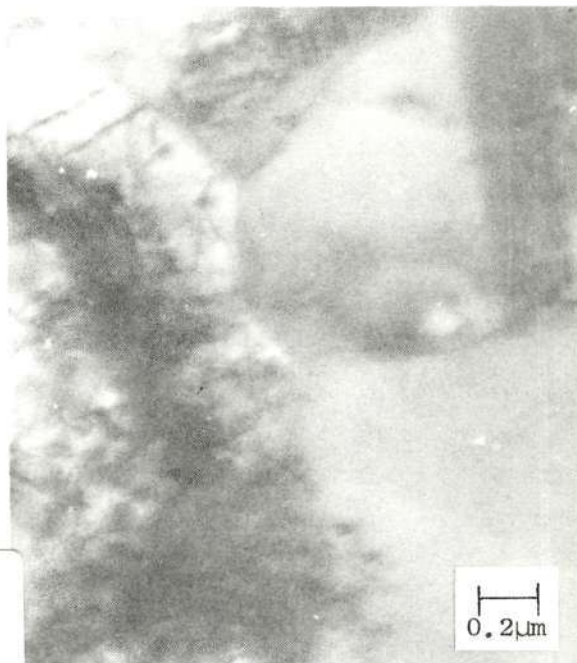
Figure 25. Transmission Electron Micrograph of Alloy A in the Recrystallized Condition, NASA CR-





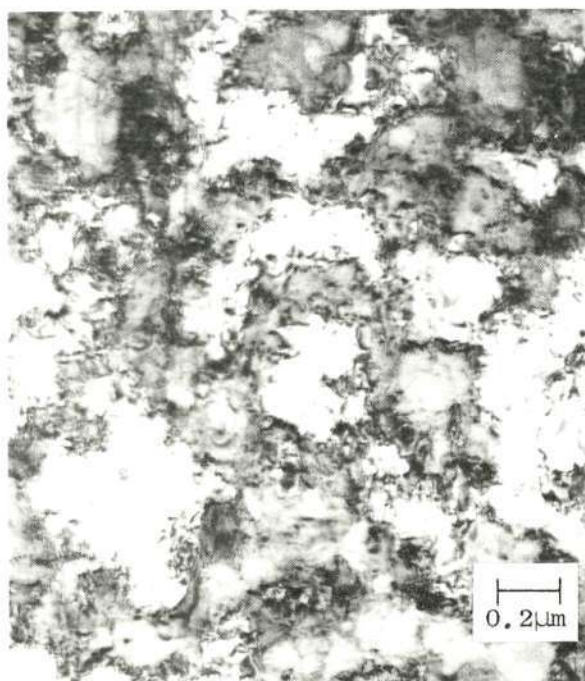
NSP

a. S-1



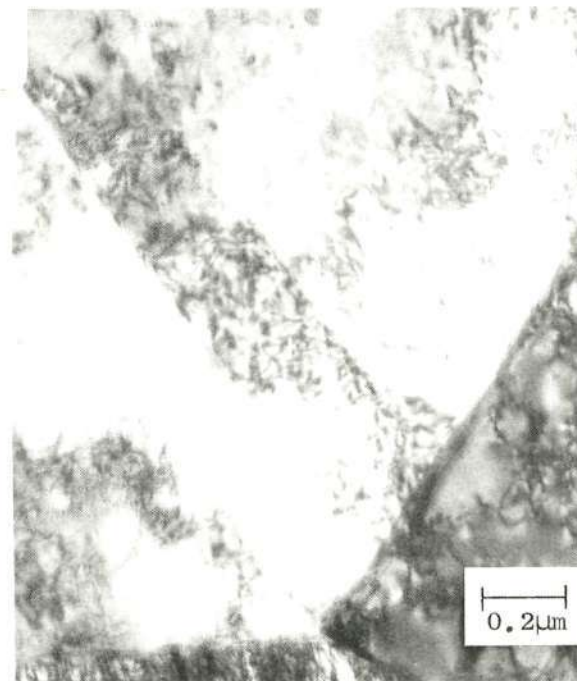
216-8

b. S-2



215-1

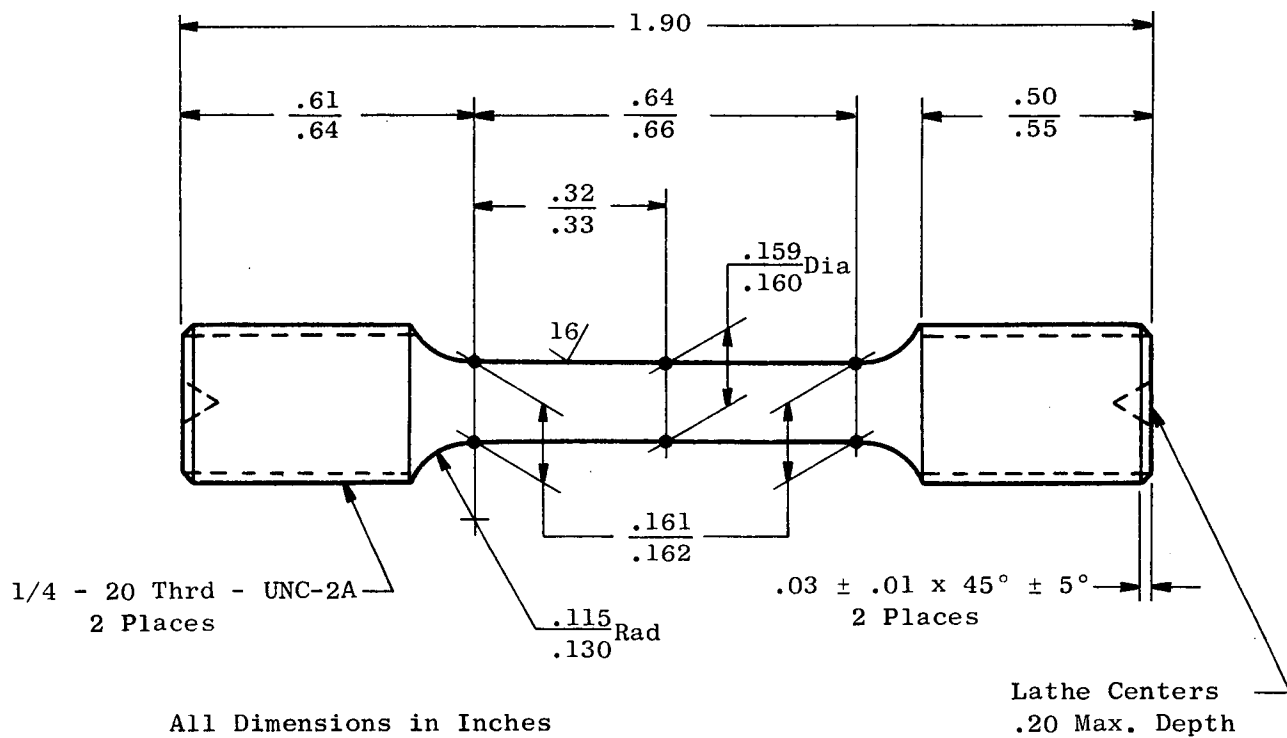
c. S-3



215-8

d. S-4

Figure 26. Transmission Electron Micrographs of Dislocation Substructures in Four Best Alloy/Process Combinations.



Note: Radius and gage section to blend smoothly without undercut. All diameters to be concentric within 0.002 tir. Remove all burrs and sharp edges with 0.015 max. rad. or cham. Unless noted all surfaces to 32/.

Figure 27. Drawing of Smooth Bar Specimens Used in Tensile, Stress Rupture, and Creep Testing. The Gage Length of the Creep Specimen was Increased from 0.65 to 1.0 Inch.



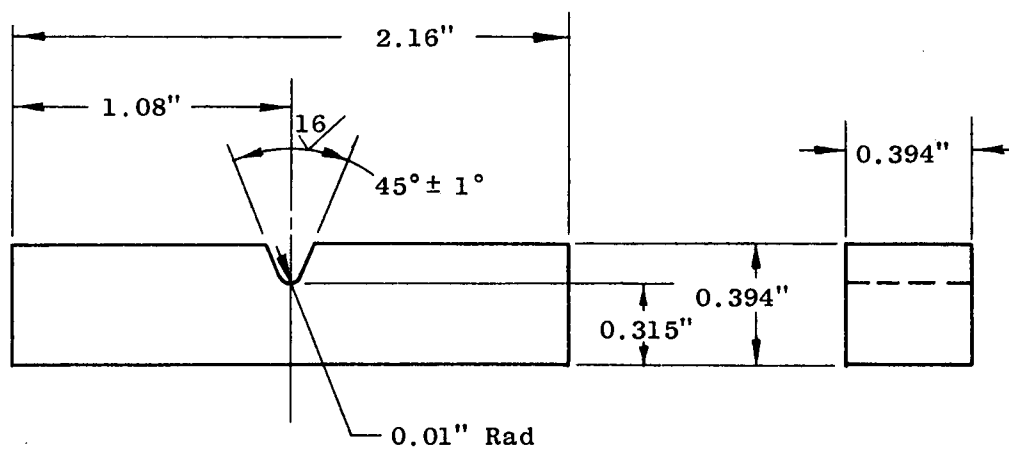


Figure 29. Design of Charpy V-Notched Bar that was Fatigue Cracked and Tested in Slow Bend.

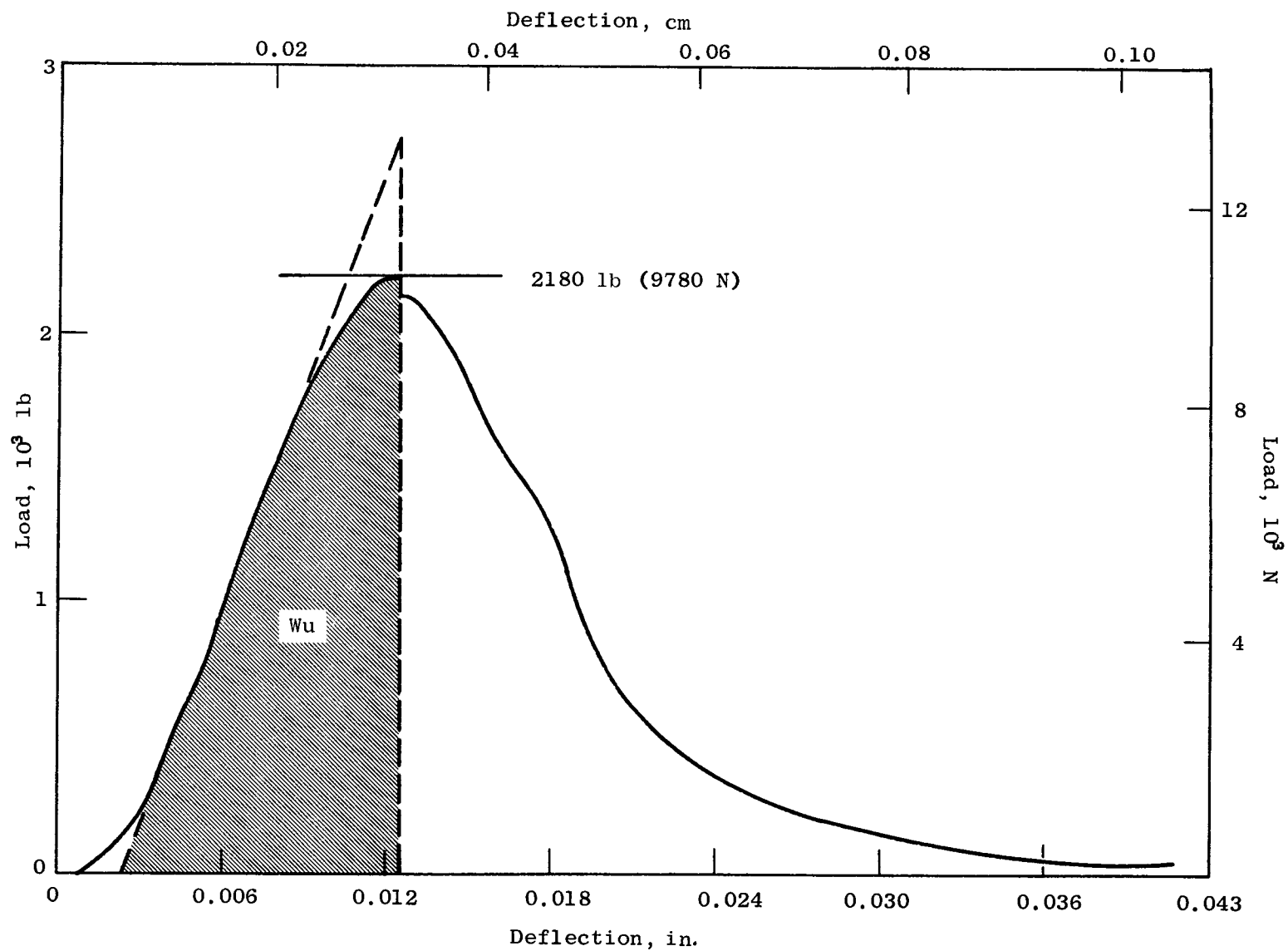


Figure 30. Typical Charpy Bend Test Record Illustrating Calculation of Energy Absorbed at Point of Crack Instability.

# DISTRIBUTION LIST

1. NASA-Lewis Research Center  
21000 Brookpark Road  
Cleveland, Ohio 44135  
Attention:

Dr. R.L. Ashbrook	MS 49-1	1
G.M. Ault	MS 3-13	1
C.P. Blankenship	MS 105-1	1
W.F. Brown	MS 105-1	1
R.L. Dreshfield	MS 49-1	1
J.C. Freche	MS 49-1	1
F.H. Harf	MS 49-1	50
Dr. A.G. Holms	MS 49-1	1
Dr. R.V. Miner	MS 49-1	1
M. Quatinetz	MS 49-1	1
N.T. Sanders	MS 105-1	1
W.J. Waters	MS 49-1	1
Library	MS 60-3	2
Aeronautics Procurement	MS 77-3	1
Patent Counsel	MS 500-311	1
Report Control Office	MS 5-5	1
Technology Utilization	MS 3-19	1
2. NASA Headquarters  
600 Independence Avenue  
Washington, D.C. 20546  
Attention:

G.C. Deutsch/RRM	1
R.H. Raring/RRM	1
J. Gangler/RRM	1
N. Rekos/RAP	1
3. NASA Ames Research Center  
Moffett Field, California 94035  
Attention: Library 1
4. NASA Goddard Space Flight Center  
Greenbelt, Maryland 20771  
Attention: Library 1
5. NASA Flight Research Center  
P.O. Box 273  
Edwards, California 93523  
Attention: Library 1

6. Jet Propulsion Laboratory  
4800 Oak Grove Drive  
Pasadena, California 91102  
Attention: Library 1
7. NASA Langley Research Center  
Langley Field, Virginia 23365  
Attention: Library 1
8. NASA Manned Space Flight Center  
Houston, Texas 77058  
Attention: Library 1
9. NASA Marshall Space Flight Center  
Huntsville, Alabama 35812  
Attention: Library 1
10. Headquarters  
Wright Patterson AFB, Ohio 45433  
Attention:  
Dr. A.M. Lovelace, AFML/MAG 1  
Dr. H.M. Burte, AFML/MAM 1  
Technical Library, AFML/MAAM 1  
Dr. I. Perlmutter, AFML/MAMP 1  
J.K. Elbaum, AFML/MAMP 1  
Dr. C.M. Pierce, AFML/MAMP 1
11. USAF Off Scientific Res  
Propulsion Research Div  
Washington, D.C. 20525  
Attention: M. Slawsky 1
12. NASA Lewis Research Center  
AFSC Liaison MS501-3  
21000 Brookpark Road  
Cleveland, Ohio 44135  
Attention: Maj. R.C. Chaplin 1
13. Army Materials and Mechanics  
Research Center  
Watertown, Massachusetts 02172  
Attention: Dr. F.R. Larson AMXMR-RM 1
14. Metallurgy Research Lab  
Frankfort Arsenal  
Philadelphia, Pennsylvania 19137  
Attention: Mr. H. Rosenthal MRL 1

15. Naval Air Systems Command  
Navy Department  
Washington, D.C. 20360  
Attention: P. Goodwin AIR-5203 1
  
16. Navy Department  
ONR Code 439  
Washington, D.C. 20525  
Attention: Dr. R. Roberts 1
  
17. Atomic Energy Commission  
Washington, D.C. 20545  
Attention:  
    Technical Reports Library 1  
    J. Simmons 1
  
18. Oak Ridge National Lab  
Technical Reports Library  
Oak Ridge, Tennessee 37830 1
  
19. Defense Documentation Center  
Cameron Station  
5010 Duke Street  
Alexandria, Virginia 22314 1
  
20. Allegheny Ludlum Steel Corp.  
Brackenridge, Pennsylvania 15014  
Attention: R.A. Lula 1
  
21. American Society for Metals  
Metals Park  
Novelty, Ohio 44073  
Attention: Dr. T. Lyman 1
  
22. Lycoming Division  
Avco Manufacturing Company  
505 South Main Street  
Stratford, Connecticut 06497  
Attention: W.H. Freeman 1
  
23. Avco Space Systems Div.  
Lowell Industrial Park  
Lowell, Massachusetts 01851  
Attention: Library 1



24. Battelle Merorial Institute  
505 King Avenue  
Columbus, Ohio 43201  
Attention:  
Cobalt Information Center 1  
DMIC 1  
Dr. R.I. Jaffee 1  
Dr. B. Wilcox
  
25. Cabot Corporation  
Stellite Division  
P.O. Box 746  
Kokomo, Indiana 46901  
Attention: Library 1
  
26. Carpenter Technology Corp.  
Res. & Dev. Center  
P.O. Box 662  
Reading, Pennsylvania 19603  
Attention: Dr. D.R. Muzyka 1
  
27. Climax Molybdenum Company  
1600 Huron Parkway  
Ann Arbor, Michigan 48106  
Attention: D. Sponseller 1
  
28. Denver Research Institute  
University Park  
Denver, Colorado 80210  
Attention: Library 1
  
29. Metallurgy Department  
Denver University  
Denver, Colorado 80210  
Attention: Prof. J.B. Newkirk 1
  
30. Dynamet, Inc.  
1720 North Main Street  
Washington, Pennsylvania 15301  
Attention: C.P. Mueller 1
  
31. Research & Development  
Federal Mogul Corporation  
Ann Arbor, Michigan  
Attention: J.G. Lebrasse 1
  
32. Firth Sterling, Inc.  
P.O. Box 71  
Pittsburgh, Pennsylvania 15230  
Attention: Powder Metals Research 1

33. Materials Development  
Ford Motor Company  
P.O. Box 2053  
Dearborn, Michigan 48123  
Attention: Dr. Y.P. Telang 1
34. Supervisor Materials Eng.  
Department 93393  
Garrett Airresearch  
Phoenix, Arizona 85034 1
35. Materials Laboratory  
Allison Division  
General Motors Corp.  
Indianapolis, Indiana 46206  
Attention: D. Hanink 1
36. Homogenous Metals Inc.  
West Canada Blvd  
Herkimer, N.Y. 13350  
Attention: R.J. Nylen 1
37. IIT Research Institute  
10 West 35th Street  
Chicago, Illinois 60616  
Attention: Dr. N.M. Parikh 1
38. Industrial Materials Technology  
127 Smith Place  
West Cambridge Ind. Pk.  
Cambridge, Massachusetts 02138  
Attention: Dr. R. Widmer 1
39. International Nickel Company  
One New York Plaza  
New York, New York 10004  
Attention: Mr. R.W. Fawley 1
40. International Nickel Co.  
Merica Research Lab  
Sterling Forest  
Suffern, New York 10901  
Attention: Dr. F. Decker 1
41. Government Relations  
Ladish Company  
Cudahy, Wisconsin 53110  
Attention: C. Burley 1

42. Director of Research  
Latrobe Steel Company  
Latrobe, Pennsylvania 15650  
Attention: Dr. E.E. Reynolds 1
43. Research Laboratory  
Lockheed-Georgia Company  
Marietta, Georgia 30060  
Attention: Dr. W.S. Cremens 1
44. Martin Marietta Corp.  
Res. Inst. Adv. Studies  
1450 S. Rolling Road  
Baltimore, Maryland 21227  
Attention: Dr. P.S. Kotval 1
45. Materials and Science Lab  
Lockheed Research Labs  
3251 Hanover Street  
Palo Alto, California 94304  
Attention: Technical Information Center 1
46. McDonnell-Douglas Corporation  
P.O. Box 516  
St. Louis, Missouri 63166  
Attention: R.E. Jackson 1
47. Micromet Laboratories  
202 South Street  
West Lafayette, Indiana 47906  
Attention: Dr. J.F. Radavich 1
48. Aeronautic Division  
Philco-Ford Corporation  
Ford Road  
Newport Beach, California 92663  
Attention: R.A. Harlow 1
49. Ploymet Corporation  
11 West Sharon Road  
Cincinnati, Ohio 45246  
Attention: G.J. Wile 1
50. Special Metals Corporation  
New Hartford, N.Y. 13413  
Attention: W.J. Boesch 1
51. Metallurgy Group  
Stanford Research Institute  
Menlo Park, California 94025  
Attention: Dr. E.S. Wright 1

52.	Dept. of Materials Science Stanford University Palo Alto, California 94305 Attention: Prof. O. Sherby	1
53.	Chem & Met Division Sylvania Electric Prod Towanda, Pennsylvania 18848 Attention: Dr. J.S. Smith	1
54.	Materials Technology TRW Equipment Group 23555 Euclid Avenue Cleveland, Ohio 44117 Attention: Dr. H.E. Collins Dr. C.S. Kortovich Dr. E.A. Steigerwald Library	1 1 1 1
56.	Pratt & Whitney Aircraft United Aircraft Corporation 400 Main Street East Hartford, Connecticut 06108 Attention: K.J. Kelly Research Library	1 1
57.	Advanced Materials R. & D. Pratt & Whitney Aircraft United Aircraft Corporation Middletown, Connecticut 06458 Attention: C.P. Sullivan	1
58.	Pratt & Whitney Aircraft United Aircraft Corporation West Palm Beach, Florida 33402 Attention: Library	1
59.	Universal Cyclops Steel Res. & Dev. Department Bridgeville, Pennsylvania 14017 Attention: L. Lherbier	1
60.	Westinghouse Electric Steam Division P.O. Box 9175 Lester, Pennsylvania 19113 Attention: F.J. Wall	1

61. Nuclear Metals Division  
Whittaker Corporation  
West Concord, Massachusetts 01781  
Attention: Library 1
62. Wyman-Gordon Company  
North Grafton, Massachusetts 01436  
Attention: W.H. Coutts 1